



Universiteit
Leiden
The Netherlands

On multifield inflation, adiabaticity, and the speed of sound of the curvature perturbations

Atal, V.

Citation

Atal, V. (2016, March 8). *On multifield inflation, adiabaticity, and the speed of sound of the curvature perturbations*. *Casimir PhD Series*. Retrieved from <https://hdl.handle.net/1887/38478>

Version: Not Applicable (or Unknown)
License: [Leiden University Non-exclusive license](#)
Downloaded from: <https://hdl.handle.net/1887/38478>

Note: To cite this publication please use the final published version (if applicable).

Cover Page



Universiteit Leiden



The handle <http://hdl.handle.net/1887/38478> holds various files of this Leiden University dissertation.

Author: Atal, Vicente

Title: On multifield inflation, adiabaticity and the speed of sound of the curvature perturbations

Issue Date: 2016-03-08

On Multifield Inflation, Adiabaticity, and the Speed of Sound of the Curvature Perturbations

Proefschrift

ter verkrijging van
de graad van Doctor aan de Universiteit Leiden,
op gezag van Rector Magnificus prof. mr. C.J.J.M. Stolker,
volgens besluit van het College voor Promoties
te verdedigen op dinsdag 8 maart 2016
klokke 15.00 uur

door

Vicente Atal

geboren te Santiago (Chile)
in 1986

Promotor: Prof. dr. A. Achúcarro

Co-Promotor: Prof. dr. G.A. Palma (Universidad de Chile, Santiago, Chile)

Promotiecommissie: Dr. D.D. Baumann (University of Amsterdam and
University of Cambridge, Cambridge, UK)

Dr. J.R. Fergusson (University of Cambridge, Cambridge, UK)

Prof. dr. S. Mataresse (Università degli Studi di Padova, Padova, Italy)

Prof. dr. E.R. Eliel

Prof. dr. K.E. Schalm

Casimir PhD series, Delft-Leiden 2016-5

ISBN 978-90-8593-249-9

An electronic version of this thesis can be found at <https://openaccess.leidenuniv.nl>

The work carried out in this thesis was supported by a Leiden Huygens Fellowship.

On the front cover: View from Utrechtse Veer 22, Leiden, by HIME.

Witrantükuneyenngé chongnoam kitra.

Inhale, deeply, to stop the pipe from going out.

Mapuche proverb

Contents

Contents	iv
1 Introduction	1
1.1 The homogeneous and isotropic model of the Universe	2
1.1.1 The contents of the Universe	6
1.2 Inflation	10
1.2.1 Primordial perturbations	13
1.2.2 Higher order correlation functions	21
2 Multifield inflation and the adiabatic condition	27
2.1 Multifield inflation	29
2.1.1 Homogeneous and isotropic backgrounds	29
2.1.2 Perturbations	32
2.1.3 Curvature and isocurvature modes	34
2.1.4 Power spectrum	35
2.1.5 The fate of isocurvature perturbations	36
2.2 The effective field theory of turning trajectories	39
2.3 Discussion: EFT with $c_s \ll 1$	42
2.3.1 Perturbativity for constant c_s	46
2.3.2 Example	47
2.3.3 Perturbativity for rapidly varying c_s	49
3 Transient reductions in the speed of sound	53
3.1 Introduction	54
3.2 Moderately sharp variations in the speed of sound: primordial power spectrum and bispectrum	55
3.2.1 Power spectrum and bispectrum with the Slow-Roll Fourier Transform method	57
3.2.2 Power spectrum in the GSR formalism	58
3.2.2.1 Test for generic variations in the speed of sound	65
3.2.3 Comparison of power spectra	65
3.2.4 Bispectrum for moderately sharp reductions	67
3.2.5 Comparison of bispectra	71
3.3 Search for features in the Planck data	72
3.3.1 Parameter space	73
3.3.2 Results	76

3.3.3	Comparison with the search for features in Planck's bispectrum . .	79
3.4	Conclusions	82
4	Slowly evolving speeds of sound	85
4.1	Introduction	85
4.2	General setup	87
4.2.1	Two-field embedding	87
4.2.2	Analytical predictions	89
4.3	Quadratic inflation	92
4.4	Linear inflation	94
4.5	Natural inflation	95
4.6	Conclusion	97
5	The two-field regime of natural inflation	99
5.1	Introduction	100
5.2	Natural models	101
5.3	Equations of motion	105
5.4	Trajectories with no mass hierarchy	107
5.4.1	Case 1: $r_0 = 1M_{\text{pl}}$	107
5.4.2	Case II: $r_0 = 0.8M_{\text{pl}}$	109
5.5	Trajectories with mass hierarchy	110
5.6	Conclusions	112
	Bibliography	113
	Publications	129
	Summary	131
	Samenvatting	139
	Curriculum Vitae	147
	Acknowledgements	149

1

Introduction

Our knowledge of the content and history of the physical cosmos has seen an unprecedented revolution in the last century. In these years we have seen how the scientific method was finally capable of providing insights to many questions that were previously only of the realm of the metaphysical experience and speculation. As a result a widely accepted cosmological model has been established, which describes a vast and evolving Universe since fractions of a second after the so-called Big-Bang until today. The history of this revolution is a good lesson on how physics is nothing more than the description of the observed natural world and that without an *observed* world, it is very difficult -if not impossible- to make definitive scientific claims. The onset of this revolution was, first, the discovery of the recession of distant galaxies in the 1920's, and later on the measurement in the 60's of a uniform cosmic microwave background radiation. The realization that the Universe is dynamical, and that the microwave radiation is a relic from a primordial era of its evolution, were the clues that finally converted cosmology into a scientific discipline.

These transformations were possible not only by the advent of new technologies which made observations possible, but also because the necessary mathematical tools to describe spacetime and its internal constituents were at hand. The advent of General Relativity in the beginning of the 20th century (exactly 100 years ago when writing this introduction) made it possible to make definite predictions which could finally be under the scrutiny of data. This fortunate conjunction between the presence of data and a variety of well motivated models for the Universe eventually made it possible to arrive at what we call today the Standard Cosmological Model.

While these developments are undoubtedly tremendous steps towards an understanding of the Universe, the Standard Cosmological Model may well be considered just a parametric model of our ignorance. Indeed, we have little idea of what the physical origin

of many of its free parameters is. As it is, the main contributions to the energy density of our present Universe come from two unknowns forms of energy, dark energy and dark matter, that together sum up to 96% of the total present energy density. While dark matter may be embedded in rather minimal extensions of the Standard Model of particles, understanding the physical origin of dark energy (in particular its incredibly small value compared to the Planck scale) may well need yet another paradigmatical revolution. Furthermore, if the Universe is an evolving system we need to understand its initial conditions. Contrary to other areas of physics, we do not have the experimental privilege to *create* Universes, and study their subsequent evolution as a function of fixed initial conditions. We can however infer them from its present stage of evolution, and the likeliness or unlikeliness of the initial conditions is also a measure on how satisfactory our cosmological model is. As we will see later, we will have to deal with the fact that the initial conditions that result in our present observed Universe may not seem natural.

While we cannot replicate the evolution of the Universe in the laboratory, the Universe can in itself be understood as a major experiment in which extremely high energy processes have occurred. This is the “poor man’s laboratory” through which we can observe the spectrum of particles present at energies which are beyond any direct experimentation. We expect these observations to be essential for resolving the problems mentioned above, knowing that any resolution will be an important step forward in the construction of a theory able to reconcile all of the fundamental forces and particles into one single consistent picture.

The question of initial conditions, and the possibilities of accessing high energy states is going to be, in a very broad sense, the framework for this thesis.

1.1 The homogeneous and isotropic model of the Universe

The first step leading to our current cosmological model is the observation that at sufficiently large scales the Universe looks homogeneous and isotropic. This can be implemented in General Relativity while still allowing for a dynamical Universe, by describing spacetime with the so-called Friedmann-Lemaître-Roberston-Walker (FLRW) metric, given by¹:

$$ds^2 = -dt^2 + a(t)^2 \left(\frac{dr^2}{1 - \kappa r^2} + r^2 d\theta^2 + r^2 \sin^2 \theta d\phi^2 \right) . \quad (1.1)$$

In this model, κ is the curvature of the three-dimensional space, and $a(t)$ -called the scale factor- parametrizes the dynamics of the metric. On large scales, where local

¹As usual done in cosmology, we work in units in which the speed of light $c = 1$.

inhomogeneities induce small displacements and velocities compared to the background cosmic flow, the physical distance R between two observers is $R(t) = a(t)\chi$, where χ is defined as the *comoving* (or coordinate) distance. The comoving distance between these observers is constant², and then all the time dependence of their physical distance is set by the scale factor $a(t)$. In a flat metric ($\kappa = 0$) and for simplicity only considering radial separations, their comoving distance is simply $\chi = \Delta r$. As only $a(t)$ determines the evolution of large scale physical distances, a history of the Universe might be understood as a history of the scale factor $a(t)$.

The time dependence of the scale factor is intimately related to the constituents of the Universe. In particular, Einstein's equations couple the scale factor and its time derivative to the density and pressure of the different 'matter' constituents. For a single fluid with pressure p and density ρ , the relevant equations are:³

$$H^2 \equiv \frac{\dot{a}(t)^2}{a^2} = \frac{\rho}{3} - \frac{\kappa}{a^2}, \quad (1.2)$$

$$\dot{\rho} + 3\frac{\dot{a}(t)}{a}(\rho + p) = 0, \quad (1.3)$$

where a dot represents a derivative with respect to cosmic time. The first equation is known as the Friedmann equation, while the latter is the continuity equation, ensuring energy conservation. We have further defined the Hubble parameter H , whose magnitude and evolution will set an important cosmological scale. The Friedmann equation (1.2) can be written in terms of the density parameter $\Omega \equiv \rho/\rho_c$ (or equivalently the curvature density parameter $\Omega_\kappa \equiv 1 - \Omega$), where $\rho_c \equiv 3H^2$ is known as the critical density, as

$$1 - \Omega = \Omega_\kappa \quad (1.4)$$

$$= -\frac{\kappa}{(aH)^2}. \quad (1.5)$$

The density parameter Ω determines whether the Universe is closed ($\Omega > 1$), flat ($\Omega = 1$) or open ($\Omega < 1$).

Additionally, from equations (1.2) and (1.3) we can derive an equation for the acceleration of the scale factor, which will later prove important:

$$\frac{\ddot{a}}{a} = -\frac{\rho}{6}(1 + 3w). \quad (1.6)$$

Here we have further introduced the equation of state parameter w which links the pressure to the density of a perfect fluid, as $p = w\rho$. Each different constituent of the

²Observers moving with the background cosmic flow are also called comoving observers

³Throughout all this thesis we work in units in which the reduced Planck mass $m_{\text{pl}} = M_{\text{pl}}/\sqrt{8\pi} \equiv 1$. In units in which $c = \hbar = 1$, the Planck mass is given by $M_{\text{pl}}^2 = G^{-1}$, where G is the gravitational constant.

Universe has a different equation of state. For example, normal matter is effectively pressureless (because of its small velocity compared to speed of light), so it is described by an equation of state parameter $w = 0$. Radiation instead is described by $w = 1/3$. An element that does not dilute as the Universe expand, i.e. that has a constant energy density, satisfies $w = -1$. This is the cosmological constant, and its value for the energy density is usually called Λ , i.e. $\rho_{c.c.} = \Lambda$.

The first observation that pointed towards a dynamical history of the scale factor $a(t)$ was the observation of the recession of distant galaxies⁴. Distant galaxies recede from each other at a velocity v that is proportional to their distance d . This is the famous Hubble law:

$$v = H_0 d . \tag{1.7}$$

The factor of proportionality H_0 is the present expansion rate, and its value is constrained with percent level precision by present cosmological data. The Hubble law has striking consequences. If galaxies are moving away from each other, it immediately follows that galaxies were closer as we go back in time. As can be deduced from eq. (1.6), if the Universe is filled with normal matter during all its evolution ($w > 0$) this process is never reversed. Using the known abundances of the different elements that contribute to the total energy density of the Universe, we can arrive at the conclusion that our observable Universe was contracted to a spacetime singularity 13.8 Gyr ago. In reality, however, we have no clue as to whether the Universe is infinitely old or not: neither the equations of General Relativity nor the matter content of the Standard Model of particles should be extrapolated back to the singularity. In particular, unknowns forms of energy may emerge, and a quantum theory of gravity would be needed. This will not be an impediment for loosely setting the starting time of the cosmic clock at the *would be* singularity, having in mind that we should not necessarily attribute to it any deep physical meaning.

In an expanding Universe, as we go back in time the same amount of matter was circumscribed to a smaller volume. This means that the energy density, and therefore the overall *temperature* of the Universe were higher. For example, far enough in the past, the energy density would have been so high that the common building blocks of our present Universe, like stars and galaxies, could not exist. As temperature is proportional to some (negative) power of the scale factor, a *thermal* history of the Universe can be derived. This is very useful since many important physical processes depend on temperature (for a detailed account, see [4]). In particular, below certain critical temperatures gauge symmetries can be spontaneously broken and phase transitions occur,

⁴While usually attributed to Hubble in 1929 [1], already in 1927 Lemaître was able to *derive* the linear relation between velocity and distance from General Relativity, and test it against data [2]. For an historical account on this discovery, see e.g. [3].

as for the electroweak and quantum chromodynamics sectors of the Standard Model of particles. Other processes like particle and antiparticle annihilation also depend on temperature (in this case, whether it is below or above the particles' rest mass), as well as the interaction rates between different particles. All of these elements make the thermal history of the Universe a very peculiar process. Considering the fundamental particles and their interactions, it was shown very early [5] that a Hot Big Bang scenario predicts the creation of light atomic elements. This is the subject of Big Bang nucleosynthesis (or BBN), and its predictions for the relative abundances of the primordial elements (from H to Li⁷) is one of the most famous and -relatively- well tested predictions of the Hot Big Bang model.

We can begin a (very) brief thermal history of the Universe 1 sec after the “singularity”, when the temperature was about 10^{10} K: back then the energy density of the Universe was dominated by a plasma consisting of electrons, protons, neutrons and photons, all of them in thermal equilibrium. As Thomson scattering between photons and electrons was very efficient, this plasma was homogeneous and opaque (in the sense that photons could not free stream for long distances). On the other hand species like neutrinos and dark matter, having smaller cross sections, were decoupled from the plasma. At a temperature of 10^9 K, or 100 s after the singularity, some of the protons and neutrons bound in the form of atomic nuclei, in particular He⁴. Eventually, when the temperature dropped to 10^3 K, 380.000 years after the singularity, atomic nuclei could bind with electrons, forming the first atoms. This process is called recombination. Soon after, with a reduced density of free electrons, Thomson scattering became inefficient: photons could travel freely, and the Universe became *transparent*. This is known as the time of decoupling, and it is the furthest event we can directly observe with photons. The photons that we observe today that scattered for the last time at recombination emerged from a thin shell that we call the surface of last scattering. After decoupling, gravity became the major driving force, making atomic clouds -mostly composed by hydrogen- collapse to form the first stars and galaxies.

At the time of decoupling the plasma was at a finite and homogeneous temperature, and then the photons that emerged from this plasma, having travelled without further interactions, should be at a finite and homogeneous temperature today. This temperature (T_0) is directly related to the temperature at decoupling (T_{dec}) by noticing that temperature drops as a^{-1} , such that $T_0 = T_{\text{dec}} a_{\text{dec}} / a_0$, where a_{dec} and a_0 are the scale factor today and at decoupling respectively. These arguments led Alpher and Herman [6] to predict that if the Universe has been expanding there should be, today, a uniform bath of radiation at a temperature of ~ 5 K. This is the famous Cosmic Microwave Background (CMB).

The observational milestone that strongly supported this Big-Bang picture (as was pejoratively named by one of its firmer detractors), was the discovery of the CMB. In 1965, Penzias and Wilson [7, 8] measured a constant and isotropic radiation, consistent with a CMB blackbody spectrum at a temperature $T_0 = 3.5 \pm 1$ K. In 1993, the COBE satellite [9] determined that the CMB indeed follows a blackbody spectrum by measuring the intensity of the signal at different wavelengths. Its temperature was measured to be $T_0 = 2.7$ K, which is consistent with the first measurement of Penzias and Wilson. Crucially, the same satellite also measured the presence of small inhomogeneities (of the order of 10^{-5} with respect to the homogeneous 2.7 K component), when comparing the temperature at different directions in the sky [10].

The discovery by COBE of these small inhomogeneities is, with the discovery of the late time accelerated expansion of the Universe, among the major recent breakthroughs in observational Cosmology. The importance of the primordial inhomogeneities is two-fold. First, they are nothing less than the initial density perturbations from which galaxies and clusters of galaxies formed. To understand the process of structure formation necessarily implies that we need to know how to characterize its initial conditions. Secondly, the initial conditions for large scale structure formation are also the final state of an earlier stage of evolution. In this sense, they are a portal to access the Universe at times way before the generation of the CMB map. These are the reasons why understanding the initial inhomogeneities is one of the major goals of modern Cosmology, and why so much effort has been made in order to measure these inhomogeneities with better precision and at a wider range of scales. The latest space mission (able to cover the full sky) designed for this purpose was the Planck satellite [11]. In figure (1.1) we show the CMB map of inhomogeneities, as measured by this experiment. By computing n -point correlation functions from this map it is possible to extract quantitative statistical information. The power spectrum, which measures the correlation in temperature between two directions separated by an angle θ in the sky, is shown in figure (1.2)

1.1.1 The contents of the Universe

Observations of the CMB have made it possible to construct a minimal model with 6 free parameters, able to consistently describe the main features of our observed Universe. In this model the Universe has been expanding for 13.8 Gyr until today. It is composed by matter, radiation, neutrinos and a cosmological constant (denoted by Λ , which as we explained above, is a form of energy that does not dilute as the Universe expands). Matter itself is composed by atoms and their internal constituents, and an elusive form of matter called dark matter. The presence of dark matter has only been inferred by its gravitational effects, so little is known about its internal constitution (for example, on

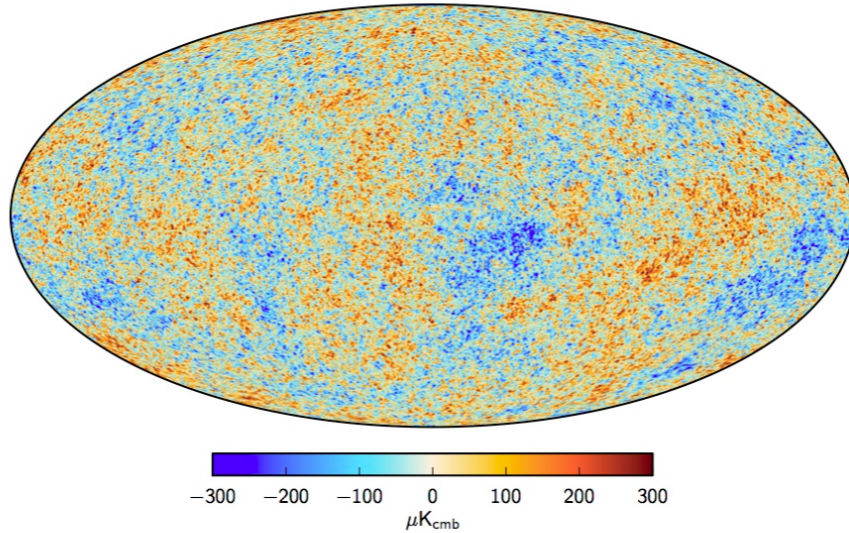


FIGURE 1.1: CMB intensity map. Colours represent inhomogeneities of the order of 10^{-5} with respect to the homogeneous 2.7 K component.

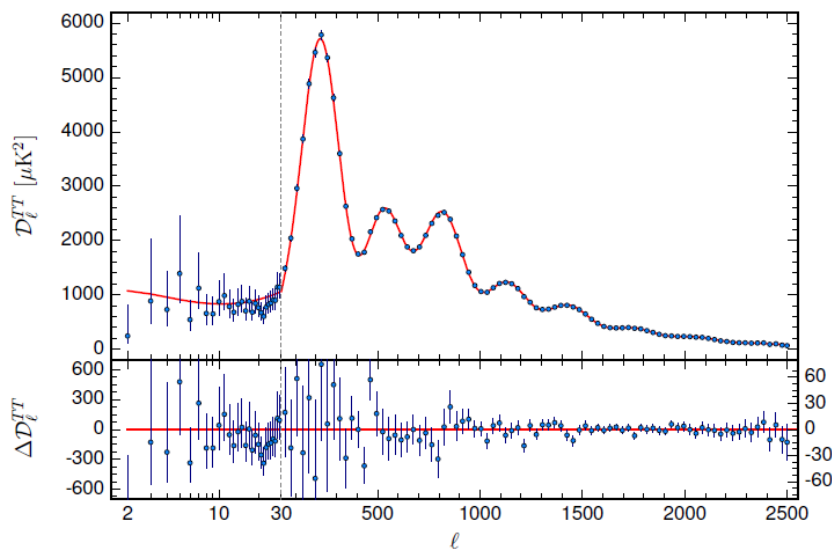


FIGURE 1.2: Power spectrum of the CMB temperature map. The horizontal axis represents the angular scale $l \sim 180/\theta$ (a logarithmic scale is used in the interval $l = [2, 49]$), while the vertical axis is the intensity of the power spectrum. The first peak is located at $l \sim 220$. The red curve is the theoretical prediction of the best fit Λ CDM model (to be explained in the following section), while blue dots are the data points taken from the map in figure 1.1. Figure taken from [12].

whether is charged under a certain gauge group). The present conclusion is that most of the matter should be composed of cold -slowly moving- dark matter (CDM). The so-called normal hierarchy is assumed for neutrinos (with an effective number $N_{\text{eff}} = 3.046$, and well approximated by a single massive neutrino), and the radiation density can be derived from the homogeneous component of the CMB temperature. As the energy density of the present Universe is dominated both by a cosmological constant and cold

dark matter, this model is called Λ CDM⁵. The Universe is just a box in which these elements (and the size of the box) evolve according to their relative abundance and initial conditions. The minimal cosmological model assumes the Universe is flat ($\kappa = 0$), and its 6 parameters are:

- Ω_b : Fraction of so-called baryonic matter. It represents atoms and their internal constituents (so, in this definition, leptons also make part of baryonic matter).
- Ω_c : Fraction of cold dark matter. This is a type of matter that has, if any at all, very suppressed interactions with Standard Model particles. We can infer its presence only by its gravitational effect.
- τ : Optical depth to the epoch of reionization. When the first stars formed, new ionizing photons were produced, so that free electrons were again present to eventually interact with CMB photons. Roughly speaking τ measures the strength of that secondary interaction (or, equivalently, the number of additional scattering events).
- θ_{MC} : Approximation to the angular scale of the sound horizon, defined as the sound horizon at the surface of last scattering divided by the distance to the surface of last scattering. The sound horizon is the distance sound waves of the photon-baryon fluid could have travel in the time up to recombination. θ_{MC} roughly corresponds to the angular size of the first peak in the two-point correlation function that can be seen in fig. 1.2.
- A_S : In order for inhomogeneities to be seen in the CMB, an initial amplitude for these inhomogeneities should have been present. A_S is the amplitude of the initial two-point function (to be defined more precisely later) at a given scale.
- n_s : The amplitude of the initial fluctuations may depend on the scale. The quantity n_s is the spectral dependence of the two-point function, when parametrized as a power law ($n_s = 1$ being scale invariance).

Given these parameters, it is possible to reproduce to a great accuracy the CMB data as well as the abundances of the primordial elements. We show in table 1.1 their best fit values as deduced from the Planck 2015 analysis [12]. Apart from the first six parameters, we have added the values of three additional parameters that, while they are not part of the baseline cosmological model, are very important for the subject of this thesis.

⁵It is very important to stress that, *within this model*, the universe is dominated by these constituents. Different cosmologies may lead to very different values for different parameters. The Λ CDM model continues to be preferred since it has the best compromise between number of parameters and goodness of fit to the data.

Parameter	Best fit value at 68% limits
$\Omega_b h^2$	0.02230 ± 0.00014
$\Omega_c h^2$	0.1188 ± 0.0010
$100\theta_{MC}$	1.04093 ± 0.00030
τ	0.066 ± 0.012
$\ln(10^{10} A_S)$	3.064 ± 0.023
n_s	0.9667 ± 0.0040
Ω_k	0.000 ± 0.005
r	< 0.09
β_{iso}	< 0.03

TABLE 1.1: Best fit parameters of the 6 parameter Λ CDM model. The factor h appearing in front of $\Omega_{c,b}$ denotes the current expansion rate, as a fraction of $100 \text{ km s}^{-1} \text{ Mpc}^{-1}$. The last three parameters are important extensions to the 6 parameter Λ CDM model.

These are the tensor-to-scalar ratio, r , which is the ratio of the initial tensor to scalar perturbations, the curvature density of the universe Ω_k (defined in 1.4) and β_{iso} , the initial isocurvature fraction. We will later define them more precisely (in particular r and β_{iso}), and their importance will become more transparent as we go further on.

In order to solve any dynamical system it is important to set the initial conditions, so we should not be surprised if we need some parameters to describe them. We should be surprised, however, if the initial conditions consistent with the observations are a very special subset of all the possible initial conditions. This is exactly what happens in the base Λ CDM cosmology. This issue is present at different levels:

- The first observation that should call our attention is the fact that the CMB can be described by a single temperature, i.e., that the CMB is a bath of radiation, of the size of the observable Universe, in thermal equilibrium. This would not be an issue if there were the means of reaching thermal equilibrium in the very early Universe, which would demand the very different patches of the Universe to be in causal contact and with large interactions among its constituents. The size of a causal patch is known as the particle horizon, and it is given by the distance light could travel from an initial time t_0 to any given time t_* . The comoving particle horizon at $t = t_*$ is given by

$$h = \int_{t_0}^{t_*} \frac{dt}{a(t)} = \int_{a_{ini}}^{a_*} \frac{d \ln a}{aH} . \quad (1.8)$$

Taking $t_0 = 0$, t_* to be the time of decoupling and assuming the scale factor is determined by the Λ CDM model, one finds that only patches separated by less than 2° in the sky could have been in causal contact. This means that patches of the CMB separated by more than 2° were never in their history in causal contact, and could not by any thermodynamical mechanism reach the very same temperature. This apparent acausal correlation is also seen at the level of the perturbations, since a non-zero correlation for the two-point function is also measured on such large scales (see fig 1.2). This is known as the horizon problem.

- Another issue concerns the observation that the Universe is flat to an incredible accuracy. If, today, the energy density associated with the curvature is measured to be negligible, it means that the curvature energy density was exponentially smaller in the past. This can be seen by considering how the curvature parameter, Ω_κ , evolves with time. From equation (1.5) this is given by

$$\frac{d\Omega_\kappa}{d \log a} = \Omega_\kappa(1 - \Omega_\kappa)(1 + 3w) . \quad (1.9)$$

Unless the Universe is exactly flat ($\Omega_\kappa = 0$), the curvature density parameter depends on time. Moreover, for $(1 + 3w) > 0$, which is the case in a Universe dominated by radiation and/or matter, small departures from flatness are said to be *unstable* since any small initial curvature density Ω_κ (positive or negative) will grow as the size of the Universe grows. Today we have an upper bound $|\Omega_k| < 10^{-2}$ which means that $|\Omega_k| < 10^{-18}$ at BBN era, and exponentially smaller as we go back in time. As there is no *a priori* reason in General Relativity to choose $\kappa = 0$ among all the possibilities, we may be puzzled by the fact that such value was initially tuned to zero to such great accuracy.

1.2 Inflation

The theory of inflation was proposed as a solution to these problems, and it can be understood as a theory for the initial conditions of the Λ CDM cosmology [13–17]. Its real achievement is that it pushes back the problem of initial conditions to $\sim 10^{-30}$ s after the singularity⁶. It is not difficult to see that both the horizon and curvature problem are linked to the fact that the comoving Hubble radius, defined as $r_H = (1/aH)$, increases as the scale factor increases. Then, one solution to the problem of the initial conditions is to impose that at some earlier period the comoving Hubble radius decreased

⁶Inflation also needs initial conditions which may or not be considered natural. Whether they are or not or whether they should be at all is of course a very important question.

with time. This would in turn mean the Universe was accelerating, as

$$\frac{d}{dt} \frac{1}{aH} < 0 \quad \rightarrow \quad \ddot{a} > 0 . \quad (1.10)$$

Inflation is just a period in which these conditions are fulfilled. This simple behaviour naturally generates the initial conditions for the primordial plasma: On the one hand, in an inflationary period the integrand in (1.8) rapidly diverges in the past, making the particle horizon substantially bigger as we go back in time. This can make all the observable Universe to have been in causal contact. Additionally, the curvature density converges at late times to zero as can directly be seen from its definition. A successful solution of these problems needs at least 60 e-folds of inflation, by which we mean that the ratio of the scale factor at the beginning and at the end of inflation is $\sim e^{60}$. As we will see shortly, this very singular causal structure, i.e. a shrinking Hubble radius, will also provide an elegant mechanism to generate the initial perturbations for the matter distribution in the Universe.

From equation (1.6) it is clear that an exotic type of matter should be dominating the energy density of the Universe such that an accelerated expansion can take place. Neither radiation nor baryons nor CDM can achieve such an expansion, since $w_{\gamma,b} > -1/3$. One possibility, though, is that the energy density is in the form of a cosmological constant, since $w_{\Lambda} = -1$. Ending inflation would demand tunneling to a different vacuum with a smaller cosmological constant, as for example, the one we measure today. While apparently satisfactory, this first order phase transition would cause bubble nucleation, spoiling the isotropy and/or the spectrum of the primordial perturbations [18]. These problems can be avoided by considering instead a scalar field classically rolling down in a potential. If the potential is flat enough, the scalar field would *resemble* a cosmological constant and produce an accelerated expansion. However, and contrary to the first scenario, in this case inflation can end smoothly if, after the required e-folds of inflation, the potential becomes steep. To see how this could happen, consider a scalar field $\phi(\mathbf{x}, t)$, canonically coupled to gravity. It is then described by an action of the form

$$S = \int d^4x \sqrt{-g} \left[\frac{1}{2} R - \frac{1}{2} g^{\mu\nu} \partial_{\mu} \phi \partial_{\nu} \phi - V(\phi) \right] . \quad (1.11)$$

Here $g_{\mu\nu}$ is the spacetime metric and R and g are respectively the Ricci scalar and the determinant of this metric. We have further introduced $\partial_{\mu} \phi \equiv \partial \phi / \partial x^{\mu}$, where μ ranges from zero (time) to three (space). In a FLRW metric the equation of motion for the homogeneous component of the field, $\phi = \phi(t)$, is given by

$$\ddot{\phi} + 3H\dot{\phi} + V_{,\phi} = 0 , \quad (1.12)$$

where $V_{,\phi} = dV/d\phi$. The Hubble parameter H is determined by the Friedmann equation (1.2), which in this case reads

$$3H^2 = \frac{1}{2}\dot{\phi}^2 + V(\phi) . \quad (1.13)$$

Equations (1.12) and (1.13) determine the joint evolution of the background component of the scalar field $\phi(t)$ and the scale factor $a(t)$. A shrinking Hubble radius is equivalent to demanding that the Hubble parameter varies slowly. Indeed, it is easy to show that

$$\frac{d}{dt} \frac{1}{aH} < 0 \quad \rightarrow \quad \epsilon \equiv \frac{\dot{H}}{H^2} = \frac{\dot{\phi}^2}{H^2} < 1 . \quad (1.14)$$

A slow variation of H ($\epsilon \ll 1$) implies then that the kinetic energy is a small fraction of the total energy, or equivalently, that the dynamics are dominated by the potential energy (which is changing slowly). In this case the scale factor grows almost exponentially

$$3H^2 \sim V(\phi) \quad \rightarrow \quad a(t) = e^{H(t_{ini}-t)} . \quad (1.15)$$

The requirement of having at least 60 e-folds of inflation demands that the condition $\epsilon \ll 1$ is maintained for a sufficient amount of time. The proper dimensionless variable quantifying the rate of change of ϵ is known as η , as is defined as

$$\eta \equiv \frac{\dot{\epsilon}}{\epsilon H} . \quad (1.16)$$

Then, both ϵ and η , the so-called slow-roll parameters, must satisfy the following conditions:

$$\epsilon \ll 1 \quad \text{and} \quad |\eta| \ll 1 . \quad (1.17)$$

Indeed, we can define an entire hierarchy of slow-roll parameters $\epsilon_{n+1} \equiv \dot{\epsilon}_n / (H\epsilon_n)$, where $\epsilon_1 = \epsilon$ and $\epsilon_2 = \eta$. For smooth potentials it is in general a good approximation to treat ϵ and η as constants, which is equivalent to neglecting all the tower of slow-roll parameters with $n > 2$. This is not however a necessary condition for having an overall exponential expansion since higher order slow-roll parameters may become large for a very small amount of time (i.e. $\epsilon < 1$ may still be satisfied while, locally in time, $|\eta| > 1$). This regime will have important observable consequences that we will address in Chapter 3. For the moment, we stick to the simple case where the slow-roll conditions (1.17) are satisfied all along the inflaton trajectory and the higher order slow-roll parameters are negligible.

In order to know whether a given potential $V(\phi)$ can sustain inflation or not, we may write the slow-roll parameters as a function of V . At leading order in slow-roll (i.e. for

$\epsilon, |\eta| \ll 1$), ϵ and η are given by

$$\epsilon = \frac{1}{2} \left(\frac{V_{\phi}}{V} \right)^2 \quad \text{and} \quad \eta = -2 \frac{V_{\phi\phi}}{V} + 2 \left(\frac{V_{\phi}}{V} \right)^2 . \quad (1.18)$$

We finish this section by saying that we may have considered different definitions for η . For example, at leading order in slow-roll it is also true that $|V_{\phi\phi}/V| \ll 1$. Furthermore, in this regime $\epsilon - \ddot{\phi}/H\dot{\phi} - V_{\phi\phi}/V = 0$, such that it is also true that $|\ddot{\phi}/H\dot{\phi}| \ll 1$. Then, as is usually found in the literature, one may rather impose that

$$\eta_V \equiv \frac{V_{\phi\phi}}{V} \ll 1 \quad \text{or} \quad \eta_{\phi} \equiv \frac{\ddot{\phi}}{H\dot{\phi}} \ll 1 . \quad (1.19)$$

The different definitions of η are related through the following equations:

$$\eta = -2\eta_V + 4\epsilon \quad \text{and} \quad \eta_V = \epsilon - 2\eta_{\phi} . \quad (1.20)$$

In the next section, we study how do perturbations evolve on top of the inflationary background.

1.2.1 Primordial perturbations

Undoubtedly, the big success of inflation is that it provides a mechanism for generating the primordial density fluctuations from which the structure of the Universe was created [19] (for a pedagogical review, see [20]). In this model, the primordial perturbations are nothing more than a combination of the quantum fluctuations of the scalar field and spacetime metric⁷. The peculiar causal structure of an accelerating Universe is responsible for converting these microscopic quantum fluctuations into classical and macroscopic density perturbations.

We begin by writing the most general perturbation of the inflaton field and metric. One possible parametrization is the following:

$$\phi(t) \rightarrow \phi(t) + \delta\phi(x, t) , \quad (1.21)$$

$$g_{\mu\nu} \rightarrow (-1 + 2\Phi)dt^2 + 2a(t)B_i dx^i + a(t)^2 [(1 - 2\Psi)\delta_{ij} + E_{ij}] dx^i dx^j . \quad (1.22)$$

where Φ , B_i , Ψ and E_{ij} are functions of both space and time. Perturbations of the metric can be classified according to their transformation properties under spatial rotations. In particular, they can be decomposed into scalar, vector and tensor modes, and it

⁷As we will argue later, it is not even important that inflation is driven by a scalar field. The only important information is that the Universe undergoes a quasi de Sitter expansion.

can be shown that these different components are decoupled at the linear level. In principle, we can directly expand the action (1.11) to second order using the expansions (1.21) and (1.22) and treat every mode independently and up to second order. We will however find that the equations of motion are overconstrained. To see this, let us note that the perturbations defined in (1.21) and (1.22) are not invariant under a generic coordinate transformation, which means that, taken individually, they are not physical. For example, by redefining time as $t \rightarrow \tilde{t} = t + \xi^0$, the perturbation to the scalar field becomes

$$\delta\phi(t, x) \rightarrow \delta\phi(t, x) + \xi^0 \dot{\delta\phi}(t, x) . \quad (1.23)$$

If we choose ξ^0 such that $\xi^0 = -\delta\phi(t, x)/\dot{\delta\phi}(t, x)$, then in the new coordinate system $\delta\phi(t, x) = 0$. This means that the perturbation to the scalar field is not a physical quantity in itself, since we can always choose a coordinate system in which it vanishes. However, we do not have the freedom to choose one single coordinate transformation in which all the perturbations vanish simultaneously. This is because the most general coordinate transformation is parametrized by only three degrees of freedom, two scalars and one vector, and that the perturbations in (1.21) and (1.22) are parametrized by 5 scalar, 2 vector and 1 tensor degrees of freedom. Thus, we do not have sufficient functions in our coordinate transformation to make all the perturbations in the metric and scalar field to disappear, and we are left with only 3 scalar, 1 vector and 1 tensor degrees of freedom (which may be later reduced by the equations of motion). There are two ways of dealing with the ambiguity of choosing the coordinate system. The first is to fix it from the beginning, which is known as *fixing a gauge*. For example, the coordinate system defined previously, in which the inflaton's perturbation vanishes, is called the *comoving gauge*⁸. There are indeed infinite ways of fixing a gauge, but in general there will be more appropriate ones depending on which calculation one wants to perform. The second possibility is to work with gauge invariant variables, which are linear combinations of the perturbation in (1.21) and (1.22) that do not transform under coordinate transformations. There is also an infinity of gauge invariant variables but some of them are more useful than others. In particular we will work with the so-called comoving curvature perturbation \mathcal{R} , defined as

$$\mathcal{R} \equiv \Psi + H \frac{\delta\phi}{\dot{\phi}} . \quad (1.24)$$

This variable is called the comoving curvature perturbation because in the comoving gauge (where $\delta\phi = 0$), it reduces to the spatial curvature of the metric. As we will see later in this section, this variable becomes constant in time for modes whose wavelength

⁸Formally, the comoving gauge is defined as the gauge in which the perturbation to the stress-energy tensor δT_{0i} vanishes. In slow-roll inflation, this is equivalent to having $\delta\phi = 0$.

exceed the Hubble radius, a crucial behavior that allows us to connect the quantum perturbations during inflation with the perturbations of the CMB.

In general, any field theory may be classified by its predictions for the n -point correlation functions of whatever observables the theory possesses. One of the predictions of the canonical single field models of inflation (as the one we have considered) is that the statistics of the curvature perturbations are nearly gaussian. Indeed, for single-field and canonical models of inflation, the smallness of the curvature perturbations and the flatness of the potential ensure that interactions other than quadratic in the field variables are highly suppressed. This means that the only relevant n -point correlation function is the two-point function (in an exactly gaussian theory all the n -point correlation functions are either zero -for n odd-, or a function of the two-point function -for n even-). We start then with the action for the comoving curvature perturbation at second order, which is given by

$$S_2 = \int d^4x a^3 \epsilon \left\{ \dot{\mathcal{R}}^2 - \frac{1}{a^2} (\nabla \mathcal{R})^2 \right\} , \quad (1.25)$$

At this point we may introduce an important time re-parametrization, known as conformal time and defined as $d\tau = adt$. In this new coordinate system, the canonical perturbation v is given by

$$v \equiv z\mathcal{R} \quad \text{with} \quad z^2 = 2a^2\epsilon, \quad (1.26)$$

where the scale factor, at first order in slow-roll, takes the following form:

$$a(\tau) = -\frac{1}{H\tau}(1 + \epsilon) . \quad (1.27)$$

Let us note that τ takes negative values, from $-\infty$ in the far past to 0 at the end of inflation. In order to find a solution to the equation of motion we expand the field in Fourier modes $v(\mathbf{x}, \tau)$ as

$$v(\mathbf{x}, \tau) = \int d^3\mathbf{k} v_{\mathbf{k}}(\tau) e^{i\mathbf{k}\cdot\mathbf{x}} . \quad (1.28)$$

The mode function $v_{\mathbf{k}}(\tau)$ satisfies the Mukhanov-Sasaki equation [21, 22]:

$$v_{\mathbf{k}}'' + \left(k^2 - \frac{z''}{z} \right) v_{\mathbf{k}} = 0 , \quad (1.29)$$

where $k^2 = \mathbf{k}\cdot\mathbf{k}$, and prime denotes derivatives with respect to conformal time. There are two independent solutions of the previous equation, only dependent on k , so we might further expand $v_{\mathbf{k}}(=v_k)$ and write

$$v(\mathbf{x}, \tau) = \int d^3\mathbf{k} \left[a_{\mathbf{k}}^- v_k(\tau) e^{i\mathbf{k}\cdot\mathbf{x}} + a_{\mathbf{k}}^{\dagger} v_k^*(\tau) e^{-i\mathbf{k}\cdot\mathbf{x}} \right] , \quad (1.30)$$

where $(a_{\mathbf{k}}^-)^* = a_{\mathbf{k}}^\dagger$ so that the solution $v(\mathbf{x}, \tau)$ is real. The Mukhanov-Sasaki equation (1.29) has an exact solution for constant ϵ and η and the integration constants can be found by imposing boundary conditions and quantum commutation relations to the mode functions. First of all, we need to promote v_k to an operator and impose the quantum commutation relations to \hat{v}_k and its conjugate momentum $\pi = v'$. This implies identifying $a_{\mathbf{k}}^-$ and $a_{\mathbf{k}}^\dagger$ as the usual creation and annihilation operators. Then, boundary conditions can be imposed in the far past ($k\tau \gg 1$), by assuming that every mode k begin its evolution in the vacuum state: high frequency modes do not feel the curvature of spacetime, and the expectation value of the Hamiltonian can be unambiguously minimized as in flat space. This is known as the Bunch-Davies vacuum [23]. Under these prescriptions, and in the most simple case of an exact de Sitter expansion, the full solution to equation (1.29) is given by:

$$v_k(\tau) = \frac{1}{\sqrt{2k}} e^{-ik\tau} \left(1 - \frac{i}{k\tau} \right). \quad (1.31)$$

As we have shown, during inflation modes go from the ultraviolet (or subhorizon) to the infrared (or superhorizon) regime⁹. We might then trace the history of a given mode v_k by analysing the different asymptotic regimes of the solution (1.31). In the far past ($|k\tau| \gg 1$), the solution to the mode function is dominated by the oscillating part $\exp(-ik\tau)$. This is nothing more than the result of imposing the Bunch-Davies vacuum prescription. As inflation proceeds, a mode initially in the short wavelength regime eventually crosses the horizon and becomes superhorizon ($|k\tau| \ll 1$). Then, the dominant contribution to the solution (??) is the divergent factor $\propto 1/\tau$. This means that the curvature perturbation \mathcal{R}_k , related to v_k through eq. (1.26), becomes constant¹⁰. When inflation ends the Hubble radius starts to grow, and this superhorizon mode k eventually re-enters inside the horizon. When it does, it will start to oscillate with an initial amplitude that was fixed when that mode crossed the Hubble radius during inflation. This is precisely the way in which perturbations generated during inflation are connected with the initial conditions for the photon-baryon plasma.

Let us note that in this description we have implicitly assumed that a superhorizon mode k remains constant after inflation ends (which we have derived *only* for the case in which there is a de Sitter background expansion). This is an important assumption, since between inflation and the decoupling of the CMB photons there are many unknown processes which may in principle invalidate the simple predictions of our calculations. For

⁹As usually done in the literature, we will say that a mode with wavelength bigger than the Hubble radius is a superhorizon mode ($k > aH$), while a mode with wavelength smaller than the Hubble radius is a subhorizon mode ($k < aH$). This terminology is not accurate since the Hubble radius is neither a particle nor an event horizon.

¹⁰In the long wavelength regime the dominant contribution to v_k comes from its imaginary part. The real part is constant for v_k which means that it is a decaying perturbation mode for \mathcal{R}_k .

example, the energy density of the inflaton has to be transferred to matter and radiation, a process -called reheating- which we know very little about. A superhorizon evolution of the curvature perturbations would mean that we need to follow the evolution of those modes through these mysterious ages, which would in practice spoil the predictability of inflation. Importantly, it is possible to show that superhorizon perturbations remain constant independently of the background FLRW cosmology, provided the perturbations are adiabatic [24]. By adiabatic perturbations we mean that for a fluid composed of different elements (and in the case in which the total stress-energy tensor is the sum of the individual stress-energy tensors), all the individual components of the fluid (labelled i) are perturbed satisfying

$$\frac{\delta\rho_i}{\dot{\rho}_i} = \frac{\delta p_i}{\dot{p}_i} = \frac{\delta\rho_t}{\dot{\rho}_t} = \frac{\delta p_t}{\dot{p}_t}, \quad (1.32)$$

where t refers to the total energy density and pressure. For adiabatic perturbations, the local perturbation to the energy density (pressure) corresponds to a time shift of the background energy density (pressure). Single field models of inflation only produce this type of perturbations, and then the conservation of superhorizon modes is guaranteed.

The two-point quantum correlation function, evaluated in the vacuum, allows us to define the power spectrum $\mathcal{P}_{\mathcal{R}}$ as

$$\langle \mathcal{R}_{\mathbf{k}} \mathcal{R}_{\mathbf{k}'} \rangle \equiv (2\pi)^3 \delta^3(\mathbf{k} + \mathbf{k}') \mathcal{P}_{\mathcal{R}}(k). \quad (1.33)$$

Using the solution (1.31) and (1.26) in the long wavelength limit, we find

$$\mathcal{P}_{\mathcal{R}}(k) = \frac{1}{8\pi^2} \frac{H^2}{\epsilon}. \quad (1.34)$$

The amplitude of the power spectrum at a given scale k depends on the value of H and ϵ at the moment in which \mathcal{R}_k became frozen. As every mode k crosses the Hubble radius and becomes constant at a different moment (thus, for slightly different values of H and ϵ) the amplitude of the power spectrum has a mild scale-dependence. This can be parametrized by the spectral index n_s , giving

$$\begin{aligned} n_s &\equiv \frac{d \ln \mathcal{P}_{\mathcal{R}}}{d \ln k} \\ &= 1 - 2\epsilon - \eta. \end{aligned} \quad (1.35)$$

Higher order derivatives of the power spectrum will depend on higher order derivatives of the slow-roll parameters, which are suppressed in the simple case considered here. Considering only the first derivative of the power spectrum is equivalent to assuming

that it is parametrized by a power law of the form

$$\mathcal{P}_{\mathcal{R}} = A_S \left(\frac{k}{k_*} \right)^{n_s - 1}, \quad (1.36)$$

in which $A_S = H^2/(8\pi^2\epsilon)$, evaluated at an arbitrary scale $k = k_*$. As we will see in the following chapters, if the slow-roll parameters are allowed to become large for some small amount of time during the inflationary trajectory (e.g. for the case of a very flat potential with a small and localized ‘bump’), higher derivatives of the power spectrum may become important and a power law expansion of the form (1.36) may not be the most adequate parametrization for the power spectrum.

Apart from scalar perturbations, the spacetime metric also has vector and tensor degrees of freedom. While the vector modes decay rapidly as the scale factor increases, tensor modes are also conserved after crossing the Hubble radius. Calculating their power spectrum is a simpler task since only the metric contributes to the total tensor perturbation. Their power spectrum is given by

$$\mathcal{P}_h = \frac{2H^2}{\pi^2}. \quad (1.37)$$

Then, we can define the tensor-to-scalar ratio, r , as the ratio between the tensor and the scalar power spectrum

$$r \equiv \frac{\mathcal{P}_h}{\mathcal{P}_{\mathcal{R}}} = 16\epsilon. \quad (1.38)$$

Before linking these predictions to the observation of the CMB, we will briefly discuss one simple extension of the model presented here. In the previous example the speed of sound c_s of the scalar curvature fluctuations was, in units of the speed of light, equal to one. This can be immediately deduced by noticing that the dispersion relation in the mode function equation (1.29) is, in the short wavelength regime, $\omega = k$. We can easily generalize the predictions above to the case in which the speed of sound c_s is a free parameter [25]. At the level of the action, a speed of sound can be introduced by generalizing (1.25) to be of the form

$$S_2 = \int d^4x a^3 \epsilon \left\{ \frac{\dot{\mathcal{R}}^2}{c_s^2} - \frac{1}{a^2} (\nabla \mathcal{R})^2 \right\}. \quad (1.39)$$

We can introduce a new variable s parametrizing the rate of change of c_s , given by

$$s \equiv \frac{\dot{c}_s}{c_s H}. \quad (1.40)$$

The Mukhanov-Sasaki equation now reads:

$$v_{\mathbf{k}}'' + \left(c_s^2 k^2 - \frac{z''}{z} \right) v_{\mathbf{k}} = 0 , \quad (1.41)$$

where this time $z = 2a^2 \epsilon c_s^{-2}$. In the limit in which the speed of sound changes slowly, i.e, $s \ll 1$, we can follow the same steps as previously in order to calculate the power spectrum and spectral index of the curvature perturbations, and we get

$$\mathcal{P}_{\mathcal{R}} = \frac{1}{8\pi^2} \frac{H^2}{c_s \epsilon} \quad \text{and} \quad n_s = 1 - 2\epsilon - \eta - s . \quad (1.42)$$

When calculating the power spectrum we must have in mind that curvature perturbations will now become constant when a mode k exists the *sound* horizon, i.e., at times satisfying $c_s k \gg aH$. For a subluminal speed of sound, this happens before the freezing of modes with $c_s = 1$. The tensor-to-scalar ratio is now¹¹

$$r = 16\epsilon c_s . \quad (1.43)$$

At this point, the motivation for considering inflation with a reduced speed sound might only seem phenomenological but, as we will see in the following chapters, reduced speeds of sound may be a *portal* to access very high energy degrees of freedom.

In order to confront theory with observations we need to evolve the initial theoretical power spectrum to a power spectrum for the CMB photons at the time of decoupling. The power spectrum of the comoving curvature perturbations determine the initial conditions for the perturbations of the photon-baryon plasma. If the perturbations are adiabatic, the initial density contrast, $\delta_i = \delta\rho_i/\rho$ for photons (γ), baryons (b), CDM (c) and neutrinos (ν) are related to the initial curvature perturbation (in the long wavelength limit) as

$$\delta_b = \delta_c = \frac{3}{4}\delta_\gamma = \frac{3}{4}\delta_\nu = \zeta . \quad (1.44)$$

Once we impose the initial conditions, the evolution of the plasma is given by a set of Boltzmann equations. The perturbations must be further projected onto the celestial sphere, since we actually measure different temperatures at different angles in the sky. The physical evolution and the geometrical projection of the initial inhomogeneities will transform the initial flat quantum spectrum into a series of temperature peaks. This process can be modelled numerically with the help of publicly available codes as CAMB [28] or CLASS [29]. The structure of the peaks has been measured to a great accuracy by a number of experiments, the last one being the Planck satellite

¹¹Contrary to curvature perturbations, the freeze-out time for tensor perturbations is not affected, as tensor modes (gravity waves) still travel at the speed of light. This difference in the time of freeze-out induces corrections to the tensor-to-scalar ratio which might be important if $c_s \ll 1$ [26, 27], but that we neglect in formula (1.43).

mission [11], which we already showed in figure 1.2. From these observations it is possible to determine the nature of the initial conditions, for example the amplitude A_S of the scalar fluctuations, the spectral index n_s and the tensor to scalar ratio r . The central values for A_S and n_s and constraints (for r) can be read from table 1.1. Every single field potential has a very precise prediction for these values, as can be seen explicitly from eqs. (1.18). The contour plot of n_s and r , together with several theoretical predictions, are shown in figure 1.3. The constraints are specified for a specific scale in the CMB, $k_* = 0.002 \text{ Mpc}^{-1}$ which may have exited the Hubble radius 50 or 60 e-folds before the end of inflation. The predictions for the models are then specified for this range of e-folds.

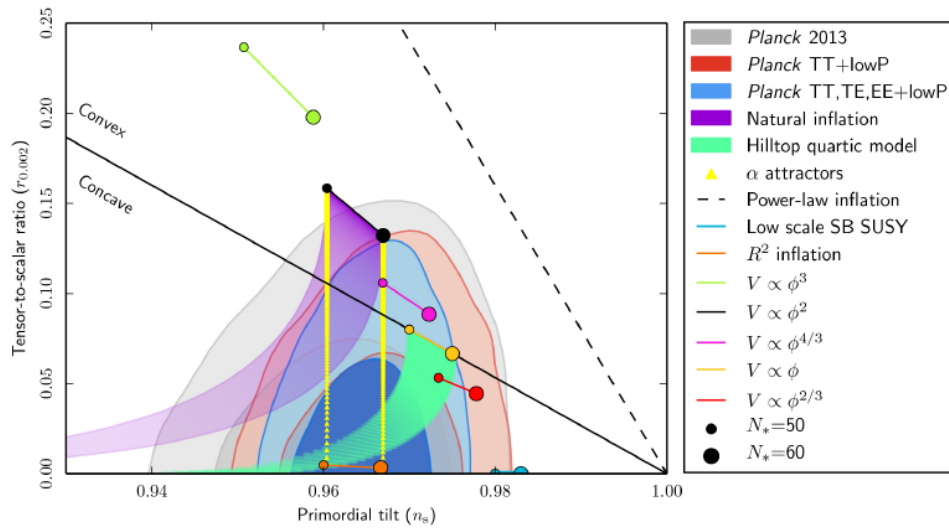


FIGURE 1.3: Marginalized joint 68% and 95% CL regions for n_s and r from Planck in combination with other data sets, compared to the theoretical predictions of selected inflationary models. From [30].

Among the theoretical predictions shown in figure 1.3, two of them are specially going to call our attention during this thesis. The first is the simplest inflationary model we can imagine, described by a quadratic potential (in black in fig. 1.3) [31]

$$V(\phi) = \frac{1}{2}m^2\phi^2 . \quad (1.45)$$

The second model is the so-called natural inflation potential (in purple in fig. 1.3) [32], described by the following potential:

$$V(\phi) = \Lambda^4 \left[1 + \cos \left(\frac{\phi}{f} \right) \right] , \quad (1.46)$$

where f is a constant parameter known as the axion decay constant. The fact that these two well motivated potentials are in tension with the data (a tension that is enhanced

when considering the BICEP2/Keck Array experiment [33]) will be a motivation for testing the robustness of their predictions. We will carry out that work in Chapters 4 and 5.

1.2.2 Higher order correlation functions

As we shall also discuss in this thesis, modifications of the canonical single-field model of inflation can generate a large non-gaussian signal. First of all, from the point of effective field theory (EFT), higher order interactions are unavoidable. In the case of inflation [34] they can be calculated relying only on the background spacetime symmetries, so we expect them to be quite universal. In particular, the curvature perturbations of every single-clock inflationary model¹² are described by a unique Lagrangian, in which only the specific value for the coefficients of the different operators depends on the microscopic origin of the model.

A well studied non-gaussian signature is the three-point correlation function (for a review, see e.g. [35]). The simplest way of generating a three-point function is through an explicit third order interaction in the Lagrangian. The first thorough calculation of this signal was performed by Acquaviva et al. [36], and later Maldacena determined its explicit k -dependence [37]. From the EFT of inflation [34], the action of the curvature perturbation, up to third order, is given by:

$$S_2 = \int d^4x a^3 \dot{H} \left\{ - \left[\frac{\dot{\pi}^2}{c_s^2} - \frac{1}{a^2} (\nabla\pi)^2 \right] + 3\dot{H}\pi^2 \right\} , \quad (1.47)$$

$$S_3 = \int d^4x a^3 \left\{ \left[\dot{\pi}^2 - \frac{(\nabla\pi)^2}{a^2} \right] \left[\dot{H}\dot{\pi} (1 - c_s^{-2}) - \ddot{H}\pi \right] + 2\dot{H} \frac{\dot{c}_s}{c_s^3} \pi \dot{\pi}^2 - \frac{4}{3} M_3^4 \dot{\pi}^3 - 3\ddot{H}\dot{H}\pi^3 \right\} , \quad (1.48)$$

where π is defined as the Goldstone boson of the broken time diffeomorphism which, at linear order, is related to the curvature perturbation as $\mathcal{R} = -H\pi$. First of all, let us note that the second order action derived from the EFT is the same as the one we wrote in section 1.2.1. At that point we derived the action for the specific case in which the curvature perturbations were identified with the scalar field and metric perturbations. The interesting point to notice is that in order to construct the EFT we do not really need to know the energy content of the Universe. More precisely, the action for the curvature perturbation is the same independently of whether the inflaton is a scalar

¹²As inflation describes a quasi de Sitter Universe, time translation is not a symmetry of the background evolution. By single-clock it is understood that time translation is broken by a single degree of freedom.

field, a composite field or any other exotic matter field (provided spatial diffeomorphism is preserved and there is only one degree of freedom dictating the background dynamics). The microscopic details of the theory are only going to be encoded in the values of c_s (which also determines s), M_3 (which is in general time dependent) and H (which has however more restrictions since it needs to support inflation).

While higher order correlation functions are unavoidable, in the simplest version of inflation they are highly suppressed. The first reason is because of the smallness of \mathcal{R} (the amplitude of the two-point function translates into $\mathcal{R} \sim 10^{-5}$). Higher order operators are described by higher powers of \mathcal{R} , and so they are small with respect to the gaussian (quadratic) component. Moreover, also the coefficients of the higher order operators are suppressed since they are composed of higher order derivatives and higher order powers of the slow-roll parameters (e.g. through \ddot{H} in (1.48)). These parameters are also small in canonical, and smooth, single-field models of inflation.

More precisely, the smallness of the three-point function is guaranteed provided some conditions are fulfilled. These conditions are i) single-clock inflation: there is only one effective degree of freedom dictating the dynamics. ii) Bunch-Davies initial conditions: modes with wavelength much smaller than the Hubble radius effectively experience Minkowski spacetime. iii) Canonical kinetic terms: the inflaton has canonical kinetic terms with speed of sound $c_s = 1$. iv) The slow-roll parameters and their time variations are small during all the observable inflationary trajectory.

The interest in studying non-gaussianity comes from the fact that any detection of primordial non-gaussianity would very likely come from the violation of any of these conditions, which would be an incredibly important step towards understanding the nature of inflation.

As the three-point correlation function depends on three momenta (which are bounded to form a triangle in k -space because of translational invariance), its comparison with data is particularly difficult. It is then useful to concentrate on a few well motivated templates, which characterizes the shape of some ‘expected signals’. A template α can be generally defined as:

$$\langle \mathcal{R}(k_1)\mathcal{R}(k_2)\mathcal{R}(k_3) \rangle^\alpha = (2\pi)^3 \delta(k_1 + k_2 + k_3) f_{NL}^\alpha \cdot F^\alpha(k_1, k_2, k_3). \quad (1.49)$$

Every template α has a scale-dependent shape $F^\alpha(k_1, k_2, k_3)$ and a corresponding amplitude f_{NL}^α , which is a number that does not depend on k_i . The current data and techniques available for the analysis of the three-point function allow us to constrain the amplitude f_{NL}^α for a finite set of templates, that we have to choose beforehand. In this sense, the non-detection of a particular template α does not imply the absence of

non-gaussianity, but rather constrains the presence of the non-gaussian signal described by that specific template. Furthermore, even if the three-point function is measured to be consistent with zero in every momentum configuration, non-gaussianities may appear in higher order correlation functions. This is the reason why complementary studies of non-gaussianities, e.g. based upon real-space statistics, are also very important.

The most studied templates for the three-point function are three (we refer the reader to [35] for a detailed account). Two of them come from noticing that, at first order in slow-roll, there are two free parameters in the cubic action (1.48), namely c_s and M_3^4 . When c_s is a constant ($\dot{c}_s = 0$), c_s and $\tilde{c}_3 \equiv 2M_3^4 c_s^2 / \dot{H}$ control the amplitude of two different templates, named equilateral and orthogonal [38]. The third template, historically the first to be considered, is the so-called local template. It describes the non-gaussian signal for the case in which there is a non-linear relation between the inflaton and the observed curvature perturbations. It borrows its name from being defined in real space [39]. The main characteristics of the templates mentioned above are:

- **Equilateral:** This is the non-gaussian signal when c_s is a constant $c_s \neq 1$, and $\tilde{c}_3 = \ddot{H} = 0$. The template peaks in the equilateral limit, which is the configuration in which the three momenta are equal, $k_1 = k_2 = k_3$. Models with constant reduced speed of sound will peak at this configuration.
- **Orthogonal:** This is a template designed to be *orthogonal* to the equilateral template, such that a basis is defined that covers all the relative contributions of c_s and \tilde{c}_3 . This template also peaks in the equilateral but has an important contribution in the flattened limit (defined as $2k_1 = 2k_2 = k_3$).
- **Local:** The local configuration comes when the non-gaussian component of the curvature perturbation \mathcal{R} is parametrized as a function of its gaussian component \mathcal{R}^g as:

$$\mathcal{R}(x) = \mathcal{R}^g(x) + \frac{3}{5} f_{NL}^{\text{loc}} (\mathcal{R}^g(x) - \langle \mathcal{R}^g(x)^2 \rangle) . \quad (1.50)$$

The parameter f_{NL}^{loc} controls the skewness of the probability density function. In momentum space this template peaks in the squeezed limit. This is an interesting configuration, in which one of the momenta is much smaller than the other two, $k_1 = k_L$ and $k_2 = k_3 = k_S$ with $k_S \gg k_L$ (S,L denoting short and long mode respectively). In [37], Maldacena showed that the amplitude of the bispectrum in the squeezed limit is proportional to the tilt of the power spectrum, as

$$\lim_{k_L \rightarrow 0} \langle \mathcal{R}(k_S) \mathcal{R}(k_S) \mathcal{R}(k_L) \rangle = -\mathcal{P}_{\mathcal{R}}(k_L) \mathcal{P}_{\mathcal{R}}(k_S) \frac{d}{d \ln k_S} \ln [k_S^3 \mathcal{P}_{\mathcal{R}}(k_S)] . \quad (1.51)$$

This is also known as the ‘consistency condition’, since any model violating this relation will have non-trivial departures from the simplest single field inflationary

models. In particular, this configuration is bound to be undetectable in the simplest inflationary models since $d \ln \mathcal{P}_{\mathcal{R}} / d \ln k \sim (n_s - 1)$ is of order slow-roll in all the observable inflationary trajectory (see equation 1.35). Contracting cosmologies, multifield models of inflation, as well as single field models with features (e.g. oscillations) in the primordial power spectra can generate however a large local signal¹³.

These configurations have been tested in the Planck 2105 data [40], and the following constraints has been derived (the amplitude of the three shapes being consistent with zero):

$$f_{NL}^{\text{local}} = 0.8 \pm 5.0 \quad , \quad f_{NL}^{\text{equi}} = -4 \pm 43 \quad , \quad f_{NL}^{\text{orth}} = -26 \pm 21 \quad (68\% \text{CL}) \quad (1.52)$$

These constraints can be related to constraints in c_s and \tilde{c}_3 , from where we can deduce an upper bound on c_s , $c_s > 0.024$ at 95% CL (the two-dimensional constraint is shown in figure (1.4)).

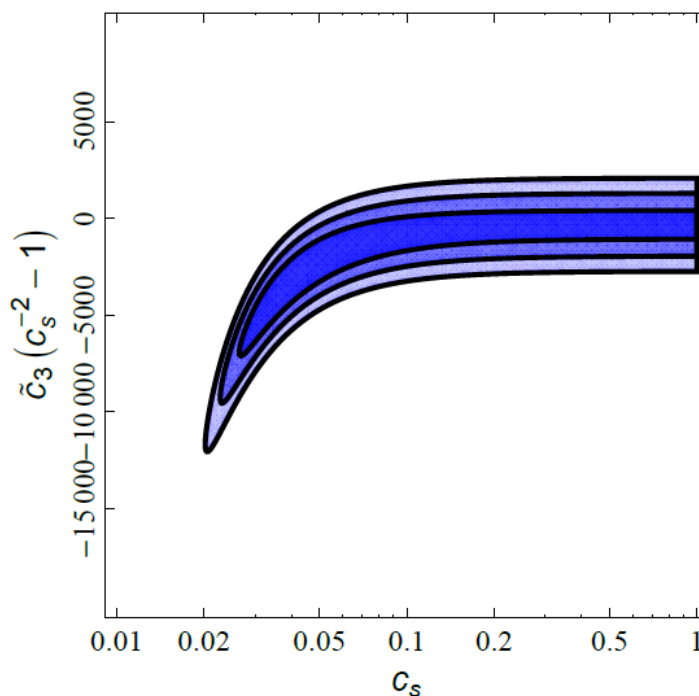


FIGURE 1.4: 68%, 95%, 99.7% confidence regions in the single field inflation parameter space (c_s, \tilde{c}_3) , with $\tilde{c}_3 \equiv 2M_3^4 c_s^2 / \dot{H}$. Figure from [40]

¹³In some of these cases the consistency condition will be violated (by violating some of the assumptions necessary for its derivation) while in others not. In particular, let us note that single field models with oscillations in the primordial power spectrum still satisfy this relation. A primordial power spectrum which is overall flat but has small oscillations on top of it has big and oscillatory values for $d \ln \mathcal{P} / d \ln k$. This family of primordial power spectrum can also provide better fits to the data than the featureless power-law primordial power spectrum, and will be an important subject of this thesis.

In the general framework of EFT, the coefficients that appear in the low energy Lagrangian are functions of the ‘UV’ completion of the theory. For example, consider a ‘UV’ theory consisting of two fields: a massless field ϕ_l and a massive field ϕ_h (with mass M) with an interaction $g\phi_l^2\phi_h$. At energies well below M , this interaction is effectively described by a 4-point self interaction of the massless field of the form $(g^2/M^2)\phi_l^4$. The strength of this 4-point self interaction is then proportional to the UV parameters of the theory, in this case g and M . So, in the context of the EFT of inflation, a natural question arises: what are the possible UV completions of inflation that give rise to non-zero values for the parameters of the low energy EFT (in our case, c_s and M_3^4 when considering up to third-order interactions)? Are they bound to be very suppressed ($\propto 1/M^2$), as in the simple two-field model showed here? Or more generally, which values for these parameters can be interpreted in terms of the UV completion?

While we will not address these questions in full generality (see e.g. [41]), in this thesis we will consider a particular embedding of inflation in which this procedure is tractable. In particular, we will consider inflation happening in a two-field landscape, in which one of the fields is light and the other is heavy (with respect to the scale of inflation), and we will show explicitly how the coefficients of the low energy operators emerge when integrating out the heavy field. In particular, we will show that the speed of sound of the curvature fluctuations is linked to the angular velocity of the inflationary trajectory. The time dependence of the speed of sound will not only determine the regime of validity of the single-field low energy effective theory but it will also demand using new techniques for calculating the n -point correlation functions. Of course, this is not the only UV completion for which the EFT of the curvature fluctuations has a reduced speed of sound¹⁴, but, as we will see explicitly, this particular embedding has enough richness to provide a better understanding of the subtleties of both decoupling in EFT and of multifield inflation. We will address these questions up to Chapter 4, while we will reserve the fifth and last chapter to study the case in which there are two light fields during some part of the inflaton trajectory.

¹⁴As in the Dirac-Born-Infeld (DBI) models of inflation [42, 43].

2

Multifield inflation and the adiabatic condition

Single field inflationary models might seem very appealing because of their theoretical minimality and their ability to fit the cosmological data. There are, however, good reasons to think that this may not be a very plausible description of the energy content of the Universe at the energy scale of inflation. Indeed, all of the completions of the Standard Model which accomplish, for example, unification of the gauge coupling constants, are populated by several new degrees of freedom at higher energies. The presence of many fields during inflation may imply a variety of observable effects departing from those predicted in standard single-field slow-roll inflation, including features in the power spectrum of primordial inhomogeneities [44–56], large primordial non-gaussianities [43, 57–62] and isocurvature perturbations [63–71]. A detection of any of these signatures would therefore represent an extremely significant step towards elucidating the fundamental nature of physics taking place during the very early universe. Likewise, the non-detection of any special feature also poses interesting challenges, in particular how to explain the symmetries protecting the smooth background in a more fundamental theory of inflation.

If inflation is well described by a single degree of freedom it does not mean that the Universe *has* one degree of freedom at those energy scales. The decoupling of different degrees of freedom is a well known phenomenon which is of course not only restricted to inflation but applies to generic physical situations (for a review see e.g. [72]). It could be further argued that this is a necessary condition for the construction of any physical theory, otherwise Planck scale physics would be necessary for describing low-energy phenomena. How different degrees of freedom decouple at different energy scales is the subject of Effective Field Theories (EFT). EFT may then be the clue to reconcile the

predictions of single field inflation, well in accordance with the data, with the unlikeliness of having just one degree of freedom at the energy scale of inflation. For example, a straightforward solution to this apparent paradox is to assume a hierarchy between the energy scale of inflation H (driven by a field with mass $m \ll H$), and all the additional degrees of freedom, such that their mass $M \gg H^1$. After these heavy degrees of freedom are integrated out, one expects a low energy EFT in which UV-physics are parametrized by non trivial operators suppressed by factors of order H^2/M^2 . The resulting low energy EFT is therefore expected to offer negligible departures from a truncated version of the same theory -single field inflation- wherein heavy fields are simply disregarded from the very beginning.

While this is a perfectly consistent scenario, there are certain situations in which the heavy degrees of freedom may leave big imprints in the low energy EFT. In the particular case of inflation, large couplings between light and heavy fields have been shown to substantially modify the properties of the low energy curvature perturbations [55, 73–81]. Would nature be so kind as to be in a such a state, the observation of its effects would offer a unique opportunity for the characterization of fields much heavier than the Hubble scale. This exciting possibility demands a thorough understanding both of the dynamics of decoupling and of data analysis.

In this chapter we will show, through a detailed study of multifield inflation, that the decoupling of different energy scales does allow for observing the effects of an additional heavy field within an effective low energy theory. After explicitly constructing a low energy EFT in the inflationary time-dependent background, we will show the restrictions that apply on the strength and time variation of the couplings of the low energy -single field- operators such that they can be interpreted in terms of the UV -multi field- theory.

The content of this chapter is based on two papers:

- “*Heavy fields, reduced speeds of sound and decoupling during inflation*”, A. Achúcarro, V. Atal, S. Cespedes, J. O. Gong, G. A. Palma and S. P. Patil, Phys. Rev. D **86** (2012) 121301 [arXiv:1205.0710 [hep-th]].
- “*On the importance of heavy fields during inflation*“, S. Cespedes, V. Atal and G. A. Palma, JCAP **1205** (2012) 008 [arXiv:1201.4848 [hep-th]].

¹Whether this is easy or difficult to achieve in specific theories is another fundamental question.

2.1 Multifield inflation

We start by defining the basics of multifield inflation. We follow the formalism developed in [55, 67, 68]. Our starting point is the action for a set of multiple scalar fields ϕ^a ($a = 1, \dots, N$, with N the total number of fields) minimally coupled to gravity

$$S = \int d^4x \sqrt{-g} \left[\frac{1}{2} R - \frac{1}{2} g^{\mu\nu} \gamma_{ab} \partial_\mu \phi^a \partial_\nu \phi^b - V(\phi) \right], \quad (2.1)$$

where R is the Ricci scalar of the spacetime metric $g_{\mu\nu}$, γ_{ab} is the sigma model metric of the space spanned by ϕ^a and V is the scalar potential. The equation of motion for ϕ^a can be written as

$$\square \phi^a + \Gamma_{bc}^a \partial_\mu \phi^b \partial^\mu \phi^c - V^a = 0, \quad (2.2)$$

where $\square = \nabla_\mu \nabla^\mu$, $V^a \equiv \gamma^{ab} V_b$ and $V_b = \partial_b V$. The Christoffel symbols Γ_{bc}^a are associated with the field space metric γ^{ab} , are given by

$$\Gamma_{bc}^a = \gamma^{ad} (\partial_b \gamma_{dc} + \partial_c \gamma_{bd} - \partial_d \gamma_{bc}) / 2. \quad (2.3)$$

We can furthermore construct a Ricci tensor and Ricci scalar associated to γ_{ab} , such that $\mathbb{R} = \gamma^{ab} \mathbb{R}_{acb}$ and \mathbb{R}_{acb} is the Riemann tensor given by:

$$\mathbb{R}_{acb}^c = \partial_c \Gamma_{bd}^a - \partial_d \Gamma_{bc}^a + \Gamma_{ce}^a \Gamma_{db}^e - \Gamma_{de}^a \Gamma_{cb}^e. \quad (2.4)$$

We now study the cosmological solutions of this system.

2.1.1 Homogeneous and isotropic backgrounds

Let us first study the equations for the homogeneous and isotropic cosmological background, characterized by a scalar field solution $\phi^a = \phi_0^a(t)$ only dependent on time. For this we consider a flat FLRW metric of the form

$$ds^2 = -dt^2 + a(t)^2 \delta_{ij} dx_i dx_j, \quad (2.5)$$

where $a(t)$ is the scale factor describing the expansion of flat spatial foliations. Then, the equations of motion determining the evolution of the system of fields are given by

$$D_t \dot{\phi}_0^a + 3H \dot{\phi}_0^a + V^a = 0, \quad (2.6)$$

$$3H^2 = \dot{\phi}_0^2 / 2 + V, \quad (2.7)$$

where $H = \dot{a}/a$ is the Hubble expansion and we have introduced the covariant time derivative

$$D_t X^a = \dot{X}^a + \Gamma_{bc}^a \dot{\phi}_0^b X^c . \quad (2.8)$$

We are further using the following definition for the total kinetic energy

$$\dot{\phi}_0^2 \equiv \gamma_{ab} \dot{\phi}_0^a \dot{\phi}_0^b , \quad (2.9)$$

from which we can write the following relation

$$\dot{H} = -\dot{\phi}_0^2/2 . \quad (2.10)$$

The equations of motion written in the field basis, as in (2.6), are not particularly useful in gaining intuition on how the system is evolving. First of all, we do not know how the kinetic energy is distributed among the different fields. As the curvature perturbations are associated with time translations of the background trajectory (see e.g. [81]), we cannot easily identify to which linear combination of the fields perturbations $\delta\phi^a$ they correspond. Additionally, if the mass matrix is non-diagonal in the field basis, we cannot know whether a hierarchy of masses, which would greatly simplify the system, exists or not.

In order to cure the first problem, we can project the equations of motion into the *kinematic* basis, which is defined as the projection of the equations of motion into the direction tangential and normal to the trajectory². For this, we define orthogonal unit vectors T^a and N^a in such a way that, at a given time t , $T^a(t)$ is tangent to the path, and $N^a(t)$ is normal to it. In this thesis we will consider two-field models, such that there is only one vector normal to the trajectory (see [83] for a generalization to more fields). In this particular case, this set of vectors can be defined as:

$$T^a = \dot{\phi}_0^a / \dot{\phi}_0 , \quad (2.11)$$

$$N^a = \gamma^{ab} N_b \quad \text{with} \quad N_a = \sqrt{\det \gamma} \epsilon_{ab} T^b , \quad (2.12)$$

where ϵ_{ab} is the Levi-Civita symbol with $\epsilon_{11} = \epsilon_{22} = 0$ and $\epsilon_{12} = -\epsilon_{21} = 1$. These definitions ensure that $T_a T^a = 1$, $N_a N^a = 1$ and $T_a N^a = 0$. The decomposition is shown in figure 2.1. Projecting the background equation of motion (2.6) along T^a yields

$$\ddot{\phi}_0 + 3H\dot{\phi}_0 + V_T = 0, \quad (2.13)$$

²An alternative decomposition which better accommodates the notion of light and heavy fields is the *mass* basis. In this basis the second covariant derivative of the potential is diagonal through all the trajectory [82]. There is not however a single basis vector associated to the curvature perturbations.

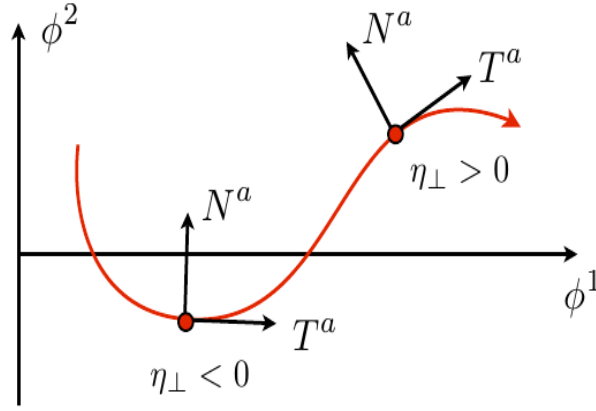


FIGURE 2.1: The decomposition of the trajectory in the kinematic basis, defined by the vectors N_a and T_a , normal and tangential to the trajectory respectively.

where $V_T \equiv T^a V_a$. On the other hand, projecting along N^a , one obtains

$$D_t T^a = -\frac{V_N}{\dot{\phi}_0} N^a, \quad (2.14)$$

where $V_N \equiv N^a \partial_a V$. Just as in single-field inflation, we may define the slow-roll parameters accounting for the time variation of various background quantities:

$$\epsilon \equiv -\dot{H}/H^2 \quad , \quad \eta^a \equiv -\frac{1}{H\dot{\phi}_0} \frac{D\dot{\phi}_0^a}{dt}. \quad (2.15)$$

Notice that η^a is a two dimensional vector field telling us how fast $\dot{\phi}_0^a$ is changing in time. We may decompose η^a along the normal and tangent directions by introducing two independent parameters η_{\parallel} and η_{\perp} as

$$\eta^a = \eta_{\parallel} T^a + \eta_{\perp} N^a. \quad (2.16)$$

Then, one finds that

$$\eta_{\parallel} = -\frac{\ddot{\phi}_0}{H\dot{\phi}_0}, \quad (2.17)$$

$$\eta_{\perp} = -\frac{V_N}{H\dot{\phi}_0}. \quad (2.18)$$

Notice that η_{\parallel} may be recognized as the usual η slow-roll parameter in single field inflation (η_{ϕ} in eq. (1.19)). On the other hand η_{\perp} tells us how fast T^a rotates in time, and therefore it parametrizes the rate of turning of the trajectory followed by the scalar field dynamics. This may be seen more clearly by using (2.14) together with (2.18) to

deduce the following relations

$$\frac{DT^a}{dt} = -H\eta_\perp N^a, \quad (2.19)$$

$$\frac{DN^a}{dt} = +H\eta_\perp T^a. \quad (2.20)$$

Thus, if $\eta_\perp = 0$, the vectors T^a and N^a remain constant along the path. On the other hand, if $\eta_\perp > 0$, the path turns to the left, whereas if $\eta_\perp < 0$ the turn is towards the right. The value of η_\perp is therefore telling us how quickly the angle determining the orientation of T^a is varying in time. By calling this angle θ we may therefore make the identification

$$\dot{\theta} \equiv H\eta_\perp. \quad (2.21)$$

With the help of this definition, one deduces that the radius of curvature κ characterizing the turning trajectory, is given by

$$\kappa^{-1} \equiv |\dot{\theta}|/\dot{\phi}_0. \quad (2.22)$$

As in conventional single-field inflation, the background dynamics may be understood in terms of the values of the dimensionless parameters ϵ , η_\parallel and η_\perp . For instance, slow-roll inflation will happen as long as:

$$\epsilon \ll 1, \quad |\eta_\parallel| \ll 1. \quad (2.23)$$

These two conditions ensure that both H and $\dot{\phi}_0$ evolve slowly. On the other hand, a large value of η_\perp does not necessarily imply a violation of the slow-roll regime (2.23). As we will see later, the regime of large η_\perp will offer the most interesting phenomenology.

2.1.2 Perturbations

We now consider the dynamics of scalar perturbations $\delta\phi^a(t, \mathbf{x}) = \phi^a(t, \mathbf{x}) - \phi_0^a(t)$. It is convenient to work with the gauge invariant quantities v^T and v^N given by:

$$v^T = aT_a\delta\phi^a + a\frac{\dot{\phi}}{H}\psi, \quad (2.24)$$

$$v^N = aN_a\delta\phi^a, \quad (2.25)$$

where ψ is the scalar perturbation of the spatial part of the metric (proportional to δ_{ij}) in flat gauge. It is useful to consider a second set of fields (u^X, u^Y) in addition to

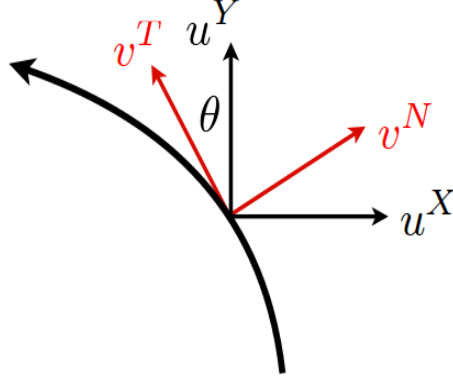


FIGURE 2.2: The u fields represent fluctuations with respect to a fixed local frame, whereas the v -fields represent fluctuations with respect to the path (parallel and normal).

(v^T, v^N) . Let us consider the following time dependent rotation in field space

$$\begin{pmatrix} u^X \\ u^Y \end{pmatrix} \equiv R(\tau) \begin{pmatrix} v^N \\ v^T \end{pmatrix}, \quad (2.26)$$

where the time dependent rotation matrix $R(\tau)$ is defined as

$$R(\tau) = \begin{pmatrix} \cos \theta(\tau) & -\sin \theta(\tau) \\ \sin \theta(\tau) & \cos \theta(\tau) \end{pmatrix}, \quad \theta(\tau) = \theta_0 + \int_{-\infty}^{\tau} d\tau a H \eta_{\perp}, \quad (2.27)$$

where θ_0 is the value of $\theta(\tau)$ at $\tau \rightarrow -\infty$. Thus, we assume that the trajectory is straight in the far past, which will help us later in properly quantizing the system. The rotation angle $\theta(\tau)$ precisely accounts for the total angle covered by all the turns during the inflationary history up to time τ , and coincides with the definition introduced in eq. (2.21). Figure (2.2) illustrates the relation between the v -fields introduced earlier and the canonical u -fields. To continue, the equations of motion for the canonically normalized fields are

$$\frac{d^2 u^I}{d\tau^2} - \nabla^2 u^I + [R(\tau) \Omega R^t(\tau)]^I_J u^J = 0, \quad I = X, Y, \quad (2.28)$$

where R^t represents the transpose of R . In addition, Ω is the mass matrix for the v -fields, whose entries are

$$\Omega_{TT} = -a^2 H^2 (2 + 2\epsilon - 3\eta_{\parallel} + \eta_{\parallel} \xi_{\parallel} - 4\epsilon \eta_{\parallel} + 2\epsilon^2 - \eta_{\perp}^2), \quad (2.29)$$

$$\Omega_{NN} = -a^2 H^2 (2 + \epsilon) + a^2 (V_{NN} + H^2 \epsilon \mathbb{R}), \quad (2.30)$$

$$\Omega_{TN} = -a^2 H^2 \eta_{\perp} (3 + \epsilon - 2\eta_{\parallel} - \xi_{\perp}), \quad (2.31)$$

where $\xi_{\parallel} = -\dot{\eta}_{\parallel}/(H\eta_{\parallel})$ and $\xi_{\perp} = -\dot{\eta}_{\perp}/(H\eta_{\perp})$. Additionally, V_{NN} is the tree level mass, defined as the second derivative of the potential projected along the perpendicular direction $V_{NN} = N^a N^b \nabla_a \nabla_b V$. To finish, expanding the original action (2.1) to quadratic order in terms of the u -fields, one finds:

$$S = \frac{1}{2} \int d\tau d^3x \left[\sum_I \left(\frac{du^I}{d\tau} \right)^2 - (\nabla u^I)^2 - [R(\tau) \Omega R^t(\tau)] u^I u^J \right]. \quad (2.32)$$

Thus, we see that the fields $u^I = (u^X, u^Y)$ correspond to the canonically normalized fields in the usual sense. Given that these fields are canonically normalized, it is now straightforward to impose Bunch-Davies conditions on the initial state of the perturbations.

2.1.3 Curvature and isocurvature modes

Another useful field parametrization for the perturbations is in terms of curvature and isocurvature fields \mathcal{R} and \mathcal{S} [66]. In terms of the v -fields, these are defined, to linear order, as

$$\mathcal{R} \equiv \frac{H}{a\dot{\phi}} v^T \quad \text{and} \quad \mathcal{S} \equiv \frac{H}{a\dot{\phi}} v^N. \quad (2.33)$$

Instead of working with \mathcal{S} , it is in fact more convenient to define ³

$$\mathcal{F} \equiv \frac{\dot{\phi}}{H} \mathcal{S}. \quad (2.34)$$

The quadratic order action for these perturbations is

$$S_2 = \frac{1}{2} \int dt d^3x a^3 \left[\frac{\dot{\phi}_0^2}{H^2} \dot{\mathcal{R}}^2 - \frac{\dot{\phi}_0^2}{H^2} \frac{(\nabla \mathcal{R})^2}{a^2} + \dot{\mathcal{F}}^2 - \frac{(\nabla \mathcal{F})^2}{a^2} - M_{\text{eff}}^2 \mathcal{F}^2 - 4\dot{\theta} \frac{\dot{\phi}_0}{H} \dot{\mathcal{R}} \mathcal{F} \right]. \quad (2.35)$$

Here M_{eff} is the effective mass of \mathcal{F} given by

$$M_{\text{eff}}^2 = m^2 - \dot{\theta}^2, \quad (2.36)$$

where $m^2 \equiv V_{NN} + \epsilon H^2 \mathbb{R}$. Notice that $\dot{\theta}$ couples both fields. In the case in which the isocurvature mode \mathcal{F} is heavy, this coupling reduces its effective mass, suggesting a breakdown of the hierarchy that would permit a single field effective description as $\dot{\theta}^2 \sim m^2$. As we are about to see, this expectation is somewhat premature. The linear

³A definition of \mathcal{R} and \mathcal{F} valid to all orders in perturbation theory is given in [81].

equations of motion in Fourier space are

$$\ddot{\mathcal{R}} + (3 + 2\epsilon - 2\eta_{||})H\dot{\mathcal{R}} + \frac{k^2}{a^2}\mathcal{R} = 2\dot{\theta}\frac{H}{\dot{\phi}_0}\left[\dot{\mathcal{F}} + \left(3 - \eta_{||} - \epsilon + \frac{\ddot{\theta}}{H\dot{\theta}}\right)H\mathcal{F}\right], \quad (2.37)$$

$$\ddot{\mathcal{F}} + 3H\dot{\mathcal{F}} + \frac{k^2}{a^2}\mathcal{F} + M_{\text{eff}}^2\mathcal{F} = -2\dot{\theta}\frac{\dot{\phi}_0}{H}\dot{\mathcal{R}}. \quad (2.38)$$

Note that $\mathcal{R} = \text{constant}$ and $\mathcal{F} = 0$ are non-trivial solutions to these equations for arbitrary $\dot{\theta}$. When \mathcal{F} is heavy, $\mathcal{F} \rightarrow 0$ shortly after horizon exit, and $\mathcal{R} \rightarrow \text{constant}$.

2.1.4 Power spectrum

From the observational point of view, the main quantities of interest coming from inflation are its predicted n -point correlation functions characterizing fluctuations. These quantities provide all the relevant information about the expected distribution of primordial inhomogeneities that seeded the observed CMB anisotropies. It is of particular interest to compute two-point correlation functions, corresponding to the variance of inhomogeneities' distribution. To deduce such quantities we have to consider the quantization of the system, and this may be achieved by expanding the canonical pair u^X and u^Y in terms of creation and annihilation operators $a_\alpha^\dagger(k)$ and $a_\alpha(k)$ respectively, as

$$u^I(\mathbf{x}, \tau) = \int \frac{d^3\mathbf{k}}{(2\pi)^{3/2}} \sum_\alpha \left[e^{i\mathbf{k}\cdot\mathbf{x}} u_\alpha^I(\mathbf{k}, \tau) a_\alpha(\mathbf{k}) + e^{-i\mathbf{k}\cdot\mathbf{x}} u_\alpha^{I*}(\mathbf{k}, \tau) a_\alpha^\dagger(\mathbf{k}) \right], \quad (2.39)$$

where $\alpha = 1, 2$ labels the two modes to be encountered by solving the second order differential equations for the fields $u_\alpha^I(k, \tau)$. In order to satisfy the conventional field commutation relations, the mode solutions need to satisfy the additional constraints consistent with the equations of motion

$$\sum_\alpha \left(u_\alpha^I \frac{u_\alpha^{J*}}{d\tau} - u_\alpha^{I*} \frac{u_\alpha^J}{d\tau} \right) = i\delta^{IJ}. \quad (2.40)$$

By examining the action (2.32) one sees that in the short wavelength limit $k^2/a^2 \gg \Omega$, where Ω symbolizes both eigenvalues of the matrix Ω , the equation of motion for the u -fields reduce to

$$\frac{d^2 u^I}{d\tau^2} - \nabla^2 u^I = 0, \quad I = X, Y, \quad (2.41)$$

In the UV limit, the mode equations are uncoupled, and they satisfy the simple harmonic oscillator equation. We can then choose the Bunch-Davies initial conditions for each one the fields, as

$$u_\alpha^X(k, \tau) = \frac{e^{-ik\tau}}{\sqrt{2k}} \delta_\alpha^1, \quad u_\alpha^Y(k, \tau) = \frac{e^{-ik\tau}}{\sqrt{2k}} \delta_\alpha^2, \quad (2.42)$$

valid in the limit $k\tau \gg 1$. Notice that here we have chosen to associate the initial state $\alpha = 1$ with the field direction X and $\alpha = 2$ with the field direction Y . This identification is in fact completely arbitrary and does not affect the computation of two-point correlation functions. In other words, we could modify the initial state (2.42) by considering an arbitrary (time independent) rotation on the right hand side, without changing the prediction of observables. Then, given the set of solutions u_α^X and u_α^Y , one finds that the two-point correlation function associated to curvature modes \mathcal{R} is given by:

$$\mathcal{P}_{\mathcal{R}}(k, \tau) = \frac{k^3}{2\pi^2} \sum_{\alpha} \mathcal{R}_{\alpha}(k, \tau) \mathcal{R}_{\alpha}^*(k, \tau) \quad (2.43)$$

where \mathcal{R}_{α} is related to the pair u_{α}^X and u_{α}^Y by the field redefinitions described in the previous sections. When (2.43) is evaluated at the end of inflation, for wavelengths k much bigger than the horizon ($k/a \ll H$), it corresponds to the power spectrum of curvature modes. One may also define the two-point correlation function $\mathcal{P}_{\mathcal{S}}(k, \tau)$ and the cross-correlation function $\mathcal{P}_{\mathcal{R}\mathcal{S}}(k, \tau)$ in analogous ways

$$\mathcal{P}_{\mathcal{S}}(k, \tau) = \frac{k^3}{2\pi^2} \sum_{\alpha} \mathcal{S}_{\alpha}(k, \tau) \mathcal{S}_{\alpha}^*(k, \tau) \quad (2.44)$$

$$\mathcal{P}_{\mathcal{R}\mathcal{S}}(k, \tau) = \frac{k^3}{2\pi^2} \sum_{\alpha} \mathcal{R}_{\alpha}(k, \tau) \mathcal{S}_{\alpha}^*(k, \tau) + h.c. \quad (2.45)$$

In the next section we discuss very briefly the observational status regarding the presence of isocurvature perturbations in the CMB, and its implications.

2.1.5 The fate of isocurvature perturbations

The presence of isocurvature modes leads to very specific effects on the angular temperature power spectra. For example, an isocurvature component will oscillate with a different phase with respect to the adiabatic components of the primordial plasma [84], changing the location of the peaks in the temperature two-point function (see figure 1.2). Because the position of the acoustic peaks are measured very accurately, CMB data can put very stringent bounds on their presence. These constraints are usually stated in terms of the primordial isocurvature fraction, defined as

$$\beta_{iso}(k) = \frac{\mathcal{P}_{\mathcal{S}}(k)}{\mathcal{P}_{\mathcal{R}}(k) + \mathcal{P}_{\mathcal{S}}(k)}. \quad (2.46)$$

The Planck constraints for β_{iso} are given specifically for models in which the isocurvature component is attributed to one of the different elements of the photon-baryon plasma (CDM, neutrino density or neutrino velocity) and different correlations are assumed between the curvature and isocurvature components. For the simplest cases with a scale

independent β_{iso} , a nominal bound can be taken to be $\beta_{iso} < 0.03$ [30], from which we can conclude that observations of the CMB highly disfavor the presence of isocurvature perturbations. The simplest way to satisfy this bound is by assuming a very heavy isocurvature field⁴. The power spectrum for a generic massive scalar field χ in a de Sitter expansion is given by [20]:

$$\mathcal{P}_\chi(k) \simeq \left(\frac{H}{2\pi}\right)^2 \left(\frac{H}{M}\right)^2 \left(\frac{k}{aH}\right)^3. \quad (2.47)$$

where M is the mass of the field χ . The power spectrum for such a field goes as $(k/aH)^3$ for superhorizon modes $(k/aH) \rightarrow 0$. An isocurvature field described by such power spectrum rapidly decays after horizon crossing, and hence its presence will be consistent with the Planck isocurvature constraints.

This is not, however, a necessary condition for not measuring isocurvature perturbations, as the bound coming from Planck really means that *at the time of decoupling* the perturbations are measured to be adiabatic. From the time of inflation to the decoupling of the CMB there is ample time and a diversity of physical processes, and there are many ways in which isocurvature perturbations during inflation may decay so that we only happen to measure adiabatic fluctuations at the time of decoupling. This is how active multifield dynamics can be consistent with the lack of observable isocurvature perturbations in the CMB. In figure 2.3 we show, schematically, the possible decays of the isocurvature fluctuations. Which dynamical process is responsible for the decay of the isocurvature field depends heavily on the mass and the evolution of the mass of this field. Ignoring particle production and effects coming from very rapid time evolution of the background (which will call our attention later), we can distinguish three situations:

- The isocurvature field is heavy throughout all the trajectory.
- The isocurvature field is light throughout all the trajectory.
- The isocurvature field has a mass which varies along the trajectory

If the isocurvature field is heavy throughout all the trajectory, the isocurvature fluctuations will decay after horizon crossing, just as we showed in eq. (2.47). This ensures that heavy scalars do not influence the dynamics of the perturbations at superhorizon scales, in particular, that they do not spoil the conservation of curvature perturbations at long wavelengths. This is case 1 in figure 2.3. If the isocurvature field is light and interacts with the curvature field, the curvature perturbations will continue to evolve after horizon crossing. Now, the isocurvature perturbations might still decay if their

⁴As usual, heavy and light field are defined with respect to the Hubble parameter. A heavy field is a field with mass $M \gg H$, while a light field has a mass $M \ll H$.

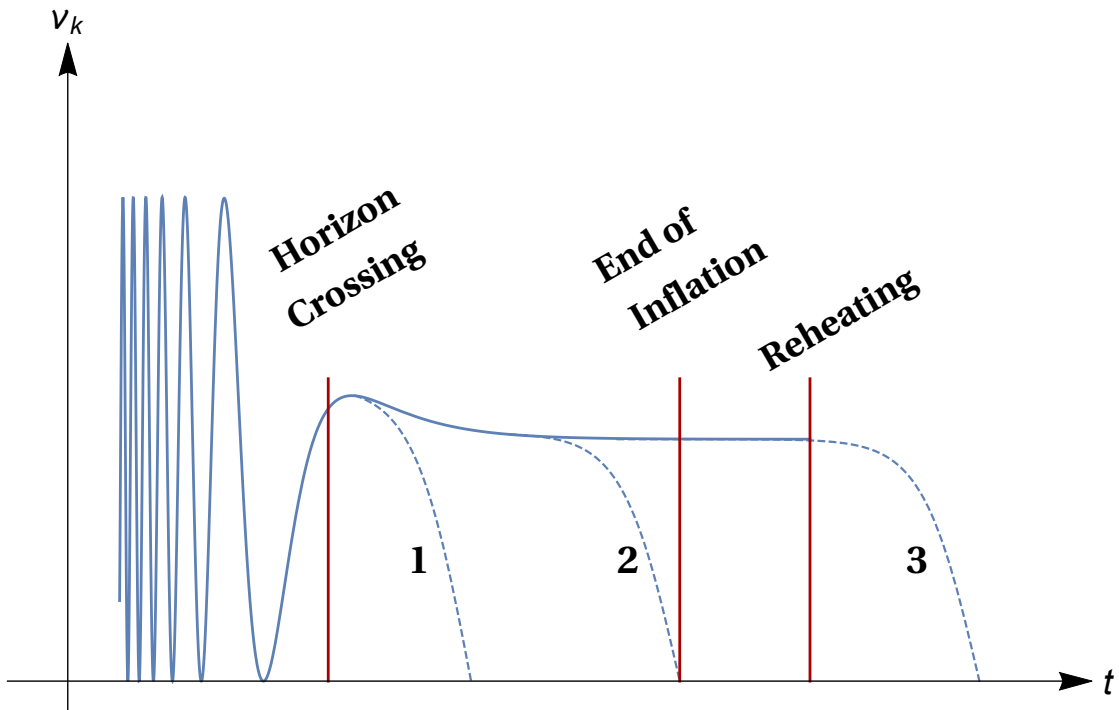


FIGURE 2.3: Schematic view, in arbitrary units, of the possible decays of an isocurvature mode v_k . An isocurvature mode may decay after it exits the horizon (if it's very massive - case 1), between horizon exit and the end of inflation (if it becomes massive during this part of the background evolution - case 2), or after thermalization in the plasma era (if it has strong interactions with radiation - case 3). While very different in nature, all these three mechanisms will be consistent with no measurable isocurvature fluctuations in the CMB spectra.

mass becomes large after the mode has exited the horizon (see e.g. [85–88]). Curvature perturbations will now freeze *after* horizon crossing. This is case 2 in figure 2.3, and we will show in the last chapter of this thesis (Chapter 5) a relevant example in which this mechanism operates. The last possibility is to rely on the thermalization process after reheating: if the isocurvature field has not yet decayed during inflation, it can thermalize with the radiation bath and reach adiabaticity [89]. This is case 3 in figure 2.3. The exact thermalization process depends on the initial condition and the couplings of the different fluids, and is thus sensitive to the physics of reheating.

If heavy isocurvature modes rapidly decay, does this mean that heavy fields are unobservable in the CMB? As we have already stated in the introduction, fortunately not. The key to answering this question comes from realizing that a heavy field may have a light propagating mode. This is a natural consequence of considering the coupled nature of the equation of motion for the heavy and light field. As we will see explicitly in the next section, whenever the coupling between both fields is large, a heavy isocurvature field will also contribute to the low energy EFT. Considering that it is impossible to

probe the energy scale of inflation directly, this scenario may be a unique way to access very high energy states observationally.

2.2 The effective field theory of turning trajectories

In this section we build the effective theory for the curvature perturbations in the case in which there is a strong turn in the inflationary trajectory supported by a heavy field (see figure 2.4 for an illustration). In this case unsuppressed interactions—kinematically coupling curvature perturbations with heavy fields—are unavoidably turned on. As a consequence, if the turning rate is large compared to the rate of expansion H , the impact of heavy physics on the low energy dynamics becomes substantially amplified, introducing large non-trivial departures from a naively truncated version of the theory.

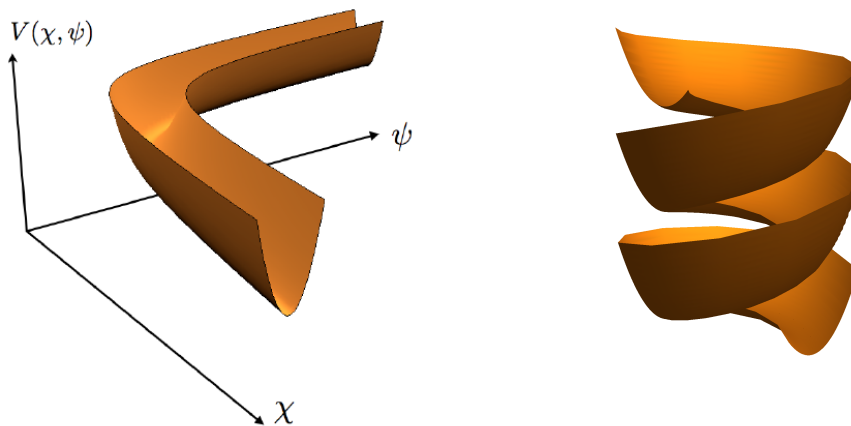


FIGURE 2.4: Two examples of strong turns in a two-field potential. They correspond to sharp (left panel) and soft (right panel) turns. In both cases the effect of the normal heavy field might be sizeable in the low energy effective theory.

It is possible to deduce an effective theory for the curvature mode \mathcal{R} by integrating out the heavy field \mathcal{F} when $M_{\text{eff}} \gg H^2$, provided that certain additional conditions are met. To see this, let us first briefly analyze the expected evolution of the fields \mathcal{R} and \mathcal{F} when the trajectory is turning at a constant rate ($\dot{\theta} = \text{constant}$). To begin with, because we are dealing with a coupled system of equations for \mathcal{R} and \mathcal{F} , in general we expect the general solutions for \mathcal{R} and \mathcal{F} to be of the form [76]

$$\mathcal{R} \sim \mathcal{R}_- e^{i\omega_- t} + \mathcal{R}_+ e^{i\omega_+ t}, \quad (2.48)$$

$$\mathcal{F} \sim \mathcal{F}_- e^{i\omega_- t} + \mathcal{F}_+ e^{i\omega_+ t}, \quad (2.49)$$

where ω_+ and ω_- denote the two frequencies at which the modes oscillate. The values of ω_- and ω_+ will depend on the mode's wave number k in the following way: In the regime $k/a \gg M_{\text{eff}}$, both fields are massless and therefore oscillate with frequencies of order $\sim k/a$. As the wavelength enters the intermediate regime $M_{\text{eff}} \gg k/a \gg H$ the degeneracy of the modes breaks down and the frequencies become of order (this estimations will be refined in the following section)

$$\omega_- \sim k/a, \quad \omega_+ \sim M_{\text{eff}}. \quad (2.50)$$

Subsequently, when the modes enter the regime $k/a < H$ the contributions coming from ω_+ will quickly decay and the contributions coming from ω_- will freeze (since they are massless). Notice that the amplitudes \mathcal{R}_+ and \mathcal{F}_- necessarily arise from the couplings mixing curvature and isocurvature perturbations, and therefore they vanish in the case $\eta_{\perp} = \dot{\theta}/H = 0$. Additionally, on general grounds, the amplitudes \mathcal{F}_+ and \mathcal{R}_+ are expected to be parametrically suppressed by k/M_{eff} in the regime $M_{\text{eff}} \gg k/a$, and therefore we may disregard high frequency contributions to (2.48) and (2.49). Then, in the regime $M_{\text{eff}} \gg k/a$, time derivatives for \mathcal{F} can be safely ignored in the equation of motion (2.38) and we may write (since $H \ll M_{\text{eff}}$ we may also disregard the friction term $3H\dot{\mathcal{F}}$):

$$\frac{k^2}{a^2}\mathcal{F} + M_{\text{eff}}^2\mathcal{F} = 2\dot{\phi}_0\eta_{\perp}\dot{\mathcal{R}}. \quad (2.51)$$

This leads to an algebraic relation between \mathcal{F} and \mathcal{R} given by:

$$\mathcal{F}_{\mathcal{R}} = \frac{2\dot{\phi}_0\eta_{\perp}\dot{\mathcal{R}}}{k^2/a^2 + M_{\text{eff}}^2}, \quad (2.52)$$

which precisely tells us the dependence of low frequency contributions \mathcal{F}_- in terms of \mathcal{R}_- defined in eqs. (2.48) and (2.49). To continue, we notice that (2.51) is equivalent to disregarding the term $\dot{\mathcal{F}}^2$ of the kinetic term in the action (2.35). Keeping this in mind, we can replace (2.52) back into the action and obtain an effective action for the curvature perturbation given by

$$S_{\text{eff}} = \frac{1}{2} \int dt d^3x a^3 \frac{\dot{\phi}_0^2}{H^2} \left[\frac{\dot{\mathcal{R}}^2}{c_s^2(k)} - \frac{k^2\mathcal{R}^2}{a^2} \right], \quad (2.53)$$

where c_s is the speed of sound of adiabatic perturbations, given by:

$$c_s^{-2} = 1 + \frac{4H^2\eta_{\perp}}{k^2/a^2 + M_{\text{eff}}^2}. \quad (2.54)$$

In deriving this expression we have assumed that $\dot{\theta}$ remained constant. In the more

general case where $\dot{\theta}$ is time dependent we expect transients that could take the system away from the simple behavior shown in eqs. (2.48) and (2.49), and the effective field theory could become invalid. The validity of the effective theory will depend on whether the kinetic terms for \mathcal{F} in eq. (2.38) can be ignored, and this implies the following condition on $\mathcal{F}_{\mathcal{R}}$ of eq. (2.52):

$$|\ddot{\mathcal{F}}_{\mathcal{R}}| \ll M_{\text{eff}}^2 |\mathcal{F}| \quad (2.55)$$

Now, recall that unless there are large time variations of background quantities, the frequency of \mathcal{R} is of order $\omega_- \sim k/a$. Thus, any violation of condition (2.55) will be due to the evolution of background quantities, which will be posteriorly transmitted to \mathcal{R} . This will allow us to ignore higher derivatives of $\dot{\mathcal{R}}$ in (2.55) and simply rewrite it in terms of background quantities as:

$$\left| \frac{d^2}{dt^2} \left(\frac{2\dot{\phi}_0 \eta_{\perp}}{k^2/a^2 + M_{\text{eff}}^2} \right) \right| \ll M_{\text{eff}}^2 \left| \frac{2\dot{\phi}_0 \eta_{\perp}}{k^2/a^2 + M_{\text{eff}}^2} \right| \quad (2.56)$$

This relation expresses the adiabaticity condition that each mode k needs to satisfy in order for the effective field theory to stay reliable. To further simplify this relation, we may take into consideration the following points: (1) When $k^2/a^2 \gg M_{\text{eff}}^2$ the two modes decouple (recall eq. (2.41)) and the turn has no influence on the evolution of curvature modes. On the other hand, in the regime $k^2/a^2 \lesssim M_{\text{eff}}^2$ contributions coming from the time variation of k^2/a^2 are always suppressed compared to M_{eff}^2 due to the fact that we are assuming $H^2 \ll M_{\text{eff}}^2$. (2) We focus on situations in which the time derivatives of quantities such as $\dot{\phi}_0$ and H , which describe the evolution of the background along the trajectory, are suppressed in comparison to $\eta_{\perp} = \dot{\theta}/H$. This corresponds to neglecting changes in the slow-roll parameters ϵ and η_{\parallel} ⁵. (3) Because of this, the rate of change of M_{eff}^2 will necessarily be at most of the same order than $\dot{\theta}$. Then, by neglecting time derivatives coming from $\dot{\phi}_0$, H , k^2/a^2 and M_{eff}^2 and focussing on the order of magnitude of the various quantities appearing in (2.56) we can write instead a simpler expression given by:

$$\left| \frac{d^2}{dt^2} \dot{\theta} \right| \ll M_{\text{eff}}^2 |\dot{\theta}| \quad (2.57)$$

Actually, a simpler alternative expression may be obtained by conveniently reducing the number of time derivatives, and disregarding effects coming from the change in sign of $\dot{\theta}$

$$\left| \frac{d}{dt} \ln \dot{\theta} \right| \ll M_{\text{eff}} \quad (2.58)$$

⁵In general, a turn in field space will also induce changes in these parameters [90, 91]. Whether the time variation of η_{\perp} or ϵ and η_{\parallel} is dominant is a model dependent issue.

This adiabaticity condition simply states that the rate of change of the turn’s angular velocity must stay suppressed with respect to the masses of heavy modes, which otherwise would become excited. Notice that, we may also choose to express this relation in terms of the variation of the speed of sound, which is a more natural quantity from the point of view of the effective field theory.

$$\left| \frac{d}{dt} \ln(c_s^{-2} - 1) \right| \ll M_{\text{eff}} . \quad (2.59)$$

We have tested the adiabaticity condition in several situations in [92], where turns induced by the potential and turns induced by the metric were studied. The validity of the adiabatic condition was demonstrated to describe very accurately the threshold between the single field and the two-field regimes. There are however some open questions: if c_s is time independent, the adiabatic condition seems to be automatically satisfied. Does this mean that we can consistently describe, in the low energy regime, a system with an arbitrarily reduced speed of sound? Furthermore, the adiabatic condition given by equation (2.59) was derived rather heuristically. Indeed, there should be a more precise condition stated in terms of the time variation of the frequency of the heavy mode. In this sense, the estimation of the eigenfrequencies in (2.50) should be done more carefully. In the next sections we tackle these question by studying more precisely the UV cut-off of the theory in the case that $\dot{\theta}$ is constant, and by precisely determining the eigenfrequencies of the two-field system.

2.3 Discussion: EFT with $c_s \ll 1$.

The observation that heavy fields can influence the evolution of adiabatic modes during inflation [73] has far reaching phenomenological implications [55, 76, 81, 92] that requires a refinement of our understanding of how high and low energy degrees of freedom decouple and how one splits “heavy” and “light” modes on a time-dependent background. As we have showed in the previous section, provided that there is only one flat direction in the inflaton potential, heavy fields (in this discussion, field excitations orthogonal to the background trajectory) can be integrated out, resulting in a low energy effective field theory (EFT) for adiabatic modes exhibiting a reduced speed of sound c_s given by (2.54). In the $k \rightarrow 0$ limit, the speed of sound is given by

$$c_s^{-2} = 1 + \frac{4\dot{\theta}^2}{M_{\text{eff}}^2} , \quad (2.60)$$

where $\dot{\theta}$ is the turning rate of the background trajectory in multi-field space, and M_{eff} is the effective mass of heavy fields, assumed to be much larger than the expansion

rate H . Given that M_{eff} is the mass of the fields we integrate out, one might doubt the validity of the EFT in the regime where the speed of sound is suppressed [77, 78, 80, 93], as this requires $\dot{\theta}^2 \gg M_{\text{eff}}^2$. In this section we elaborate on this issue by studying the dynamics of light and heavy degrees of freedom when $c_s^2 \ll 1$. To this end, we draw a distinction between isocurvature and curvature field excitations, and the true heavy and light excitations. We show that the light (curvature) mode \mathcal{R} indeed stays coupled to the heavy (isocurvature) modes when strong turns take place ($\dot{\theta}^2 \gg M_{\text{eff}}^2$), however, decoupling between the physical low and high energy degrees of freedom persists in such a way that the deduced EFT remains valid. This is confirmed by a simple setup in which H decreases adiabatically, allowing for a sufficiently long period of inflation. In this construction, *high energy degrees of freedom* are never excited, and yet *heavy fields* do play a role in lowering the speed of sound of adiabatic modes.

We are interested in (2.37) and (2.38) in the particular case where $\dot{\theta}$ is constant and much greater than M_{eff} . We first consider the short wavelength limit where we can disregard Hubble friction terms and take $\dot{\phi}_0/H$ as a constant. In this regime, the physical wavenumber $p \equiv k/a$ may be taken to be constant, and (2.37) and (2.38) simplify to

$$\begin{aligned}\ddot{\mathcal{R}}_c + p^2 \mathcal{R}_c &= +2\dot{\theta}\dot{\mathcal{F}}, \\ \ddot{\mathcal{F}} + p^2 \mathcal{F} + M_{\text{eff}}^2 \mathcal{F} &= -2\dot{\theta}\dot{\mathcal{R}}_c,\end{aligned}\tag{2.61}$$

where we have defined $\mathcal{R}_c = (\dot{\phi}_0/H)\mathcal{R}$. The solutions to these equations are found to be [76]

$$\begin{aligned}\mathcal{R}_c &= \mathcal{R}_+ e^{i\omega_+ t} + \mathcal{R}_- e^{i\omega_- t}, \\ \mathcal{F} &= \mathcal{F}_+ e^{i\omega_+ t} + \mathcal{F}_- e^{i\omega_- t}.\end{aligned}\tag{2.62}$$

The two frequencies ω_- and ω_+ are precisely given by

$$\omega_{\pm}^2 = \frac{M_{\text{eff}}^2}{2c_s^2} + p^2 \pm \frac{M_{\text{eff}}^2}{2c_s^2} \sqrt{1 + \frac{4p^2(1-c_s^2)}{M_{\text{eff}}^2 c_s^{-2}}},\tag{2.63}$$

with c_s given by (2.60). The pairs $(\mathcal{R}_-, \mathcal{F}_-)$ and $(\mathcal{R}_+, \mathcal{F}_+)$ represent the amplitudes of both low and high frequency modes respectively, and satisfy

$$\mathcal{F}_- = \frac{-2i\dot{\theta}\omega_-}{M_{\text{eff}}^2 + p^2 - \omega_-^2} \mathcal{R}_-, \quad \mathcal{R}_+ = \frac{-2i\dot{\theta}\omega_+}{\omega_+^2 - p^2} \mathcal{F}_+.\tag{2.64}$$

Thus the fields in each pair oscillate coherently. Of course, we may only neglect the friction terms if both frequencies satisfy $H \ll \omega_{\pm}$. This implies $H \ll pc_s$, which is what is meant by short wavelength regime. Integrating out the heavy mode consists in ensuring that the high frequency degrees of freedom do not participate in the dynamics

of the adiabatic modes. This can only be done in a sensible way if there is a hierarchy of the form $\omega_-^2 \ll \omega_+^2$, which given (2.63) necessarily requires

$$p^2 \ll M_{\text{eff}}^2 c_s^{-2}. \quad (2.65)$$

This defines the regime of validity of the EFT, in which one has

$$\omega_+^2 \simeq M_{\text{eff}}^2 c_s^{-2} = m^2 + 3\dot{\theta}^2, \quad (2.66)$$

$$\omega_-^2 \simeq p^2 c_s^2 + (1 - c_s^2)^2 p^4 / (M_{\text{eff}}^2 c_s^{-2}), \quad (2.67)$$

and one can clearly distinguish between low and high energy degrees of freedom. The adiabatic condition can then be more precisely stated as

$$\frac{\dot{\omega}_+}{\omega_+^2} \ll 1 \quad (2.68)$$

with ω_+ given by (2.66). Notice that the dispersion relation for the light mode may change depending on M_{eff} and c_s as:

$$\omega_-^2 \simeq p^2 c_s^2 \quad \text{for } p^2 \ll M_{\text{eff}}^2 / (1 - c_s^2)^2, \quad (2.69)$$

$$\omega_-^2 \simeq (1 - c_s^2)^2 p^4 / (M_{\text{eff}}^2 c_s^{-2}) \quad \text{for } M_{\text{eff}}^2 / (1 - c_s^2)^2 \ll p^2 \ll M_{\text{eff}}^2 c_s^{-2}. \quad (2.70)$$

This last possibility, in which $\omega_-^2 \sim p^4$ is only possible if $c_s^2 \ll 1$. Then, we see that condition (2.65) may be rewritten as

$$\omega_-^2 \ll M_{\text{eff}}^2 c_s^{-2}, \quad (2.71)$$

which allows to recognize the cut-off scale Λ_{UV} (which we use interchangeably with ω_+) given by

$$\Lambda_{\text{UV}}^2 = \omega_+^2 \simeq M_{\text{eff}}^2 c_s^{-2}. \quad (2.72)$$

One can also re-express (2.65) using (2.60) and (2.36) as

$$p^2 \ll 4m^2 / (3c_s^2 + 1). \quad (2.73)$$

From this, we see that contrary to the naive expectation based on M_{eff} , the range of comoving momenta for low energy modes *actually increases as the speed of sound decreases*. Furthermore, upon quantization [76] one finds $|\mathcal{R}_-|^2 \sim c_s^2 / (2\omega_-)$ and $|\mathcal{F}_+|^2 \sim 1 / (2\omega_+)$, implying that high frequency modes are relatively suppressed in amplitude. Thus, we can safely consider only low frequency modes, in which case \mathcal{F} is completely determined by \mathcal{R}_c as $\mathcal{F} = -2\dot{\theta}\dot{\mathcal{R}}_c / (M_{\text{eff}}^2 + p^2 - \omega_-^2)$. Notice that $\omega_-^2 \ll M_{\text{eff}}^2 + p^2$, so ω_-^2 may be disregarded here.

We now outline four crucial points that underpin our general conclusions:

1. The mixing between fields \mathcal{R} and \mathcal{F} , and modes with frequencies ω_- and ω_+ is *inevitable* when the background trajectory bends. If one attempts a rotation in field space in order to uniquely associate fields with frequency modes, the rotation matrix would depend on the scale p , implying a non-local redefinition of the fields.
2. Even in the absence of excited high frequency modes, the heavy field \mathcal{F} is forced to oscillate in pace with the light field \mathcal{R} at a frequency ω_- , so \mathcal{F} continues to participate in the low energy dynamics of the curvature perturbations.
3. When $\dot{\theta}^2 \gg M_{\text{eff}}^2$, the high and low energy frequencies become $\omega_+^2 \simeq M_{\text{eff}}^2 c_s^{-2} \sim 4\dot{\theta}^2$ and $\omega_-^2 \simeq p^2(M_{\text{eff}}^2 + p^2)/(4\dot{\theta}^2)$. Thus the gap between low and high energy degrees of freedom is amplified, and one can consistently ignore high energy degrees of freedom in the low energy EFT.
4. In the low energy regime, the field \mathcal{F} exchanges kinetic energy with \mathcal{R} resulting in a reduction in the speed of sound c_s of \mathcal{R} , the magnitude of which depends on the strength of the kinetic coupling $\dot{\theta}$. This process is adiabatic and consistent with the usual notion of decoupling in the low energy regime (2.65), as implied by (2.68).

At the core of these four observations is the simple fact that in time-dependent backgrounds, the eigenmodes and eigenvalues of the mass matrix along the trajectory do not necessarily coincide with the curvature and isocurvature fluctuations and their characteristic frequencies. With this in mind, it is possible to state more clearly the refined sense in which decoupling is operative: *while the fields \mathcal{R} and \mathcal{F} inevitably remain coupled, high and low energy degrees of freedom effectively decouple.*

We now briefly address the evolution of modes in the ultraviolet (UV) regime $p^2 \gtrsim M_{\text{eff}}^2 c_s^{-2}$. Here both modes have similar amplitudes and frequencies, and so in principle could interact via relevant couplings beyond linear order (which are proportional to $\dot{\theta}$). Because these interactions must allow for the non-trivial solutions $\mathcal{R} = \text{constant}$ and $\mathcal{F} = 0$ (a consequence of the background time re-parametrization invariance), their action is very constrained [81]. Moreover, in the regime $p^2 \gg M_{\text{eff}}^2 c_s^{-2}$ the coupling $\dot{\theta}$ becomes negligible when compared to p , and one necessarily recovers a very weakly coupled set of modes, whose $p \rightarrow \infty$ limit completely decouples \mathcal{R} from \mathcal{F} . This can already be seen in (2.52), where contributions to the effective action for the adiabatic mode at large momenta from having integrated out \mathcal{F} , are extremely suppressed for $k^2/a^2 \gg M_{\text{eff}}^2$, leading to high frequency contributions to (2.53) with $c_s = 1$.

Given that we have established the UV cut-off of the theory from the perspective of the full two-field theory, we can compare this scale to the strong coupling scale as given by the single field EFT. Indeed, the EFT will come with an intrinsic strong coupling scale $\Lambda_{s.c.}$ at which perturbative unitarity in the scattering matrix is lost. If we want the predictions for the power spectrum and bispectrum coming from the EFT to be reliable, it is important that the strong coupling scale $\Lambda_{s.c.}$ is much above the Hubble scale ($\Lambda_{s.c.} \gg H$). Furthermore, re-establishing unitarity demands that new degrees of freedom appears at an energy scale $E \leq \Lambda_{s.c.}$. As we have previously showed, the new degrees of freedom are characterized by the scale Λ_{UV} (or equivalently ω_+), and then it will also be important to ensure that this scale satisfies $\Lambda_{UV} \leq \Lambda_{s.c.}$.

2.3.1 Perturbativity for constant c_s

Demanding that the curvature perturbations are weakly coupled at the energy scale of inflation implies bounds on the strength of the non linear interactions of the low energy EFT. The operators of the EFT and their hierarchy vary according to whether they are time dependent or not. The perturbative regime will then be sensitive to this time dependence, so we might divide the discussion in whether the operators -in our case, functions of the speed of sound- are time dependent or not.

For the case in which the speed of sound is constant (we will later refer to the time dependent case), the strong coupling scale can be calculated from the action (1.48) with $\dot{c}_s = \ddot{H} = M_3^4 = 0$. The strong coupling scale is precisely defined as the scale at which quantum corrections to correlation functions become comparable to the tree level contribution. It is given by [34, 79]

$$\Lambda_{s.c.}^4 = 4\pi M_{pl}^2 \dot{H} |c_s^5 (1 - c_s^2)^{-1} . \quad (2.74)$$

Imposing that the observable modes were in the weakly coupled regime at the time they exited the horizon, $\Lambda_{s.c.} > H$, implies the following bound on c_s

$$c_s > 0.01 . \quad (2.75)$$

This is consistent with the bound coming from the absence of observed non-gaussianities, $c_s > 0.024$ [40]. The bound in (2.75) comes however with an important drawback: it is possible that the theory becomes strongly coupled at an energy which is below the energy at which the heavier degrees of freedom becomes excited, Λ_{UV} , given by

$$\Lambda_{UV} \sim M^2 c_s^{-2} . \quad (2.76)$$

This clashes with the general idea that it should be possible to define an EFT below the UV cut-off of the theory. The key to circumvent this problem is by noticing that the speed of sound we have derived has an energy dependence

$$c_s^{-2}(k) = 1 + \frac{4\dot{\theta}^2}{(k^2/a^2 + M_{\text{eff}}^2)}. \quad (2.77)$$

As we showed explicitly in eqs. (2.69) and (2.70), at sufficiently high energies the dispersion relation changes from $\omega(p) \propto p$ to $\omega(p) \propto p^2$. The strong coupling bound (2.74) is derived assuming a constant dispersion relation, and we may expect deviations when assuming a momentum dependent dispersion relation. This was done in [79, 94], and the new strong coupling scale was found to be:

$$\Lambda_{s.c.} = (8\pi c_s^2)^{2/5} \left(\frac{2\epsilon H^2 M_{\text{pl}}^2}{\Lambda_{\text{UV}}^4} \right)^{2/5} \Lambda_{\text{UV}}, \quad (2.78)$$

which implies, as expected, $\Lambda_{s.c.} > \Lambda_{\text{UV}}$. Furthermore, an extended version of the EFT action (1.48) can be constructed such that the *new physics regime* (in which the dispersion relation becomes $\propto p^2$) is incorporated [94].

2.3.2 Example

We now analyse a model of slow-roll inflation that executes a constant turn in field space, implying an almost constant and heavily suppressed speed of sound for the adiabatic mode. We will show that very simple two-field models of inflation exhibit all of these features. These are models that have a spiral structure in field space, just as in the right panel of figure 2.4. Further phenomenological implications of these models will be discussed in Chapter 4. To begin, let us consider fields $\phi^1 = \theta$, $\phi^2 = \rho$ with a metric $\gamma_{\theta\theta} = \rho^2$, $\gamma_{\rho\rho} = 1$, $\gamma_{\rho\theta} = \gamma_{\theta\rho} = 0$ (thus $\Gamma_{\rho\theta}^\theta = \Gamma_{\theta\rho}^\theta = 1/\rho$ and $\Gamma_{\theta\theta}^\rho = -\rho$), and potential

$$V(\theta, \rho) = V_0 - \alpha\theta + \frac{1}{2}m^2(\rho - \rho_0)^2. \quad (2.79)$$

This model would have a shift symmetry along the θ direction were it not broken by a non-vanishing α . This model is a simplified version of one studied in [74], where the focus instead was on the regime $M_{\text{eff}} \sim m \sim H$ (see also [95] where the limit $M_{\text{eff}}^2 \gg H^2 \gg \dot{\theta}^2$ is analysed). The background equations of motion are

$$\begin{aligned} \ddot{\theta} + 3H\dot{\theta} + 2\dot{\theta}\frac{\dot{\rho}}{\rho} &= \frac{\alpha}{\rho^2}, \\ \ddot{\rho} + 3H\dot{\rho} + \rho(m^2 - \dot{\theta}^2) &= m^2\rho_0. \end{aligned} \quad (2.80)$$

The slow-roll attractor is such that $\dot{\rho}$, $\ddot{\rho}$ and $\ddot{\theta}$ are negligible. This means that H , ρ and $\dot{\theta}$ remain nearly constant and satisfy the following algebraic equations near $\theta = 0$

$$\begin{aligned} 3H\dot{\theta} &= \frac{\alpha}{\rho^2}, \\ \dot{\theta}^2 &= m^2 \left(1 - \frac{\rho_0}{\rho}\right), \\ 3H^2 &= \frac{1}{2}\rho^2\dot{\theta}^2 + V_0 + \frac{1}{2}m^2(\rho - \rho_0)^2. \end{aligned} \quad (2.81)$$

These equations describe circular motion with a radius of curvature ρ and angular velocity $\dot{\theta}$. Here $M_{\text{eff}}^2 = m^2 - \dot{\theta}^2$, implying the strict bound $m^2 > \dot{\theta}^2$. Thus the only way to obtain a suppressed speed of sound is if $\dot{\theta}^2 \simeq m^2$. Our aim is to find the parameter ranges such that the background attractor satisfies $\epsilon \ll 1$, $c_s^2 \ll 1$ and $H^2 \ll M_{\text{eff}}^2$ simultaneously. This is given by

$$1 \gg \frac{\rho_0}{4} \left(\frac{m\sqrt{3V_0}}{\alpha}\right)^{1/2} \gg \frac{V_0}{6m^2} \gg \frac{\alpha}{4\sqrt{3V_0}m}. \quad (2.82)$$

If these hierarchies are satisfied, the solutions to (2.81) are well approximated by

$$\rho^2 = \frac{\alpha}{\sqrt{3V_0}m}, \quad \dot{\theta} = m - \frac{m\rho_0}{2} \left(\frac{m\sqrt{3V_0}}{\alpha}\right)^{1/2}, \quad (2.83)$$

and $H^2 = V_0/3$, up to fractional corrections of order ϵ , c_s^2 and H^2/M_{eff}^2 . We note that the first inequality in (2.82) implies $\rho \gg \rho_0$, and so the trajectory is displaced off the adiabatic minimum at ρ_0 . However, the contribution to the total potential energy implied by this displacement is negligible compared to V_0 . After n cycles around $\rho = 0$ one has $\Delta\theta = 2\pi n$, and the value of V_0 has to be adjusted to $V_0 \rightarrow V_0 - 2\pi n\alpha$. This modifies the expressions in (2.83) accordingly, and allows us to easily compute the adiabatic variation of certain quantities, such as $s \equiv \dot{c}_s/(c_s H) = -\epsilon/4$, and $\eta_{\parallel} = -\epsilon/2$, where $\epsilon = \sqrt{3}\alpha m^2/(2V_0^{3/2})$. These values imply a spectral index $n_{\mathcal{R}}$ for the power spectrum $\mathcal{P}_{\mathcal{R}} = H^2/(8\pi^2\epsilon c_s)$ given by $n_{\mathcal{R}} - 1 = -4\epsilon + 2\eta_{\parallel} - s = -19\epsilon/4$. It is now possible to find reasonable values of the parameters in such a way that observational bounds are satisfied. Using (2.83) we can relate the values of V_0 , α , m and ρ_0 to the measured values $\mathcal{P}_{\mathcal{R}}$ and $n_{\mathcal{R}}$, and to hypothetical values for c_s and $\beta \equiv H/M_{\text{eff}}$ as

$$\begin{aligned} V_0 &= \frac{96}{19}\pi^2(1 - n_{\mathcal{R}})\mathcal{P}_{\mathcal{R}}c_s, \\ m^2 &= \frac{8}{19}\pi^2(1 - n_{\mathcal{R}})\mathcal{P}_{\mathcal{R}}c_s^{-1}\beta^{-2}, \\ \alpha &= 6\left(\frac{16}{19}\right)^2\pi^2(1 - n_{\mathcal{R}})^2\mathcal{P}_{\mathcal{R}}c_s^2\beta, \\ \rho_0 &= 16c_s^3\beta\sqrt{\frac{2}{19}(1 - n_{\mathcal{R}})}. \end{aligned} \quad (2.84)$$

Following WMAP7, we take $\mathcal{P}_{\mathcal{R}} = 2.42 \times 10^{-9}$ and $n_{\mathcal{R}} = 0.98$ [96]. Then, as an application of relations (2.84), we look for parameters such that

$$c_s^2 \simeq 0.06, \quad M_{\text{eff}}^2 \simeq 250H^2, \quad (2.85)$$

(which imply $H^2 \simeq 1.4 \times 10^{-10}$), according to which $V_0 \simeq 5.9 \times 10^{-10}$, $\alpha \simeq 1.5 \times 10^{-13}$, $m \simeq 4.5 \times 10^{-4}$ and $\rho_0 \simeq 6.8 \times 10^{-3}$, from which we note that m , ρ_0 and $\alpha^{1/4}$ are naturally all of the same order. We have checked numerically that the background equations of motion are indeed well approximated by (2.83), up to fractional corrections of order c_s^2 . More importantly, we obtain the same nearly scale invariant power spectrum $\mathcal{P}_{\mathcal{R}}$ using both the full two-field theory described by (2.37) and (2.38), and the single field EFT described by the action (2.53). The evolution of curvature perturbations in the EFT compared to the full two-field theory for the long wavelength modes is almost indistinguishable given the effectiveness with which (2.65) is satisfied, with a marginal difference $\Delta\mathcal{P}_{\mathcal{R}}/\mathcal{P}_{\mathcal{R}} \simeq 0.008$. This is of order $(1 - c_s^2)H^2/M_{\text{eff}}^2$, which is consistent with we made in [92]. Despite the suppressed speed of sound in this model, a fairly large tensor-to-scalar ratio of $r = 16\epsilon c_s \simeq 0.020$ is predicted.

As expected, for $c_s^2 \ll 1$ a sizable value of $f_{\text{NL}}^{(\text{eq})}$ is implied. The cubic interactions leading to this were deduced in Ref. [81] which for constant turns is given by

$$f_{\text{NL}}^{(\text{eq})} = \frac{125}{108} \frac{\epsilon}{c_s^2} + \frac{5}{81} \frac{c_s^2}{2} \left(1 - \frac{1}{c_s^2}\right)^2 + \frac{35}{108} \left(1 - \frac{1}{c_s^2}\right). \quad (2.86)$$

This result is valid for any single-field system with constant c_s obtained by having integrated out a heavy field. Recalling that the spectral index n_T of tensor modes is $n_T = -2\epsilon$, for $c_s \ll 1$ we find a consistency relation between three potentially observable parameters, given by $f_{\text{NL}}^{(\text{eq})} = -20.74 n_T^2/r^2$. In the specific case of the values in (2.85), we have $f_{\text{NL}}^{(\text{eq})} \simeq -4.0$. This value is relatively large, so future observations could constrain this type of scenario. Finally, one can ask if the EFT corresponding to (2.85) remains weakly coupled throughout. As we have already mentioned, for small values of c_s , the dispersion relation has a dominant quartic piece which implies a strong coupling scale (2.78). For the values (2.85), we find $\Lambda_{\text{s.c.}}/\Lambda_{\text{UV}} \simeq 2$, implying that the EFT obtained by integrating a heavy field remains weakly coupled all the way up to its cut-off scale $\Lambda_{\text{s.c.}}$.

2.3.3 Perturbativity for rapidly varying c_s

So far, the analysis has been made assuming that the speed of sound is constant in time. In the case in which the speed of sound is varying with time there is a new scale,

the characteristic time of variation of c_s , that might affect the discussion above. While a constant $c_s \neq 1$ implies the appearance of a third order interaction, a time varying c_s creates an infinite number of interactions (in which the coupling of the higher order operators are given by higher order derivatives of c_s). This demands recalculating the strong coupling scale as given in eq. (2.74).

For the case in which the slow-roll parameter ϵ has a sharp change during inflation it is indeed possible to easily organize all the higher order interactions (assuming they all come from ϵ and its derivatives), and give an order of magnitude for the strong coupling scale. This was done by Cannone, Bartolo and Matarrese in [97] (and also by Adshead and Hu using different estimators [98]). We might expect these results to hold also for the speed of sound case. In [97] the change in ϵ was parametrized as a step in the Hubble parameter as

$$\dot{H}(t) = \dot{H}_0(t) \left[1 + \epsilon_{\text{step}} F \left(\frac{t - t_b}{b} \right) \right] \quad (2.87)$$

where ϵ_{step} is the magnitude of the step and F is a function centred at t_b , where the step happened, and b parametrizes its sharpness. Defining $\beta = 1/bH$, it was showed that the perturbative expansion is valid if we impose

$$\beta \ll 160 . \quad (2.88)$$

We will refer to this condition as the feature unitarity bound. While we will make use of this bound, let us note that a quantitative analysis might in principle shows some deviations from this result. First of all, the previous result was obtained taking into account only the time dependence of the Hubble parameter. The n th-order lagrangian can then be calculated by Taylor expanding the Hubble parameter up to that order. Then it is possible to group all the terms at n th-order in a single vertex (for example π^n) by successive integration by parts, greatly simplifying the calculation.

There are however many more terms that are allowed by the symmetries of the system. In particular, there is a tower of M_n^4 coefficients multiplying n th-order operators (just as M_3^4 was needed for computing \mathcal{L}_3) which are in principle time dependent and different from zero. In the absence of a UV theory that gives us a recipe for consistently calculating M_n^4 , any estimate on how they determine the perturbative regime must be made with caution. Additionally, the intuition in terms of scattering amplitudes is borrowed from the standard QFT techniques which assume time-independent vertex coefficients. Intuitively, this will be applicable to time-dependent coefficients if they obey an adiabatic condition of the form $|\dot{\lambda}/\lambda T| \ll 1$, where T is the timescale of the scattering process. Within this regime, higher order interactions should be suppressed. Although

this might relax the strong coupling bound coming from the scattering amplitudes, it is not clear how time dependence would affect the other strong coupling scales [98].

Let us note that a very sharp change in the speed of sound might also violate the two-field adiabatic condition, $\dot{\omega}_+ \ll \omega_+^2$. We can express this bound in terms of u and s as:

$$\begin{aligned} \frac{\dot{\omega}_+}{\omega_+^2} &= \frac{c_s^2}{M_{\text{eff}}^2} \frac{d}{dt} \left(\frac{M_{\text{eff}}}{c_s} \right) \\ &= s \left(\frac{H}{M_{\text{eff}}} \right) \left(\frac{-3c_s^4}{1+3c_s^2} \right) \ll 1. \end{aligned} \quad (2.89)$$

The parameter H/M_{eff} may take a wide range of values, from a minimal of $H/M_{\text{eff}} \sim 10^{-2}$ to $H/M_{\text{eff}} \sim 10^{-16}$ in the extreme cases of inflation happening just below the Planck scale or at the TeV scale (see e.g. [99, 100]). The feature unitarity bound given by equation (2.88) can also be expressed in terms of s and c_s . For this, we need to choose a functional form for the speed of sound. We will use the following ansatz

$$c_s^2(t) = \bar{c}_s^2(t) \left[1 + \sigma F \left(\frac{t - t_b}{b} \right) \right], \quad (2.90)$$

where \bar{c}_s is the unperturbed value of c_s , and σ and F are respectively the amplitude and the shape of the feature. We choose an exponential for F in e-folds, such that

$$F = e^{-\beta^2(N-N_f)^2}. \quad (2.91)$$

Under this parametrization, we can write a relation between s and c_s in the following form (for definitiveness with signs we choose $\sigma < 0$)

$$|s| = \beta \left(\frac{c_s^2}{\bar{c}_s^2} - 1 \right) \sqrt{-\ln \left(\frac{c_s^2/\bar{c}_s^2 - 1}{\sigma} \right)}. \quad (2.92)$$

Then, the bound (2.88) can be written as

$$\beta = |s| \left[-\ln \left(\frac{c_s^2/\bar{c}_s^2 - 1}{\sigma} \right) \right]^{-1/2} \left(\frac{c_s^2}{\bar{c}_s^2} - 1 \right)^{-1} \ll 160. \quad (2.93)$$

We compare the bounds (2.89) (with $H/M_{\text{eff}} \sim 10^{-2}$) and (2.93) (with $\bar{c}_s = 1$) in figure 2.5. In orange we show the region excluded either by dynamical excitation of the heavy field (when $\dot{\omega}_+ \sim \omega_+^2$) or by loss of unitarity given by the constant speed of sound bound (2.78). We also show the speed of sound trajectories that satisfy the feature unitarity bound (2.93), given the gaussian ansatz for the shape of the speed of sound feature (we do not expect different qualitative results when considering different shapes, e.g. a *tanh* step in the speed of sound). We see that all the trajectories that satisfy the feature

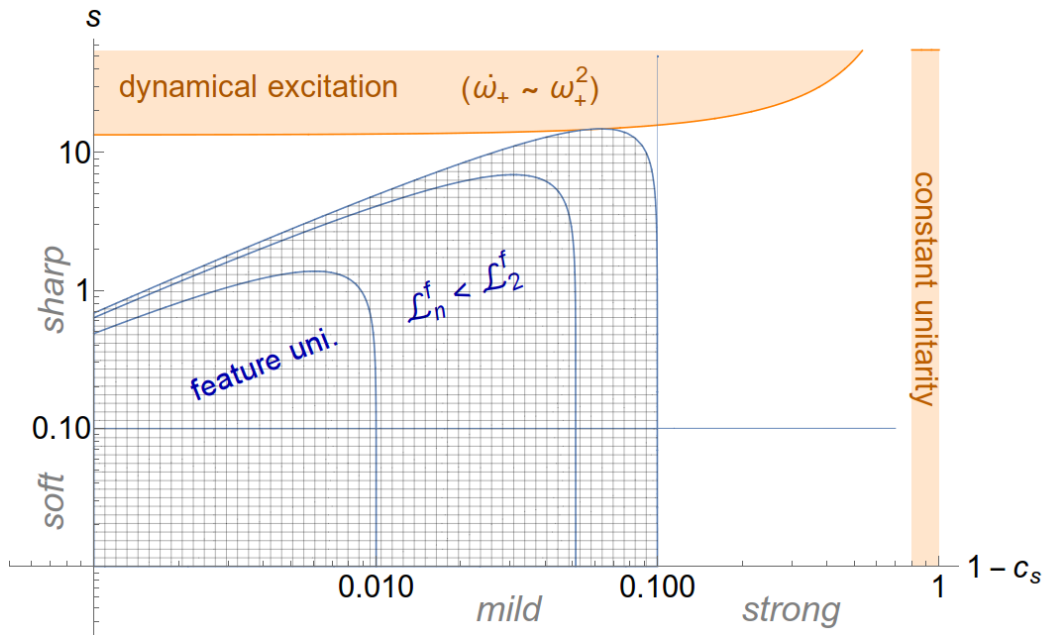


FIGURE 2.5: Different regimes for reduction in the speed of sound. Regions in orange are forbidden either by violation of the unitarity bound for constant c_s eq. (2.78) (in the plot this region is enlarged for visualization) or adiabaticity ($\dot{\omega}_+ \sim \omega_+^2$), as given in eq. (2.89). The meshed gray region is allowed by imposing the feature unitarity bound for the gaussian transient reduction, as given in eq. (2.93). We arbitrarily consider the soft/sharp limit to be at $s = 0.1$ and the mild/strong limit to be at $1 - c_s = 0.1$.

unitarity bound also satisfy the dynamical excitation bound. The zone in which feature unitarity is lost but the heavy field is not excited demands to be studied in more detail.

Independently of its origin, the speed of sound of the adiabatic mode during inflation may be phenomenologically divided into whether it has a slow or a fast time evolution. In figure 2.5 we have also plotted these different regimes in terms of $1 - c_s$ and s . While s determines whether the time variation of the speed of sound is *soft* or *sharp*, $1 - c_s$ determines whether the reductions in the speed of sound is *mild* or *strong*⁶. These different regions will result in n -point correlation functions with different characteristics. On the one hand, if the speed of sound evolves slowly, we can use the standard slow-roll techniques. This is the soft regime of figure 2.5. In this case the predictions for both the mild and strong regime can be analytically calculated. On the other hand, a fast evolution of the speed of sound will demand the use of different techniques for calculating the spectra of the curvature perturbations. In this case the mildness of the feature will prove important for using perturbative techniques, so we will restrict our study to the sharp and mild regime. We will devote the two following chapters to studying the observational constraints for these two different phenomenological regions, the sharp and mild (Chapter 3) and the soft (Chapter 4) regime.

⁶Let us note that here strong does not refer to the strong coupling regime, but rather to reductions in c_s that satisfy $1 - c_s < 0.1$.

3

Transient reductions in the speed of sound

In this chapter we will study the observational consequences of a fast evolving speed of sound for the curvature perturbations. This could correspond to inflating in a two-field potential with a sharp turn, as in the left panel of figure 2.4. Transient phenomena during inflation will imply that the predictions for the n -point correlation functions can be modified with respect to the slow-roll predictions shown in Chapter 1. This will demand adopting new techniques both for calculating the observables and for testing the predictions against the CMB data.

First, we apply, compare and extend different techniques for calculating both the power spectrum and bispectrum, based on applying perturbation theory to the Hamiltonian or to the equations of motion. We further check for the possibility that some of the anomalous features found in the Planck data have a common physical origin in a transient reduction of the inflaton speed of sound. We do this by exploiting predicted correlations between the power spectrum and bispectrum. Our results suggest that current data might already be sensitive enough to detect transient reductions in the speed of sound as mild as a few percent. Since this is a signature of interactions, it opens a new window for the detection of extra degrees of freedom during inflation.

This chapter is based on the following two papers:

- *Inflation with moderately sharp features in the speed of sound: Generalized slow roll and in-in formalism for power spectrum and bispectrum*,
A. Achucarro, V. Atal, B. Hu, P. Ortiz and J. Torrado, Phys. Rev. D **90** (2014) 2, 023511 [arXiv:1404.7522 [astro-ph.CO]].

- “*Localized correlated features in the CMB power spectrum and primordial bispectrum from a transient reduction in the speed of sound,*”,
A. Achúcarro, V. Atal, P. Ortiz and J. Torrado, Phys. Rev. D **89** (2014) 10, 103006 [arXiv:1311.2552 [astro-ph.CO]].

We have also enlarged the discussion made in these papers in order to contrast our results with the new data analysis of the Planck collaboration.

3.1 Introduction

As we have previously discussed, when an additional heavy field can be consistently integrated out [80, 81, 92, 101–103] (see also [51]), inflation is described by an effective single-field theory [34, 80, 81, 101, 104, 105] with a variable speed of sound. In particular, changes in the speed of sound result from derivative couplings, or equivalently, turns in field space [55, 73, 79, 81, 82, 92, 95, 101, 106]. The effect of a variable speed of sound has been analyzed both in the power spectrum [55, 107, 108] (for sudden variations see [109–113]) and bispectrum [108, 114, 115] (see [112, 113] for sudden variations). Transient variations in the speed of sound will produce *oscillatory* and *correlated* features in the correlation functions of the adiabatic curvature perturbation [34, 108, 109, 111, 113, 116–119]. These effects are worth taking into account since an oscillatory component in the correlation functions may improve the fits in comparison with a flat primordial spectra, and because we expect correlations to be very good model selectors.

Apart from reduction in the speed of sound, several other mechanisms during inflation also produce oscillatory features. As first noted in [44], a step in the inflaton potential causes features in the spectra [47–49, 113, 120–126]. Different initial vacuum states (see e.g. [127–130]) or multi-field dynamics [82, 117, 131, 132] may also cause oscillations in the primordial spectra.

Whether an oscillatory primordial power spectrum is preferred in the data is a question that has been asked by several authors. Searches in the CMB power spectrum data have been performed for a variety of scenarios, such as transient slow-roll violations [110, 124, 133–138], superimposed oscillations in the primordial power spectrum [139–145] and more general parametric forms (see [30] and references therein). In addition, the Planck collaboration searched for features in the CMB bispectrum for a number of theoretically motivated templates [40]. In none of these cases the statistical significance of the extended models has been found high enough to claim a detection. Still, it is becoming clear that hints of new physics (if any) are most likely to be detected in the correlation between different observables.

The detection of transients poses some interesting challenges. In particular, the effects of a feature in the potential or a localized change in the speed of sound depend on its *location* (in time or e-folds), its *amplitude* and its *sharpness* (or inverse duration). If transients are too sharp, they can excite higher frequency modes that make the single-field interpretation inconsistent (as extensively discussed in Chapter 2). Notably, some of the best fits found so far in the data for a step feature in the potential [136, 146, 147] falls outside the weakly coupled regime that is implicitly required for its interpretation as a step in the single field potential [97, 98]. On the other hand, if the features are too broad, their signature usually becomes degenerate with cosmological parameters, making their presence difficult to discern. There is however an interesting intermediate regime where the features are mild (small amplitude) and moderately sharp, which makes them potentially detectable in the CMB/LSS data, while they also remain under good theoretical control. This regime is particularly important if the inflaton field excursion is large and can reveal features in the inflationary potential and the presence of other degrees of freedom. At the same time, if slow-roll is the result of a (mildly broken) symmetry that protects the background in the UV completion, the same symmetry might presumably preclude very sharp transients.

In this chapter we first review and enlarge several methods to calculate correlation functions when there are transient phenomena happening during inflaton. Finally, we perform a search for transient reductions in the speed of sound in the CMB data. We do this by exploiting a very simple correlation between power spectrum and bispectrum noted in [108], valid in the mild and sharp regime defined above.

3.2 Moderately sharp variations in the speed of sound: primordial power spectrum and bispectrum

In order to compare any model with data, it is important to develop fast and accurate techniques to compute the relevant observables of the theory, in this case, correlations functions of the adiabatic curvature perturbation. The calculation of correlation functions is often rather complicated and the use of approximate methods is needed. The study of transients often involves deviations from slow-roll and may be analysed in the generalized slow-roll (GSR) formalism [110, 113, 114, 119, 148–152]. This approach is based on solving the equations of motion iteratively using Green’s functions method. This formalism can cope with general situations with both slow-roll and speed of sound

features, but one usually needs to impose extra hierarchies between the different parameters to obtain simple analytic solutions.

A notable exception that is theoretically well understood is a transient, mild, and moderately sharp reduction in the speed of sound. They are better defined as those for which the effects coming from a varying speed of sound are small enough to be treated at linear order, but large enough to dominate over the slow-roll corrections. This carries an implicit assumption of uninterrupted slow-roll¹. We will show that this regime ensures the validity of the effective single-field theory, even though our analysis is blind to the underlying inflationary model. In this regime, an alternative approach is possible, that makes the correlation between power spectrum and bispectrum manifest [108]. This approach is based on applying perturbation theory at the level of the Hamiltonian for both the power spectrum and bispectrum. The change in the power spectrum is then simply given by the Fourier transform of the reduction in the speed of sound, and the *complete* bispectrum can be calculated to leading order in slow-roll as a function of the power spectrum. Hence we name this approximation Slow-Roll Fourier Transform (SRFT). One of the aims of this chapter is to compare the GSR and SRFT approaches. In order to do this, we develop simple expressions within the GSR approach and the in-in formalism for computing the changes in the power spectrum and bispectrum due to moderately sharp features in the speed of sound. These are new and extend the usual GSR expressions for very sharp features.

Additionally, we compute the bispectrum. We compute it from the cubic action for the curvature perturbation $\mathcal{R}(t, \mathbf{x})$ using an approximation for sharp features as in [113], but including the next order correction and additional operators. We check that the agreement with the SRFT result [108] is excellent. An important point we show is that the contributions to the bispectrum arising from the terms proportional to $(1 - c_s^{-2})$ and s in the cubic action are of the same order, *independently of the sharpness of the feature*. We also eliminate the small discrepancy found in [113] between their bispectrum and the one obtained with GSR [124] for step features in the scalar potential, due to a missing term in the bispectrum.

Our starting point is the action for the adiabatic curvature perturbation $\mathcal{R}(t, \mathbf{x})$. In the framework of the effective field theory (EFT) of inflation [34], this is directly linked to the effective action for the Goldstone boson of time diffeomorphisms $\pi(t, \mathbf{x})$, via the

¹Here we mean that $\epsilon, \eta \ll 1$. This is not however a necessary condition for making use of the techniques we are presenting, as they can be generalized to the case in which both the speed of sound and the slow roll parameters are subject to transient changes (and hence $\eta > 1$ is allowed) [91]

linear relation² $\mathcal{R} = -H\pi$. Let us focus on a slow-roll regime and write the quadratic and cubic actions for π (as written in Chapter 1):

$$S_2 = \int d^4x a^3 M_{\text{Pl}}^2 \epsilon H^2 \left\{ \frac{\dot{\pi}^2}{c_s^2} - \frac{1}{a^2} (\nabla\pi)^2 \right\}, \quad (3.1)$$

$$S_3 = \int d^4x a^3 M_{\text{Pl}}^2 \epsilon H^2 \left\{ -2Hs c_s^{-2} \pi \dot{\pi}^2 - (1 - c_s^{-2}) \dot{\pi} \left[\dot{\pi}^2 - \frac{1}{a^2} (\nabla\pi)^2 \right] \right\}, \quad (3.2)$$

where $\epsilon = -\dot{H}/H^2$ and we are neglecting higher order slow-roll corrections ($\propto \ddot{H}$). We recall that s parametrizes changes in the speed of sound, $s \equiv \dot{c}_s/c_s H$, and for convenience we define a new variable u as

$$u \equiv 1 - c_s^{-2}. \quad (3.3)$$

In this section we compare the different approaches to evaluating the power spectrum and bispectrum of the adiabatic curvature perturbation from eqs. (3.1) and (3.2) with a variable speed of sound, and show the excellent agreement between them.

3.2.1 Power spectrum and bispectrum with the Slow-Roll Fourier Transform method

Corrections to the two-point function due to a transient reduction in the speed of sound can be calculated using the in-in formalism [153, 154]. We can do it assuming an uninterrupted slow-roll regime, which, as we showed in the Chapter 2, is perfectly consistent with turns along the inflationary trajectory. In order to calculate the power spectrum, we separate the quadratic action (3.1) in a free part and a small perturbation:

$$S_2 = \int d^4x a^3 M_{\text{Pl}}^2 \epsilon H^2 \left\{ \dot{\pi}^2 - \frac{1}{a^2} (\nabla\pi)^2 \right\} - \int d^4x a^3 M_{\text{Pl}}^2 \epsilon H^2 \left\{ \dot{\pi}^2 (1 - c_s^{-2}) \right\}, \quad (3.4)$$

Then, using the in-in formalism, the change in the power spectrum due to a small transient reduction in the speed of sound can be calculated to first order in u , and it is found to be [108]

$$\frac{\Delta \mathcal{P}_{\mathcal{R}}}{\mathcal{P}_{\mathcal{R},0}}(k) = k \int_{-\infty}^0 d\tau u(\tau) \sin(2k\tau), \quad (3.5)$$

where $k \equiv |\mathbf{k}|$, $\mathcal{P}_{\mathcal{R},0} = H^2/(8\pi^2 \epsilon M_{\text{Pl}}^2)$ is the featureless power spectrum with $c_s = 1$, and τ is the conformal time. We made the implicit assumption that the speed of sound approaches to one asymptotically, since we are perturbing around that value³. Here we see that the change in the power spectrum is simply given by the Fourier transform of

²In this work, we do not need to consider non-linear correction terms, since we are in a slow-roll regime. For further details on this, see [37].

³At the level of the power spectrum, the generalization to arbitrary initial and final values of the speed of sound $c_{s,0}$ is straightforward, provided they are sufficiently close to each other.

the reduction in the speed of sound. Notice that the result above is independent of the physical origin of such reduction.

For the three-point function, we take the cubic action (3.2), and calculate the bispectrum at first order in u and s , which implies that we must have $|u|_{\max}, |s|_{\max} \ll 1$ ⁴. We also disregard the typical slow-roll contributions that one expects for a canonical featureless single-field regime [37]. Therefore, for the terms proportional to u and s to give the dominant contribution to the bispectrum, one must require that u and/or s are much larger than the slow-roll parameters, i.e. $\max(u, s) \gg \mathcal{O}(\epsilon, \eta)$. Let us note that eq. (3.5) can be inverted, so that we might write u (or, equivalently c_s) as a function of $\Delta\mathcal{P}_{\mathcal{R}}/\mathcal{P}_{\mathcal{R},0}$. As the bispectrum is a function of c_s as its derivative, we can write the bispectrum as a function of $\Delta\mathcal{P}_{\mathcal{R}}/\mathcal{P}_{\mathcal{R},0}$. Using again the in-in formalism, one finds [108]:

$$\begin{aligned} \Delta B_{\mathcal{R}}(\mathbf{k}_1, \mathbf{k}_2, \mathbf{k}_3) = & \frac{(2\pi)^4 \mathcal{P}_{\mathcal{R},0}^2}{(k_1 k_2 k_3)^2} \left\{ -\frac{3}{2} \frac{k_1 k_2}{k_3} \left[\frac{1}{2k} \left(1 + \frac{k_3}{2k} \right) \frac{\Delta\mathcal{P}_{\mathcal{R}}}{\mathcal{P}_{\mathcal{R},0}} - \frac{k_3}{4k^2} \frac{d}{d \log k} \left(\frac{\Delta\mathcal{P}_{\mathcal{R}}}{\mathcal{P}_{\mathcal{R},0}} \right) \right] \right. \\ & + 2 \text{ perm} + \frac{1}{4} \frac{k_1^2 + k_2^2 + k_3^2}{k_1 k_2 k_3} \left[\frac{1}{2k} \left(4k^2 - k_1 k_2 - k_2 k_3 - k_3 k_1 - \frac{k_1 k_2 k_3}{2k} \right) \frac{\Delta\mathcal{P}_{\mathcal{R}}}{\mathcal{P}_{\mathcal{R},0}} \right. \\ & \left. \left. - \frac{k_1 k_2 + k_2 k_3 + k_3 k_1}{2k} \frac{d}{d \log k} \left(\frac{\Delta\mathcal{P}_{\mathcal{R}}}{\mathcal{P}_{\mathcal{R},0}} \right) + \frac{k_1 k_2 k_3}{4k^2} \frac{d^2}{d \log k^2} \left(\frac{\Delta\mathcal{P}_{\mathcal{R}}}{\mathcal{P}_{\mathcal{R},0}} \right) \right] \right\} \Bigg|_{k=\frac{1}{2} \sum_i k_i}, \quad (3.6) \end{aligned}$$

where $k_i \equiv |\mathbf{k}_i|$, $k \equiv (k_1 + k_2 + k_3)/2$, and $\Delta\mathcal{P}_{\mathcal{R}}/\mathcal{P}_{\mathcal{R},0}$ and its derivatives are evaluated at k . From the result above it is clear how features in the power spectrum seed correlated features in the bispectrum. Note that in the squeezed limit ($k_1 \rightarrow 0, k_2 = k_3 = k$) one recovers the single-field consistency relation [37, 155].

In the following sections, we compute the power spectrum and bispectrum using alternative methods and compare the results.

3.2.2 Power spectrum in the GSR formalism

Instead of applying perturbation theory at the level of the Hamiltonian (as we do in the in-in formalism), one can calculate the power spectrum by solving iteratively the full equations of motion (first in [148, 149] and further developed in [107, 114, 119, 124, 150, 151]). The idea is to consider the Mukhanov-Sasaki equation of motion with a

⁴This is a conservative choice, values of $s > 1$ might be consistent with perturbativity, as discussed in Chapter 2

time-dependent speed of sound. We recall it from eq. (1.41), namely:

$$\frac{d^2 v_{\mathbf{k}}(\tau)}{d\tau^2} + \left(c_s^2 k^2 - \frac{1}{z} \frac{d^2 z}{d\tau^2} \right) v_{\mathbf{k}}(\tau) = 0, \quad (3.7)$$

with $v = z\mathcal{R}$, $z^2 = 2a^2\epsilon c_s^{-2}$ and

$$\frac{1}{z} \frac{d^2 z}{d\tau^2} = a^2 H^2 \left[2 + 2\epsilon - 3\tilde{\eta} - 3s + 2\epsilon(\epsilon - 2\tilde{\eta} - s) + s(2\tilde{\eta} + 2s - t) + \tilde{\eta}\tilde{\xi} \right], \quad (3.8)$$

where we have used the following relations:

$$\epsilon = -\frac{\dot{H}}{H^2}, \quad \tilde{\eta} = \epsilon - \frac{\dot{\epsilon}}{2H\epsilon}, \quad s = \frac{\dot{c}_s}{Hc_s}, \quad t = \frac{\ddot{c}_s}{H\dot{c}_s}, \quad \tilde{\xi} = \epsilon + \tilde{\eta} - \frac{\dot{\tilde{\eta}}}{H\tilde{\eta}}, \quad (3.9)$$

and here the dot denotes the derivative with respect to cosmic time. Defining a new time variable $d\tau_c = c_s d\tau$ and a rescaled field $y = \sqrt{2k c_s} v$, the above equation can be written in the form:

$$\frac{d^2 y}{d\tau_c^2} + \left(k^2 - \frac{2}{\tau_c^2} \right) y = \frac{g(\ln \tau_c)}{\tau_c^2} y, \quad (3.10)$$

where

$$g \equiv \frac{f'' - 3f'}{f}, \quad f = 2\pi z c_s^{1/2} \tau_c, \quad (3.11)$$

and $'$ denotes derivatives with respect to $\ln \tau_c$. Throughout this section (and only in this section), unless explicitly indicated, we will adopt the convention of positive conformal time ($\tau, \tau_c \geq 0$) in order to facilitate comparison with [107, 151]. Note that g encodes all the information with respect to features in the background. In this sense, setting g to zero represents solving the equation of motion for a perfect de Sitter universe, where the solution to the mode function is well known. Considering the r.h.s. of equation (3.10) as an external source, a solution to the mode function can be written in terms of the homogeneous solution. In doing so, we need to expand the mode function in the r.h.s. as the homogeneous solution plus deviations and then solve iteratively. To first order, the contribution to the power spectrum is of the form [151]:

$$\ln \mathcal{P}_{\mathcal{R}} = \ln \mathcal{P}_{\mathcal{R},0} + \int_{-\infty}^{\infty} d \ln \tau_c W(k\tau_c) G'(\tau_c), \quad (3.12)$$

where the logarithmic derivative of the source function G reads:

$$G' = -2(\ln f)' + \frac{2}{3}(\ln f)'', \quad (3.13)$$

and the window function W and its logarithmic derivative (used below) are given by

$$W(x) = \frac{3 \sin(2x)}{2x^3} - \frac{3 \cos(2x)}{x^2} - \frac{3 \sin(2x)}{2x}, \quad (3.14)$$

$$W'(x) \equiv \frac{dW(x)}{d \ln x} = \left(-3 + \frac{9}{x^2}\right) \cos(2x) + \left(\frac{15}{2x} - \frac{9}{2x^3}\right) \sin(2x). \quad (3.15)$$

If we consider moderately sharp features in the speed of sound, such that $\epsilon, \tilde{\eta} \ll s, t$, the leading contribution to the function G' is the following:

$$G' = -\frac{2}{3}s + \frac{2}{3} \left(\frac{aH\tau_c}{c_s} - 1\right)^2 + \frac{2}{3} \left(\frac{aH\tau_c}{c_s} - 1\right) (4 - s) + \frac{1}{3} \left(\frac{aH\tau_c}{c_s}\right)^2 s (-3 + 2s - t), \quad (3.16)$$

where t is defined in (3.9). Moreover, when $|s| \ll 1$ but $t \gtrsim \mathcal{O}(1)$, the logarithmic derivative of G is approximately given by:

$$G' \simeq s - \frac{\dot{s}}{3H}, \quad (3.17)$$

where we have used that $aH\tau_c/c_s \simeq 1 + s$. This result agrees with the results of [107] in the mentioned limits. In this approximation, the leading contribution to the power spectrum is:

$$\ln \mathcal{P}_{\mathcal{R}} \simeq \ln \mathcal{P}_{\mathcal{R},0} + \int_{-\infty}^{\infty} d \ln \tau_c \left[W(k\tau_c) s(\tau_c) - \frac{1}{3} W(k\tau_c) \frac{ds}{d \ln \tau_c} \right]. \quad (3.18)$$

Integrating by parts the term proportional to the derivative of s we obtain:

$$\begin{aligned} \ln \mathcal{P}_{\mathcal{R}} &\simeq \ln \mathcal{P}_{\mathcal{R},0} + \int_{-\infty}^{\infty} d \ln \tau_c \left[W(k\tau_c) + \frac{1}{3} W'(k\tau_c) \right] s(\tau_c) \\ &= \ln \mathcal{P}_{\mathcal{R},0} + \int_{-\infty}^{\infty} d \ln \tau_c \left[\frac{\sin(2k\tau_c)}{k\tau_c} - \cos(2k\tau_c) \right] s(\tau_c). \end{aligned} \quad (3.19)$$

This is the result that we will later on compare with the SRFT result given in equation (3.5). Let us recall that the regime in which this expression has been derived is for moderately sharp reductions such that $\mathcal{O}(\epsilon, \eta) \ll s \ll 1$ and $t \gtrsim \mathcal{O}(1)$. We would like to point out that the s term in the source function (3.17) provides the dominant contribution to the power spectrum on large scales. This can be seen by comparing W and W' in eqs. (3.19), which carry the contribution of s and \dot{s} , respectively. We will later show that when including this term, the power spectrum at large scales matches the numerical solution considerably better (see figure 3.3).

In the following, we will: **(i)** derive an analytic expression for the power spectrum as in (3.19) solely in terms of c_s in order to connect with the SRFT approach. **(ii)** Find

an analytic approximation for arbitrary functional forms of the speed of sound in the moderately sharp regime specified above.

(i) For the first point, one can integrate by parts (3.19) in order to get a formula than only involves the speed of sound. Doing so, we obtain:

$$\ln \mathcal{P}_{\mathcal{R}} = \ln \mathcal{P}_{\mathcal{R},0} - \int_{-\infty}^{\infty} d \ln \tau_c \left[2 \cos(2k\tau_c) - \frac{\sin(2k\tau_c)}{k\tau_c} + 2k\tau_c \sin(2k\tau_c) \right] \ln c_s(\tau_c) , \quad (3.20)$$

where we have used that $s \simeq d \ln c_s / d \ln \tau_c$ and that the asymptotic value of the speed of sound is one, otherwise the boundary term would not vanish. Therefore, the expression above is only valid for functional forms of the speed of sound that satisfy $c_s(\tau = 0) = c_s(\tau = \infty) = 1$. Let us restrict our attention to mild reductions of the speed of sound $|u| = |1 - c_s^{-2}| \ll 1$, in which the SRFT approach is operative. In that case, for mild and moderately sharp reductions, the time τ_c is very well approximated by $\tau_c \simeq \tau$. Furthermore, the logarithmic term of the speed of sound can be expanded as follows:

$$\ln c_s(\tau) \simeq \frac{1}{2} (1 - c_s^{-2}(\tau)) + \mathcal{O}(u^2) . \quad (3.21)$$

Using the expansion above and the fact that $\ln(\mathcal{P}_{\mathcal{R}}/\mathcal{P}_{\mathcal{R},0}) = \ln(1 + \Delta\mathcal{P}_{\mathcal{R}}/\mathcal{P}_{\mathcal{R},0}) \simeq \Delta\mathcal{P}_{\mathcal{R}}/\mathcal{P}_{\mathcal{R},0}$, we can write:

$$\begin{aligned} \frac{\Delta\mathcal{P}_{\mathcal{R}}}{\mathcal{P}_{\mathcal{R},0}} &\simeq k \int_{-\infty}^0 d\tau (1 - c_s^{-2}) \left[\sin(2k\tau) + \frac{1}{k\tau} \cos(2k\tau) - \frac{1}{2k^2\tau^2} \sin(2k\tau) \right] \quad (3.22) \\ &\simeq \begin{cases} \frac{\Delta\mathcal{P}_{\mathcal{R}}}{\mathcal{P}_{\mathcal{R},0}} \Big|_{\text{SRFT}} + \mathcal{O}[(k\tau)^2] , & k\tau \ll 1 \\ \frac{\Delta\mathcal{P}_{\mathcal{R}}}{\mathcal{P}_{\mathcal{R},0}} \Big|_{\text{SRFT}} + \mathcal{O}[(k\tau)^{-1}] , & k\tau \gg 1 \end{cases} \end{aligned}$$

where we have already returned to negative conformal time. Notice that when $k\tau \ll 1$ we retrieve the SRFT expression (3.5) with a subleading correction $\mathcal{O}(k\tau)$ inside the integral, and that for $k\tau \gg 1$ we also retrieve the SRFT result. The regime $k\tau \sim 1$ will generally involve large scales, where the change in the power spectrum is small, as can be seen in figure 3.3.

(ii) In what follows we derive an analytic approximation to the power spectrum (3.19) for *generic* forms of the speed of sound, provided they are moderately sharp, i.e. $\mathcal{O}(\epsilon, \eta) \ll s \ll 1$ and $t \gtrsim \mathcal{O}(1)$. As in (i), in this regime we can safely consider $\tau_c \simeq c_{s,0}\tau$. Let us drop the rest of assumptions made in point (i), which were only made to establish connection with the SRFT approach. We define the function $X(k\tau_c) \equiv -W'(k\tau_c) -$

$3W(k\tau_c)$, which in general can be decomposed as follows:

$$X(kc_{s,0}\tau) = p_c(kc_{s,0}\tau) \cos(2kc_{s,0}\tau) + p_s(kc_{s,0}\tau) \sin(2kc_{s,0}\tau) , \quad (3.23)$$

where p_c and p_s denote the polynomials multiplying the cosine and sine, respectively. Following [113], we will parametrize c_s^2 in terms of the height σ_* and the sharpness β_s of the feature, and a function F describing the shape of the variation of the speed of sound:

$$c_s^2(\tau) = c_{s,0}^2 \left[1 - \sigma_* F \left(-\beta_s \ln \frac{\tau}{\tau_f} \right) \right] , \quad (3.24)$$

where τ_f is the characteristic time of the feature and we take $\sigma_* \ll 1$ to focus on small variations. The rate of change in the speed of sound can be written at first order in σ_* as follows:

$$s(\tau) = -\frac{1}{2} \sigma_* \beta_s F' \left(-\beta_s \ln \frac{\tau}{\tau_f} \right) + \mathcal{O}(\sigma_*^2) , \quad (3.25)$$

where $'$ denotes the derivative with respect to the argument. Since we are considering sharp features happening around the time τ_f , the functions involved in the integral of equation (3.19) will only contribute for values in the neighborhood of τ_f . Note that for polynomials with negative powers of $k\tau$, the approximation of evaluating them at $k\tau_f$ fails for small values of $k\tau$, since in that region they vary very rapidly. This may cause infrared divergences in the spectrum which, as we will see, can be cured by approximating the polynomials to first order around $k\tau_f$.

First, we define the variable $y \equiv -\beta_s \ln(\tau/\tau_f)$, and we expand the functions around $\tau = \tau_f$, which is equivalent to $y/\beta_s \ll 1$. Then, at first order, the expansion of X in (3.23) reads:

$$\begin{aligned} X(kc_{s,0}\tau) \simeq & \left[p_c(kc_{s,0}\tau_f) - y \frac{k\tau_f}{\beta_s} \frac{dp_c}{d(k\tau)} \Big|_{\tau_f} \right] \cos \left[2kc_{s,0}\tau_f \left(1 - \frac{y}{\beta_s} \right) \right] \\ & + \left[p_s(kc_{s,0}\tau_f) - y \frac{k\tau_f}{\beta_s} \frac{dp_s}{d(k\tau)} \Big|_{\tau_f} \right] \sin \left[2kc_{s,0}\tau_f \left(1 - \frac{y}{\beta_s} \right) \right] . \end{aligned} \quad (3.26)$$

Substituting in (3.19) the above expansion and the definition of s (3.25), the change in the power spectrum is given by:

$$\begin{aligned} \frac{\Delta \mathcal{P}_{\mathcal{R}}}{\mathcal{P}_{\mathcal{R},0}} = & \frac{\sigma_*}{6} \left\{ \left[p_c \cos(2kc_{s,0}\tau_f) + p_s \sin(2kc_{s,0}\tau_f) \right] \int_{-\infty}^{\infty} dy \cos\left(\frac{2kc_{s,0}\tau_f}{\beta_s} y\right) F'(y) \right. \\ & + \left[p_c \sin(2kc_{s,0}\tau_f) - p_s \cos(2kc_{s,0}\tau_f) \right] \int_{-\infty}^{\infty} dy \sin\left(\frac{2kc_{s,0}\tau_f}{\beta_s} y\right) F'(y) \\ & - \frac{k\tau_f}{\beta_s} \left[\left. \frac{dp_s}{d(k\tau)} \right|_{\tau_f} \sin(2kc_{s,0}\tau_f) + \left. \frac{dp_c}{d(k\tau)} \right|_{\tau_f} \cos(2kc_{s,0}\tau_f) \right] \int_{-\infty}^{\infty} dy \cos\left(\frac{2kc_{s,0}\tau_f}{\beta_s} y\right) y F'(y) \\ & \left. + \frac{k\tau_f}{\beta_s} \left[\left. \frac{dp_s}{d(k\tau)} \right|_{\tau_f} \cos(2kc_{s,0}\tau_f) - \left. \frac{dp_c}{d(k\tau)} \right|_{\tau_f} \sin(2kc_{s,0}\tau_f) \right] \int_{-\infty}^{\infty} dy \sin\left(\frac{2kc_{s,0}\tau_f}{\beta_s} y\right) y F'(y) \right\}. \end{aligned}$$

Note that the integrals above are the Fourier transforms of the symmetric and antisymmetric parts of the derivative of the shape function $F = F(y)$. We define the envelope functions resulting from these integrals as follows:

$$\int dy \cos\left(\frac{2kc_{s,0}\tau_f}{\beta_s} y\right) F' \equiv \frac{1}{2} \mathcal{D}_A, \quad \int dy y F' \cos\left(\frac{2kc_{s,0}\tau_f}{\beta_s} y\right) = \frac{\beta_s}{4c_{s,0}\tau_f} \frac{d}{dk} \mathcal{D}_S \quad (3.27)$$

$$\int dy \sin\left(\frac{2kc_{s,0}\tau_f}{\beta_s} y\right) F' \equiv \frac{1}{2} \mathcal{D}_S, \quad \int dy y F' \sin\left(\frac{2kc_{s,0}\tau_f}{\beta_s} y\right) = -\frac{\beta_s}{4c_{s,0}\tau_f} \frac{d}{dk} \mathcal{D}_A, \quad (3.28)$$

where \mathcal{D}_S and \mathcal{D}_A are the envelope functions corresponding to the symmetric and anti-symmetric parts of F , respectively. Finally, the change in the power spectrum can be written as:

$$\begin{aligned} \frac{\Delta \mathcal{P}_{\mathcal{R}}}{\mathcal{P}_{\mathcal{R},0}} = & \frac{\sigma_*}{12} \left\{ \left[p_c \cos(2kc_{s,0}\tau_f) + p_s \sin(2kc_{s,0}\tau_f) \right] \mathcal{D}_A + \left[p_c \sin(2kc_{s,0}\tau_f) - p_s \cos(2kc_{s,0}\tau_f) \right] \mathcal{D}_S \right\} \\ & - \frac{\sigma_*}{24c_{s,0}} \left\{ \left[\left. \frac{dp_s}{d(k\tau)} \right|_{\tau_f} \sin(2kc_{s,0}\tau_f) + \left. \frac{dp_c}{d(k\tau)} \right|_{\tau_f} \cos(2kc_{s,0}\tau_f) \right] k \frac{d}{dk} \mathcal{D}_S \right. \\ & \left. + \left[\left. \frac{dp_s}{d(k\tau)} \right|_{\tau_f} \cos(2kc_{s,0}\tau_f) - \left. \frac{dp_c}{d(k\tau)} \right|_{\tau_f} \sin(2kc_{s,0}\tau_f) \right] k \frac{d}{dk} \mathcal{D}_A \right\} \quad (3.29) \end{aligned}$$

Let us stress that the contributions from the second and third lines are comparable to the ones in the first line. The infrared limit of the symmetric part is finite and tends to zero, which would not have been the case if we had only considered the zeroth order terms (first line). We will now substitute the values of the polynomials for the particular regime we are analyzing, $p_c = 1/3$ and $p_s = -1/(3kc_{s,0}\tau)$. In this case, the change in

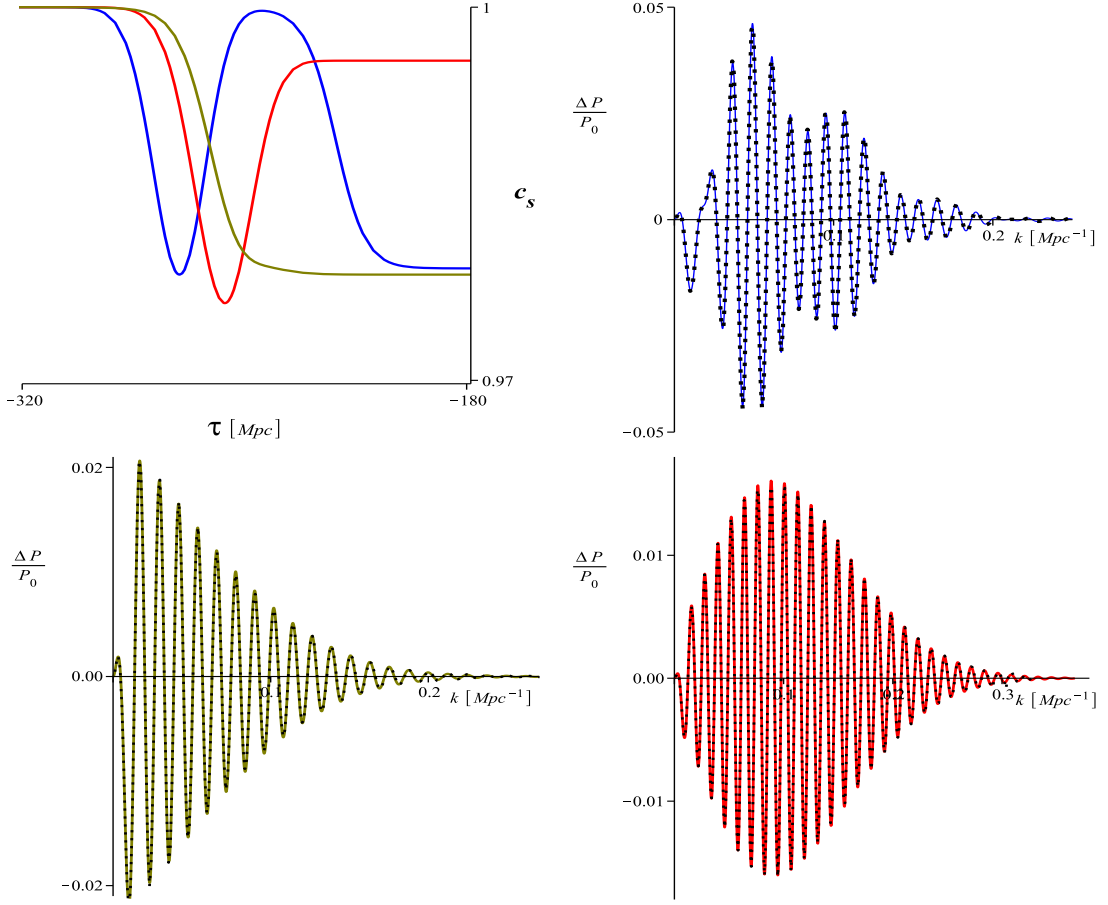


FIGURE 3.1: Speed of sound as defined in (3.31) for three different values of the parameters. We show the power spectra calculated with the full integral (3.19) (dotted line) and with the approximation (3.29) (solid line). The parameters, for the blue, olive and red figures, are respectively given by: $A = [-0.021, -0.0215, -0.0043]$, $B = [-0.043, -0.0086, -0.043]$, $\alpha^2 = [\exp(6.3), \exp(6.3), \exp(7)]$, $\beta_s^2 = [\exp(6.3), \exp(6.3), \exp(7)]$, $\tau_{0_g} = [-\exp(5.6), -\exp(5.55), -\exp(5.55)]$, $\tau_{0_t} = [-\exp(5.4), -\exp(5.55), -\exp(5.55)]$. For the first set of parameters the symmetric and antisymmetric parts have comparable magnitude, while for the second (third) set of parameters the antisymmetric (symmetric) part dominates. As can be seen by the very good agreement between the full integral and the approximation, the chosen parameters are all of them in the sharp feature regime.

the power spectrum reads:

$$\begin{aligned} \frac{\Delta \mathcal{P}_{\mathcal{R}}}{\mathcal{P}_{\mathcal{R},0}} = & \frac{\sigma_*}{36} \left\{ \left[\cos(2kc_{s,0}\tau_f) - \frac{\sin(2kc_{s,0}\tau_f)}{kc_{s,0}\tau_f} \right] \mathcal{D}_A + \left[\sin(2kc_{s,0}\tau_f) + \frac{\cos(2kc_{s,0}\tau_f)}{kc_{s,0}\tau_f} \right] \mathcal{D}_S \right\} \\ & - \frac{\sigma_*}{72} \left\{ \left[\frac{\sin(2kc_{s,0}\tau_f)}{(kc_{s,0}\tau_f)^2} \right] k \frac{d}{dk} \mathcal{D}_S + \left[\frac{\cos(2kc_{s,0}\tau_f)}{(kc_{s,0}\tau_f)^2} \right] k \frac{d}{dk} \mathcal{D}_A \right\}. \end{aligned} \quad (3.30)$$

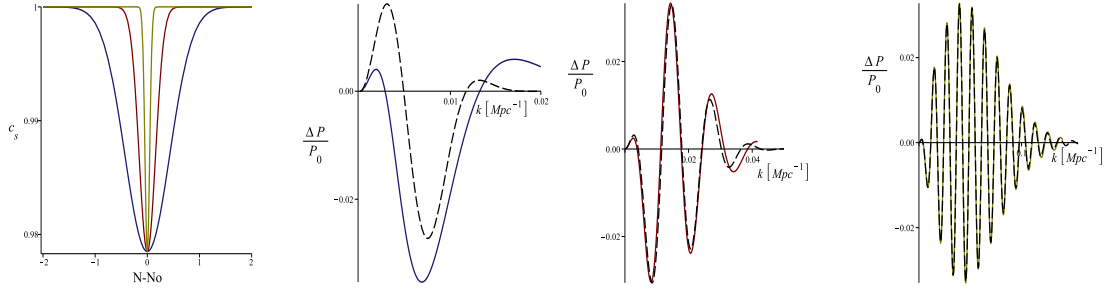


FIGURE 3.2: Here we test when the approximation (3.29) starts to break down. The full integral (3.19) is represented by dashed lines while the approximation (3.29) is given by solid lines. We take $A = 0$, $B = -0.043$, $\tau_{0g} = -\exp(5.55)$ for the three profiles of the speed of sound, and $\beta_g = [\exp(1), \exp(3), \exp(11/2)]$ for the blue, red and olive figures respectively. We see that the approximation starts to fail for features with $\Delta N \gtrsim 1$.

3.2.2.1 Test for generic variations in the speed of sound

In this section we will test the sharp feature approximation (3.29) in comparison with the full integral (3.19). We explicitly decompose c_s^2 into its symmetric and antisymmetric parts. We choose the following functional form for c_s

$$c_s^2 = 1 + A \left[1 - \tanh \left(\alpha \ln \frac{\tau}{\tau_{0t}} \right) \right] + B \exp \left[-\beta_s^2 \left(\ln \frac{\tau}{\tau_{0g}} \right)^2 \right] \\ = \left\{ 1 + A + B \exp \left[-\beta_s^2 \left(\ln \frac{\tau}{\tau_{0g}} \right)^2 \right] \right\}_S + \left\{ -A \tanh \left(\alpha \ln \frac{\tau}{\tau_{0t}} \right) \right\}_A. \quad (3.31)$$

From the definitions given in eqs. (3.24) and (3.27), the envelope functions are given by

$$\mathcal{D}_A = -\frac{4\pi A k \tau_{0t}}{\sigma_*} \frac{1}{\alpha \sinh(\pi k \tau_{0t}/\alpha)} \quad , \quad \mathcal{D}_S = \frac{4\sqrt{\pi} B k \tau_{0g}}{\sigma_* \beta_s} \exp \left(-\frac{k^2 \tau_{0g}^2}{\beta_s^2} \right). \quad (3.32)$$

Since the symmetric and antisymmetric parts do not necessarily peak at the same time, the integrands involved in each part take values around τ_{0g} and τ_{0t} , respectively. We test our approximation for different values of the parameters above, and show our results in figure 3.1. We can see that the approximation is indeed very good, and that it allows to reproduce highly non-trivial power spectra. By allowing β_s and/or α to be small, we can see where the approximation starts to fail. We show these results in figure 3.2, where one can see that for features with $\Delta N \gtrsim 1$ the approximation breaks down.

3.2.3 Comparison of power spectra

In this section we apply both SRFT and GSR methods for moderately sharp reductions to calculate the change in the power spectrum, and compare them with the power

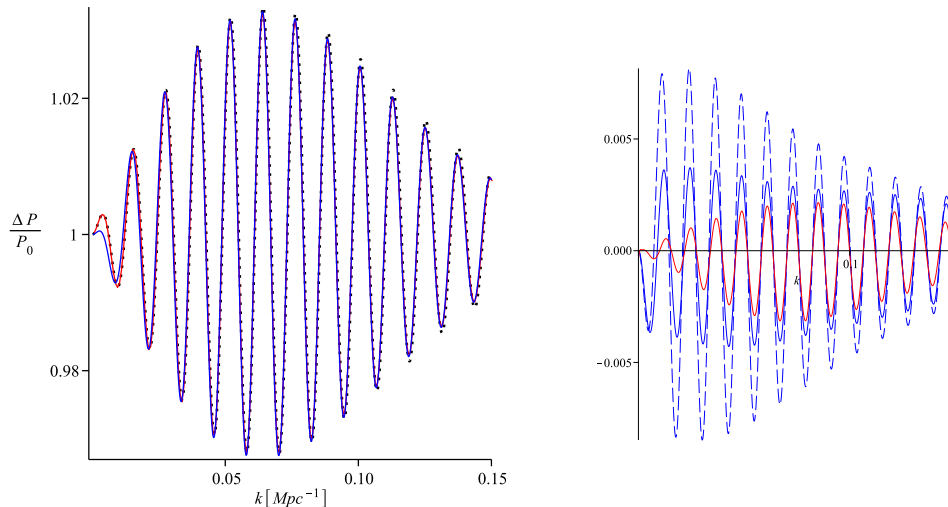


FIGURE 3.3: Change in the power spectrum due to a reduced speed of sound given by (3.33), with the following choice of parameters: $B = -0.043$, $\beta_s = 23.34$, $\ln(\tau_f) = 5.55$, corresponding to one of our best fits to the Planck CMB power spectrum [156]. LEFT: different methods to compute the primordial power spectrum: GSR in the sharp feature approach (blue), SRFT (red), and a solution obtained from the numerical solution to the mode equation (3.7) (black dotted). RIGHT: differences of the GSR sharp feature method (solid blue) and SRFT (red) against the numerical solution. The dashed blue line is the GSR sharp feature approach if we had not taken into account the term proportional to s in the source function (3.17). The numerical solution is calculated choosing $\epsilon \simeq 1.25 \times 10^{-4}$ and $\tilde{\eta} \simeq -0.02$. Higher values of ϵ need a proper accounting for the slow-roll corrections.

spectrum calculated from the numerical solution to the mode equation (3.7). We will test a reduction in the speed of sound purely symmetric in the variable $y = -\beta_s \ln(\tau/\tau_f)$:

$$u = 1 - c_s^{-2} = B e^{-\beta_s^2 (N - N_f)^2} = B e^{-\beta_s^2 \left(\ln \frac{\tau}{\tau_f}\right)^2}. \quad (3.33)$$

In figure 3.3 we show the comparison between the power spectrum coming from the GSR result (3.29) with the one coming from the SRFT method (3.5), and with a numerical solution. In general terms, both methods are in good agreement with the numerical solution. We also note that at large scales the SRFT method reproduces the numerical results better than the GSR method. This is partly due to the fact that in the GSR approximation we have only taken a subset of the terms in the source function. The agreement would have been much worse if we had not taken into account the term proportional to s , as the dashed line in the right plot of figure 3.3 indicates. Note that $k\tau_f \sim 1$ corresponds to the first peak in the left plot of figure 3.3, precisely the regime where we expect a discrepancy, as anticipated in eq. (3.23).

This shows that, in the regime of moderately sharp variations of the speed of sound, the simple SRFT formula (3.5) is capable of reproducing the effect of *all* the terms in the equation of motion, and that there is no need to impose any further hierarchy between

the different terms of the equation of motion in order to have a simple expression, as long as slow-roll is uninterrupted.

3.2.4 Bispectrum for moderately sharp reductions

In this section we will compute the change in the bispectrum due to moderately sharp reductions in the speed of sound using the in-in formalism. Instead of the SRFT method reviewed in section 3.2.1, we will compute the bispectrum using an approximation based on sharp features [113], as for the power spectrum. Our starting point is the cubic action in the effective field theory of inflation, where we will only take into account the contribution from variations in the speed of sound at first order:

$$S_3 = \int d^4x a^3 M_{\text{Pl}}^2 \frac{\epsilon}{H} \left\{ 2Hsc_s^{-2} \mathcal{R} \dot{\mathcal{R}}^2 + (1 - c_s^{-2}) \dot{\mathcal{R}} \left[\dot{\mathcal{R}}^2 - \frac{1}{a^2} (\nabla \mathcal{R})^2 \right] \right\}, \quad (3.34)$$

with $\mathcal{R} = -\pi H$. For sharp features ($\beta_s \gg 1$) and given the parametrization in (3.24) and (3.25), one is tempted to think that the contribution of s will dominate over the contribution of $(1 - c_s^{-2})$. However, we will show that the contributions arising from both terms are of the same order, *independently of the sharpness* β_s . As dictated by the in-in formalism, the three-point correlation function reads:

$$\begin{aligned} \langle \mathcal{R}_{\mathbf{k}_1} \mathcal{R}_{\mathbf{k}_2} \mathcal{R}_{\mathbf{k}_3} \rangle = & \left\langle \text{Re} \left\{ 2i \mathcal{R}_{\mathbf{k}_1}(0) \mathcal{R}_{\mathbf{k}_2}(0) \mathcal{R}_{\mathbf{k}_3}(0) \int_{-\infty}^0 d\tau \int d^3x a^4 M_{\text{Pl}}^2 \frac{\epsilon}{H} \left[2Hsc_s^{-2} \mathcal{R} \dot{\mathcal{R}}^2 \right. \right. \right. \\ & \left. \left. \left. + (1 - c_s^{-2}) \dot{\mathcal{R}}^3 - H^2 \tau^2 (1 - c_s^{-2}) \dot{\mathcal{R}} (\nabla \mathcal{R})^2 \right] \right\} \right\rangle \end{aligned}$$

Expressing the functions $\mathcal{R}(\tau, \mathbf{x})$ in Fourier space and using the Wick theorem, we obtain

$$\begin{aligned} \langle \mathcal{R}_{\mathbf{k}_1} \mathcal{R}_{\mathbf{k}_2} \mathcal{R}_{\mathbf{k}_3} \rangle = & \text{Re} \left\{ 2i u_{\mathbf{k}_1}^0 u_{\mathbf{k}_2}^0 u_{\mathbf{k}_3}^0 \int_{-\infty}^0 \frac{d\tau}{\tau^2} \frac{\epsilon M_{\text{Pl}}^2}{H^2} (2\pi)^3 \int d^3q_1 \int d^3q_2 \int d^3q_3 \delta(\mathbf{q}_1 + \mathbf{q}_2 + \mathbf{q}_3) \right. \\ & \times \left[4sc_s^{-2} u_{\mathbf{q}_1}^*(\tau) u_{\mathbf{q}_2}^{*'}(\tau) u_{\mathbf{q}_3}^{*'}(\tau) \left(\delta(\mathbf{k}_1 - \mathbf{q}_1) \delta(\mathbf{k}_2 - \mathbf{q}_2) \delta(\mathbf{k}_3 - \mathbf{q}_3) + \{\mathbf{k}_1 \leftrightarrow \mathbf{k}_2\} + \{\mathbf{k}_1 \leftrightarrow \mathbf{k}_3\} \right) \right. \\ & - 6\tau (1 - c_s^{-2}) u_{\mathbf{q}_1}^{*'}(\tau) u_{\mathbf{q}_2}^{*'}(\tau) u_{\mathbf{q}_3}^{*'}(\tau) \delta(\mathbf{k}_1 - \mathbf{q}_1) \delta(\mathbf{k}_2 - \mathbf{q}_2) \delta(\mathbf{k}_3 - \mathbf{q}_3) \\ & - 2\tau (1 - c_s^{-2}) (\mathbf{q}_2 \cdot \mathbf{q}_3) u_{\mathbf{q}_1}^{*'}(\tau) u_{\mathbf{q}_2}^*(\tau) u_{\mathbf{q}_3}^*(\tau) \left(\delta(\mathbf{k}_1 - \mathbf{q}_1) \delta(\mathbf{k}_2 - \mathbf{q}_2) \delta(\mathbf{k}_3 - \mathbf{q}_3) \right. \\ & \left. \left. \left. + \{\mathbf{k}_1 \leftrightarrow \mathbf{k}_2\} + \{\mathbf{k}_1 \leftrightarrow \mathbf{k}_3\} \right) \right] \right\}, \end{aligned}$$

where $u_{\mathbf{k}_1}^0 \equiv u_{\mathbf{k}_1}(0)$. For the leading order contribution, it suffices to use the zeroth-order mode function

$$u_{\mathbf{k}}(\tau) = \frac{iH}{\sqrt{4\epsilon c_{s,0} k^3}} (1 + ikc_{s,0}\tau) e^{-ikc_{s,0}\tau}, \quad (3.37)$$

and the three-point correlation function is then:

$$\begin{aligned} \langle \mathcal{R}_{\mathbf{k}_1} \mathcal{R}_{\mathbf{k}_2} \mathcal{R}_{\mathbf{k}_3} \rangle &= \frac{\mathcal{P}_{\mathcal{R},0}^2 (2\pi)^7 M_{\text{Pl}}^6}{8k_1^3 k_2^3 k_3^3} \delta(\mathbf{k}_1 + \mathbf{k}_2 + \mathbf{k}_3) \int_{-\infty}^0 d\tau \left\{ \cos(Kc_{s,0}\tau) \right. \\ &\times \left[4sc_s^{-2} c_{s,0}^3 \tau k_1 k_2 k_3 (k_1 k_2 + 2 \text{ perm}) - 2\tau c_{s,0} (1 - c_s^{-2}) [k_1^2 (k_2 + k_3)(\mathbf{k}_2 \cdot \mathbf{k}_3) + 2 \text{ perm}] \right] \\ &- \sin(Kc_{s,0}\tau) \left[4sc_s^{-2} c_{s,0}^2 (k_1^2 k_2^2 + 2 \text{ perm}) - 6\tau^2 c_{s,0}^4 (1 - c_s^{-2}) k_1^2 k_2^2 k_3^2 - 2(1 - c_s^{-2}) \right. \\ &\left. \times [k_1^2 (\mathbf{k}_2 \cdot \mathbf{k}_3) + 2 \text{ perm}] + 2\tau^2 c_{s,0}^2 (1 - c_s^{-2}) k_1 k_2 k_3 [k_1 (\mathbf{k}_2 \cdot \mathbf{k}_3) + 2 \text{ perm}] \right] \left. \right\}, \quad (3.38) \end{aligned}$$

where $K \equiv k_1 + k_2 + k_3$ and $\mathcal{P}_{\mathcal{R},0} = H^2 / (8\pi^2 \epsilon M_{\text{Pl}}^2 c_{s,0})$. Before we proceed, some comments are in order:

- For steps in the potential, one also has to calculate the contribution to the three-point function coming from similar cubic operators. It is easy to track the polynomials in k_i arising from the different operators if one pays attention to the form of the mode functions (3.37). This way, we noticed that the result for steps in the potential in [113, eq. 3.32] is missing a term, so it should display as follows:

$$\begin{aligned} \frac{\mathcal{G}}{k_1 k_2 k_3} &= \frac{1}{4} \epsilon_{\text{step}} \mathcal{D} \left(\frac{K\tau_f}{2\beta} \right) \left[\left(\frac{k_1^2 + k_2^2 + k_3^2}{k_1 k_2 k_3 \tau_f} - K\tau_f \right) K\tau_f \cos(K\tau_f) \right. \\ &\left. - \left(\frac{k_1^2 + k_2^2 + k_3^2}{k_1 k_2 k_3 \tau_f} - \frac{\sum_{i \neq j} k_i^2 k_j}{k_1 k_2 k_3} K\tau + K\tau \right) \sin(K\tau_f) \right] \quad (3.39) \end{aligned}$$

This is indeed good news, since the missing term ($+K\tau$) above was the source of a small discrepancy found by the authors of [113] with respect to previous results [124], of order 10 – 15% on large scales. We have checked that this discrepancy vanishes when the extra term is introduced.

- We consider sharp features ($\beta_s \gg 1$) peaking in τ_f and define the new variable y through $\tau = \tau_f e^{-y/\beta_s}$, as we did for the power spectrum. There are two kinds of functions appearing in equation (3.38): polynomials and oscillating functions. For the latter, we substitute $\tau \simeq \tau_f (1 - y/\beta_s)$ and do not expand further, in order

to keep the Fourier transforms. For the former, the zeroth order approximation $\tau \simeq \tau_f$ (as in [113]) provides excellent results⁵, although we take the next order and evaluate them at $\tau \simeq \tau_f(1 - y/\beta_s)$ to test for not-so-sharp features. We will therefore calculate the first order correction to previous results. Furthermore we consider, apart from the operator $\mathcal{R}\dot{\mathcal{R}}^2$ (proportional to s), two extra contributions $\dot{\mathcal{R}}^3$ and $\dot{\mathcal{R}}(\nabla\mathcal{R})^2$ (proportional to u) and show that they all contribute at the same order, independently of the sharpness β_s . This is because, although s is proportional to the sharpness β_s , it is also proportional to the derivative of the shape function, F' , defined in eq. (3.25). On the other hand, u is proportional to the shape function, but the Fourier transform of F introduces an additional factor β_s relative to the Fourier transform of F' , cf. eqs. (3.27),(3.28) and (3.41)–(3.43).

- The integrals in (3.38) contain Fourier transforms of the shape function F and its derivative, given the definitions in eqs. (3.24) and (3.25). The symmetric and antisymmetric envelope functions arising from the Fourier transform of F' were already defined in equations (3.27) and (3.28). For completeness, we will give the complementary definitions obtained when integrating by parts:

$$\int_{-\infty}^{\infty} dy F(y) \cos\left(\frac{K c_{s,0} \tau_f}{\beta_s} y\right) = -\frac{\beta_s}{2K c_{s,0} \tau_f} \mathcal{D}_S \quad , \quad (3.40)$$

$$\int_{-\infty}^{\infty} dy F(y) \sin\left(\frac{K c_{s,0} \tau_f}{\beta_s} y\right) = \frac{\beta_s}{2K c_{s,0} \tau_f} \mathcal{D}_A \quad , \quad (3.41)$$

$$\int_{-\infty}^{\infty} dy y F(y) \cos\left(\frac{K c_{s,0} \tau_f}{\beta_s} y\right) = \frac{1}{2} \left(\frac{\beta_s}{K c_{s,0} \tau_f}\right)^2 \left(K \frac{d\mathcal{D}_A}{dK} - \mathcal{D}_A\right) \quad , \quad (3.42)$$

$$\int_{-\infty}^{\infty} dy y F(y) \sin\left(\frac{K c_{s,0} \tau_f}{\beta_s} y\right) = \frac{1}{2} \left(\frac{\beta_s}{K c_{s,0} \tau_f}\right)^2 \left(K \frac{d\mathcal{D}_S}{dK} - \mathcal{D}_S\right) \quad , \quad (3.43)$$

where the slight change of notation between these definitions and those in equations (3.27) and (3.28) is given by $K \leftrightarrow 2k$. We also imposed that F asymptotically vanishes when integrating by parts, which will be the case in this calculation.

Taking into account the comments above, we calculate the bispectrum to leading order for the particular case in which $c_{s,0} = 1$, so that we can compare to the SRFT method. We will express the bispectrum in terms of the normalized scale-dependent function

⁵As opposed to the power spectrum, in this case we only have polynomials with positive powers of $k\tau$, and therefore evaluating them at $k\tau_f$ is already a good approximation for sufficiently sharp features.

$f_{\text{NL}}(\mathbf{k}_1, \mathbf{k}_2, \mathbf{k}_3)$ defined by:

$$\begin{aligned} \langle \mathcal{R}_{\mathbf{k}_1} \mathcal{R}_{\mathbf{k}_2} \mathcal{R}_{\mathbf{k}_3} \rangle &= (2\pi)^3 \delta(\mathbf{k}_1 + \mathbf{k}_2 + \mathbf{k}_3) \Delta B_{\mathcal{R}} \\ &= (2\pi)^7 \delta(\mathbf{k}_1 + \mathbf{k}_2 + \mathbf{k}_3) \frac{3}{10} f_{\text{NL}}(\mathbf{k}_1, \mathbf{k}_2, \mathbf{k}_3) \mathcal{P}_{\mathcal{R},0}^2 \frac{k_1^3 + k_2^3 + k_3^3}{k_1^3 k_2^3 k_3^3} \end{aligned} \quad (3.44)$$

and we will use the following identities for a triangle of vectors $\{\mathbf{k}_1, \mathbf{k}_2, \mathbf{k}_3\}$:

$$\begin{aligned} k_1(\mathbf{k}_2 \cdot \mathbf{k}_3) + 2 \text{ perm} &= \frac{1}{2} [k_1^3 + k_2^3 + k_3^3 - K(k_1 k_2 + 2 \text{ perm}) + 3k_1 k_2 k_3] , \\ k_1^2(\mathbf{k}_2 \cdot \mathbf{k}_3) + 2 \text{ perm} &= \frac{1}{2} [k_1^4 + k_2^4 + k_3^4 - 2(k_1^2 k_2^2 + 2 \text{ perm})] , \\ k_1^2(k_2 + k_3)(\mathbf{k}_2 \cdot \mathbf{k}_3) + 2 \text{ perm} &= \frac{1}{2} [K(k_1^4 + k_2^4 + k_3^4) - (k_1^5 + k_2^5 + k_3^5) - K(k_1^2 k_2^2 + 2 \text{ perm}) \\ &\quad - k_1 k_2 k_3 (k_1 k_2 + 2 \text{ perm})] . \end{aligned}$$

Finally, the bispectrum contribution due to variations in the speed of sound as considered in the cubic action (3.34), to first order in the size of the feature σ_* , and to first order in the polynomial expansion $\tau \simeq \tau_f(1 - y/\beta_s)$ reads:

$$\begin{aligned} f_{\text{NL}}(\mathbf{k}_1, \mathbf{k}_2, \mathbf{k}_3) &= \frac{5}{24} \frac{\sigma_*}{k_1^3 + k_2^3 + k_3^3} \times \left\{ \cos(K\tau_f) \left\{ \tau_f^2 \frac{k_1 k_2 k_3}{K} [(k_1^3 + k_2^3 + k_3^3) \right. \right. \\ &\quad \left. \left. + K(k_1 k_2 + 2 \text{ perm}) - 3k_1 k_2 k_3] \mathcal{D}_A + \frac{\tau_f}{K} [K(k_1^4 + k_2^4 + k_3^4) - (k_1^5 + k_2^5 + k_3^5) \right. \right. \\ &\quad \left. \left. + K(k_1^2 k_2^2 + 2 \text{ perm}) - 4k_1 k_2 k_3 (k_1 k_2 + 2 \text{ perm}) + 3 \frac{k_1 k_2 k_3}{K} (k_1^3 + k_2^3 + k_3^3) - 9 \frac{k_1^2 k_2^2 k_3^2}{K}] \mathcal{D}_S \right. \right. \\ &\quad \left. \left. - 3\tau_f \frac{k_1 k_2 k_3}{K} [(k_1^3 + k_2^3 + k_3^3) + \frac{1}{3} K(k_1 k_2 + 2 \text{ perm}) - 3k_1 k_2 k_3] \frac{d\mathcal{D}_S}{dK} \right. \right. \\ &\quad \left. \left. - \frac{1}{K^2} [3K(k_1^4 + k_2^4 + k_3^4) - 2(k_1^5 + k_2^5 + k_3^5) - 4K(k_1^2 k_2^2 + 2 \text{ perm}) \right. \right. \\ &\quad \left. \left. - 2k_1 k_2 k_3 (k_1 k_2 + 2 \text{ perm})] \mathcal{D}_A + \frac{1}{K} [2K(k_1^4 + k_2^4 + k_3^4) - 2(k_1^5 + k_2^5 + k_3^5) \right. \right. \\ &\quad \left. \left. - 2k_1 k_2 k_3 (k_1 k_2 + 2 \text{ perm})] \frac{d\mathcal{D}_A}{dK} - \frac{1}{\tau_f K^2} [(k_1^4 + k_2^4 + k_3^4) - 2(k_1^2 k_2^2 + 2 \text{ perm})] \left(\mathcal{D}_S - K \frac{d\mathcal{D}_S}{dK} \right) \right\} \\ &\quad \left. + \sin(K\tau_f) \left\{ \{ \mathcal{D}_S \leftrightarrow \mathcal{D}_A , \tau_f \leftrightarrow -\tau_f \} \right\} \right\} , \end{aligned} \quad (3.45)$$

where the $\sin(K\tau_f)$ in the last line contains the same terms as the $\cos(K\tau_f)$, but changing $\mathcal{D}_S \leftrightarrow \mathcal{D}_A$ and $\tau_f \leftrightarrow -\tau_f$, as indicated. This is the formula we want to compare with equation (3.6), after proper normalization. Below, we show the comparison for different

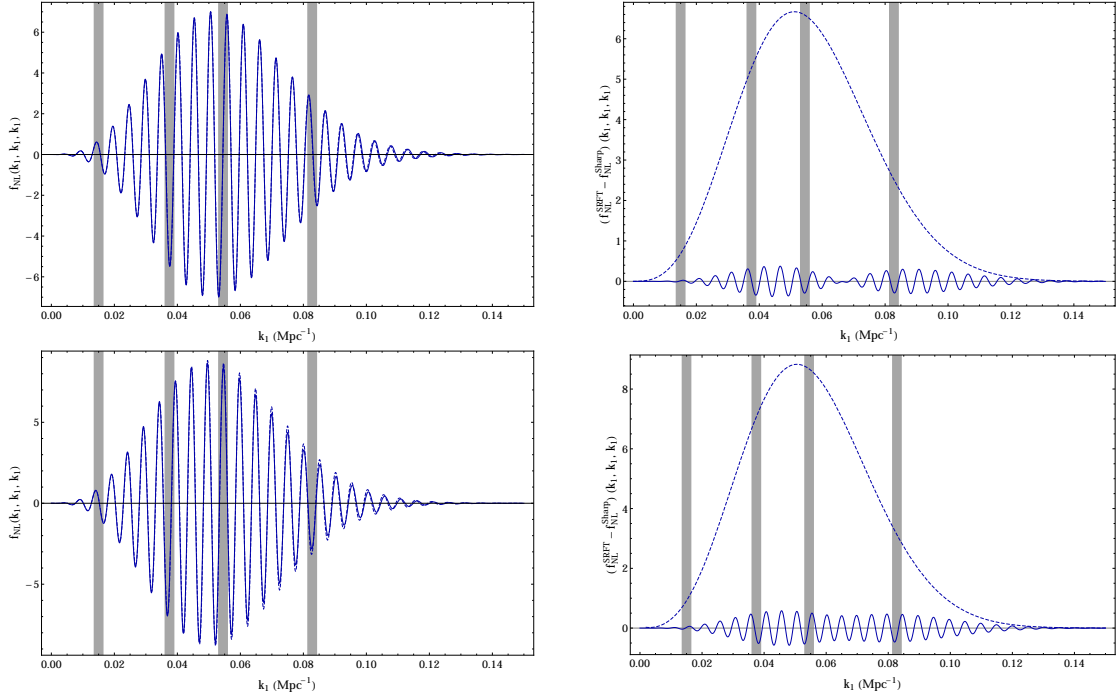


FIGURE 3.4: *left*: bispectrum f_{NL} signal in the equilateral limit with the normalization indicated in eq. (3.44), given by a symmetric reduction in the speed of sound as in (3.46) (*top*) and an asymmetric reduction as in (3.48) (*bottom*), calculated with the SRFT formula (3.6) (solid) and with the sharp approximation (3.45) (dashed). *right*: absolute difference between the signals showed in the left plot (solid), together with the envelope of the signal (dashed). The grey strips represent the approximate scales of the first four acoustic peaks of the CMB temperature spectrum. The parameters are $\sigma_* = 0.04$, $\beta_s = 25.5$, $\ln(-\tau_f) = 6$. This gives $|s|_{\text{max}} \simeq 0.42$ for the symmetric case and $|s|_{\text{max}} \simeq 0.55$ for the asymmetric case. In both cases the relative difference with respect to the envelope is large only at very small scales, which will be indistinguishable at the observational level. We are also within the limit $|s|_{\text{max}} < 1$, where these signatures are reliable but sharp enough so that the sharp approximation works.

functional forms of the speed of sound.

3.2.5 Comparison of bispectra

In this section we compare the bispectrum obtained using the SRFT method (3.6) with that using the first order approximation for sharp features (3.45). As a first example, one can reproduce our test case of gaussian reductions in the speed of sound, cf. equation (3.51), by taking:

$$F = \exp \left[-\beta_s^2 \left(\ln \frac{\tau}{\tau_f} \right)^2 \right] \Rightarrow 1 - c_s^{-2} = -\sigma_* e^{-\beta_s^2 \left(\ln \frac{\tau}{\tau_f} \right)^2} + \mathcal{O}(\sigma_*)^2, \quad (3.46)$$

where the correspondence between this set of parameters and the one used in [156] is $\sigma_* \leftrightarrow -B$, $\tau_f \leftrightarrow \tau_0$, and $\beta_s \leftrightarrow \sqrt{\beta}$. In this case F is symmetric in the variable $y = -\beta_s \ln \frac{\tau}{\tau_f}$ and therefore only the symmetric envelope function \mathcal{D}_S contributes, which

is given by

$$\mathcal{D}_S = -\frac{2K\tau_f}{\beta_s} \sqrt{\pi} \exp\left(-\frac{K^2\tau_f^2}{4\beta_s^2}\right), \quad \mathcal{D}_A = 0. \quad (3.47)$$

In figure 3.4 we show the excellent agreement between the results obtained with equations (3.6) and (3.45) for the equilateral limit $k_1 = k_2 = k_3$. We have checked that for other configurations in momentum space, such as the folded or the squeezed shapes, the agreement is very similar. Note that in figure 3.4 we are plotting the absolute difference in f_{NL} and comparing with the total envelope of the signal⁶. At small scales one can see that the relative difference compared to the total signal is high, due to the fact that the approximation for sharp features starts to fail for large values of $K\tau$. However, the absolute signal is insignificant at such small scales.

As a second example, we propose a shape function with an antisymmetric part:

$$F = \exp\left[-\beta_s^2 \left(\ln \frac{\tau}{\tau_f}\right)^2 + \beta_s \ln \frac{\tau}{\tau_f}\right], \quad (3.48)$$

so that

$$1 - c_s^{-2} = -\sigma_* \left(\frac{\tau}{\tau_f}\right)^{\beta_s} e^{-\beta_s^2 \left(\ln \frac{\tau}{\tau_f}\right)^2} + \mathcal{O}(\sigma_*^2). \quad (3.49)$$

Then, the symmetric and antisymmetric envelope functions read

$$\begin{aligned} \mathcal{D}_S &= -\frac{2K\tau_f}{\beta_s} \sqrt{\pi} \exp\left(\frac{\beta_s^2 - K^2\tau_f^2}{4\beta_s^2}\right) \cos\left(\frac{K\tau_f}{2\beta_s}\right), \\ \mathcal{D}_A &= -\frac{2K\tau_f}{\beta_s} \sqrt{\pi} \exp\left(\frac{\beta_s^2 - K^2\tau_f^2}{4\beta_s^2}\right) \sin\left(\frac{K\tau_f}{2\beta_s}\right). \end{aligned} \quad (3.50)$$

We show in figure 3.4 the equilateral bispectrum signal produced by the asymmetric shape given by eq. (3.48), again derived using equations (3.6) and (3.45). As one can see in figure 3.4, the agreement is also remarkable for functions with an antisymmetric part.

3.3 Search for features in the Planck data

Equipped with accurate analytical predictions for the effect of a varying speed of sound in the power spectrum and bispectrum, we are in a position to search for these features in the CMB data. We choose to parametrize the reduction in the speed of sound as a

⁶We point out that the total envelope of the signal is not given by \mathcal{D}_S or \mathcal{D}_A alone. The total envelope is a combination of both functions, their derivatives, and the polynomials of k_i that appear in Equation 3.45.

gaussian in e-folds N as previously defined in eq. (3.33), i.e.

$$u = 1 - c_s^{-2} = B e^{-\beta(N-N_0)^2} = B e^{-\beta\left(\ln\frac{\tau}{\tau_0}\right)^2}, \quad (3.51)$$

where $\beta > 0$, $B < 0$ and N_0 (or τ_0) is the instant of maximal reduction. Assuming slow-roll, $\ln(-\tau) = (N_{\text{in}} - N) - \ln(a_{\text{in}}H_0)$, where $a_{\text{in}} = a(N_{\text{in}})$ and N_{in} is the time when the last ~ 60 e-folds of inflation start.

This functional form is inspired by soft turns along a multi-field inflationary trajectory with a large hierarchy of masses, a situation that is consistently described by an effective single-field theory [55, 76, 81, 92] (see also [82, 131]). Here, the value of the speed of sound asymptotes to one at the beginning and at the end of inflation (as opposed to step features in which the value at the beginning and at the end of inflation are different). Nevertheless we stress that reductions in the speed of sound are a more general phenomenon within effective field theory (and hence may have diverse shapes and physical origins).

3.3.1 Parameter space

The template for the speed of sound feature (3.51) has three parameters, namely B (the amplitude), β (the sharpness) and τ_0 (equivalently N_0 , the time of maximum reduction). There are two main criteria that we followed in order to determine the explored parameter regions:

- (a) The angular scales probed by Planck ($\ell = 2 - 2500$) roughly correspond to certain momentum scales crossing the Hubble sound horizon during the first $N_{\text{CMB}} \simeq 7$ e-folds of the last ~ 60 e-folds of inflation. If the data resembles features due to a reduced speed of sound, it is most likely to find them in this ‘‘CMB window’’. The sharpness β and the position N_0 are chosen so that the reduction happens well within this window⁷. As a by-product, we avoid degeneracies with the spectral index n_s and the optical depth τ_{reio} that would be present in very wide reductions.
- (b) The Slow Roll Fourier Transform (SRFT) calculation of the power spectrum and the bispectrum (reviewed in section 3.2.1) is valid for mild and moderately sharp reductions of the speed of sound. Also, the slow-roll contributions to the bispectrum are disregarded with respect to the terms arising from the reduced speed of sound [108]. This means that the amplitude $|u|$ and the rate of change $s \equiv \frac{\dot{c}_s}{c_s H}$ must be much smaller than one, while being (at least one of them) much larger than

⁷As we explain later, this a sufficient but not necessary condition for inducing changes in the power spectrum at these scales.

the slow-roll parameters. More precisely we demand the following hierarchy to be present

$$\mathcal{O}(\epsilon, \eta) \ll \text{Max} (|u|, |s|) \ll 1 . \quad (3.52)$$

We took a very conservative definition for the total width of the reduction (in e-folds): ten standard deviations, $\Delta N = 10/\sqrt{2\beta}$. Then, from **(a)**, the position N_0 and the sharpness β should satisfy $5\sqrt{2\beta} < N_0 < N_{\text{CMB}} - 5\sqrt{2\beta}$ and $10\sqrt{2\beta} < N_{\text{CMB}}$. As to the perturbative regime, the rate of change s of the speed of sound (3.51) reads:

$$s(N) = \frac{1}{c_s} \frac{dc_s}{dN} = -\frac{B\beta(N - N_0) e^{-\beta(N - N_0)^2}}{1 - B e^{-\beta(N - N_0)^2}} . \quad (3.53)$$

Since we have to impose $|s| \ll 1$ for all values of N , it suffices to impose this condition at the point where $|s|$ takes its maximum value $|s(N_*)| = |s|_{\text{max}}$, determined by:

$$N_* = N_0 \pm \frac{1}{\sqrt{2\beta}} \sqrt{1 + \mathcal{O}(B)} \simeq N_0 \pm \frac{1}{\sqrt{2\beta}} , \quad (3.54)$$

which approximately corresponds to one standard deviation of our gaussian, and we have used that $|B| \ll 1$. Then the condition $|s|_{\text{max}} \ll 1$ translates into $\beta \ll \frac{2e}{B^2} + \mathcal{O}(B^{-1})$. Altogether, the allowed region of our parameter space is taken to be:

$$\mathcal{O}(\epsilon, \eta) \ll |B| \ll 1 , \quad (3.55a)$$

$$\frac{50}{N_{\text{CMB}}^2} < \beta \ll \frac{2e}{B^2} , \quad (3.55b)$$

$$\frac{5}{\sqrt{2\beta}} < N_0 < N_{\text{CMB}} - \frac{5}{\sqrt{2\beta}} . \quad (3.55c)$$

Notice that, as explained above in **(b)**, the bound $|B| \gg \mathcal{O}(\epsilon, \eta)$ can be avoided if $|s|_{\text{max}} \gg \mathcal{O}(\epsilon, \eta)$. For computational purposes, we use the parameter $\ln(-\tau_0)$ instead of N_0 for the data analysis. We take uniform priors on B , $\ln \beta$ and $\ln(-\tau_0)$. The range for the parameter $\ln(-\tau_0)$ is taken to be more strongly restricted than by equation (3.55c):

$$4.4 \leq \ln(-\tau_0) \leq 6 , \quad (3.56)$$

Before we proceed with the search in the data, a few comments are in order. The chosen region of parameter space (3.55) is a very conservative choice. First, equation (3.55c) and the lower bound in equation (3.55b) are more restrictive than the condition that the feature be observable. For example, we expect observable effects when the reduction occurs before the CMB window, since it would effectively modify the initial conditions of the modes subsequently leaving the sound horizon. We are also trying to avoid very broad features that could be degenerate with cosmological parameters as the spectral

index n_s and the optical depth τ_{reio} , as well as highly oscillating features (for large values of $|\tau_0|$) that make computational control difficult.

Secondly, this range is well within the region of the parameter space where the theory is weakly coupled. As we explained in Chapter 2 following [97], a hard upper bound on the sharpness of the feature can be derived by imposing that the theory is weakly coupled at the energy scale where the changes in the mode functions are induced. Our sharpness parameter β is related to that of [97] (that we will call β_{CBM}) by $\beta = 50\beta_{\text{CBM}}^2$, where we took the conservative definition of the width to be ten standard deviations. The feature unitarity bound eq. (2.88) imposes that our sharpness parameter must satisfy:

$$\ln \beta < 14 . \quad (3.57)$$

Since we restrict our search to $2 < \ln \beta < 7.5$, we are perfectly consistent with the bound given above. Even if we take the crude definition for the width of only one standard deviation, the correspondence would be $\beta = \beta_{\text{CBM}}^2$, and the bound would translate to $\ln \beta < 10$, which still leaves us in a safe region. Given that we *a priori* constrained our search to a region of the parameter space where the perturbative and adiabatic regimes are respected, the predictions obtained are consistently interpreted by the underlying theory.

Let us note that respecting the weak coupling condition (3.57) has important consequences. Indeed, it was found [97, 98] that some of the best fits found so far for steps in the potential in the CMB [136, 146, 147] do not lie within this bound. This calls into question the consistency of the framework in which these predictions are derived. More interestingly, this motivates a new theoretical framework able to consistently describe those predictions, since the data is blind to whether a theory is internally consistent or not. An important and evident conclusion of these analyses is that very sharp features are problematic from the theoretical point of view. In addition, one could speculate that if the data finally points to inflationary scenarios with large field excursions, a (slightly broken) symmetry should protect the background, and then we would not expect to find sharp features in the potential. This further motivates the study of moderately sharp features, which are still safely described by an underlying theory. In the following, we present the results of our search.

3.3.2 Results

As already stated in precedent section, a variation in the speed of sound will generate a primordial power spectrum given by:

$$\frac{\Delta \mathcal{P}_{\mathcal{R}}}{\mathcal{P}_{\mathcal{R},0}}(k) = k \int_{-\infty}^0 d\tau u(\tau) \sin(2k\tau) , \quad (3.58)$$

This primordial power spectrum feature is computed using a Fast Fourier Transform, and added to the primordial spectrum of the Λ CDM Planck baseline model described in ref. [157, sec. 2]. The resulting CMB power spectrum, calculated using the CLASS Boltzmann code [29, 158], is fitted to the Planck 2013 CMB temperature data [159] and the WMAP CMB low- ℓ polarization data [160], using MONTE PYTHON [161] as a Markov chain Monte Carlo (MCMC) sampler. We varied all cosmological, nuisance and feature parameters. For those last ones, the likelihood probability distribution is found to be multi-modal. Though multi-modal distributions are more efficiently sampled using other methods (e.g. MULTINEST [162, 163]), we were able to perform the search using only MCMC's.

Our statistical analysis of the Planck CMB power spectrum reveals several fits with a moderately improved likelihood compared to the best Λ CDM fit. Having discarded small signals with $\Delta\chi^2 > -2$ (defined in ⁸) over Λ CDM, we find a series of five well-isolated bands of almost constant $\ln(-\tau_0)$, with variable significance, see table 3.1 and figure 3.5. For each of those fits we give the associated full primordial bispectrum. At the time of writing this thesis the Planck bispectrum data have not yet been released, but templates similar to our predictions have already been tested by the Planck collaboration. We find, through a heuristic and limited comparison, that the predicted bispectra have frequencies which are not favoured by the latest data.

The amplitude B of the fits is rather small, $\mathcal{O}(10^{-2})$, and therefore comparable with neglected slow-roll terms. This means the bispectrum is dominated by terms of order $s = \dot{c}_s/(Hc_s)$. The maximum values of s at the best fits for the modes \mathcal{A} to \mathcal{E} in table 3.1 are respectively 0.33, 0.42, 0.40, 0.48, 0.05. Notice that the value of s for \mathcal{E} is also comparable to neglected terms, so the prediction for the bispectrum based on eq. (3.6) cannot be trusted in this case. We therefore disregard this mode in the comparison with the bispectrum.

For the modes \mathcal{A} , \mathcal{B} and \mathcal{C} the table shows the 68% c.l. ranges. For bands \mathcal{B} and \mathcal{C} we were unable to put an upper bound on $\ln \beta$ due to a degeneracy between that parameter

⁸Hereafter, χ^2 refers to the *effective* quantity defined as $\chi_{\text{eff}}^2 = -2 \ln \mathcal{L}$, see [164, p. 10]; in turn, Δ stands for the difference with the corresponding best fit value of Planck baseline model, using the same likelihood.

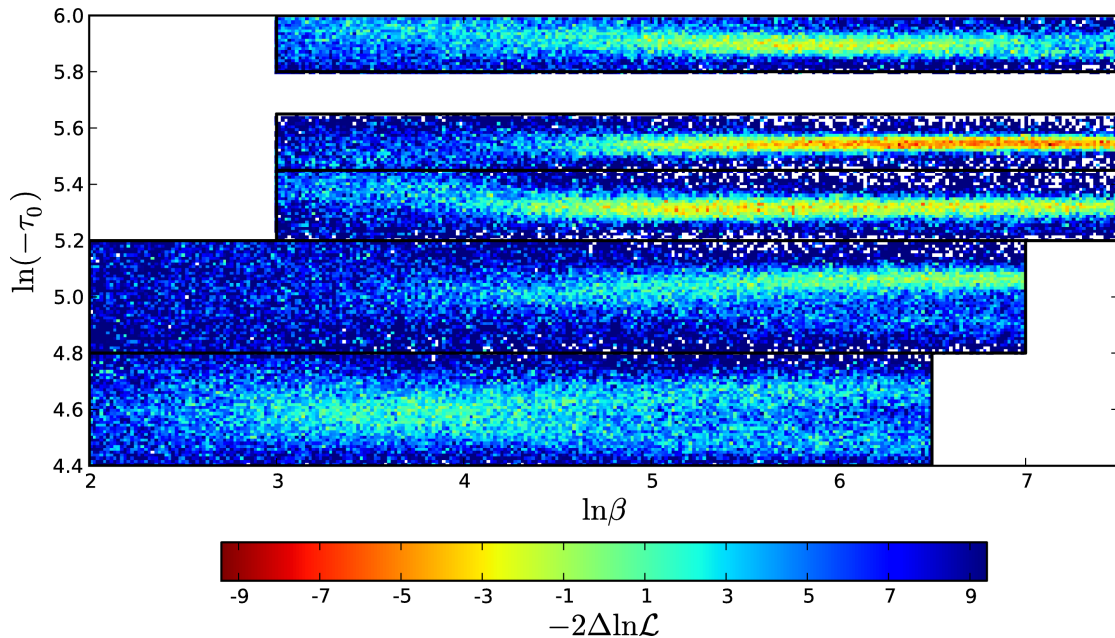


FIGURE 3.5: Profile of $\Delta\chi_{\text{eff}}^2 = -2\Delta\ln\mathcal{L}$ for the features in the CMB power spectrum in the $(\ln\beta, \ln(-\tau_0))$ plane.

#	$-B \times 10^2$	$\ln\beta$	$\ln(-\tau_0)$	$\Delta\chi^2$
\mathcal{A}	(4.5) $3.7^{+1.6}_{-3.0}$	(5.7) $5.7^{+0.9}_{-1.0}$	(5.895) $5.910^{+0.027}_{-0.035}$	-4.3
\mathcal{B}	(4.2) 4.3 ± 2.0	(6.3) $6.3^{+1.2}_{-0.4}$	(5.547) $5.550^{+0.016}_{-0.015}$	-8.3
\mathcal{C}	(3.6) $3.1^{+1.6}_{-1.9}$	(6.5) $5.6^{+1.9}_{-0.7}$	(5.331) $5.327^{+0.026}_{-0.034}$	-6.2
\mathcal{D}	(4.4)	(6.5)	(5.06)	-3.3
\mathcal{E}^*	(1.5)	(4.0)	(4.61)	-2.2

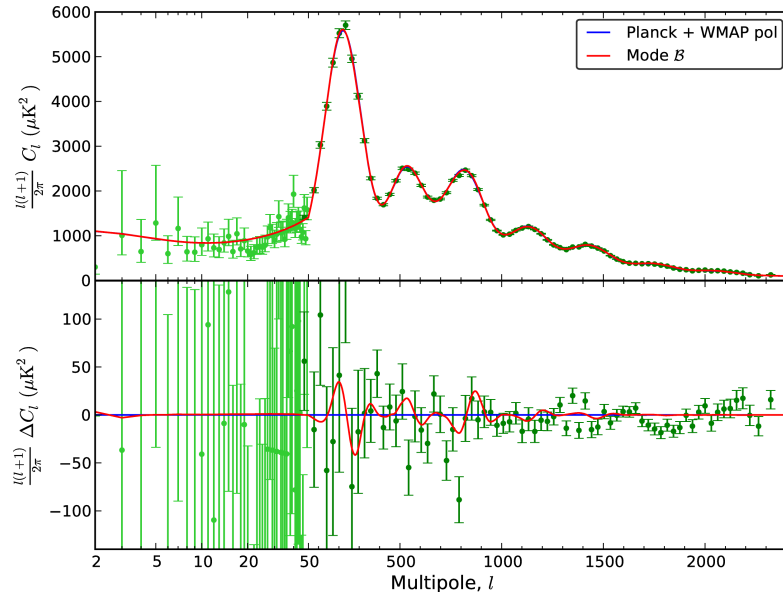
TABLE 3.1: CMB power spectrum best fits (in parentheses), 68% c.l. intervals and effective $\Delta\chi^2$ at the best fit value for each of the different modes. The prediction for the bispectrum for \mathcal{E} is not reliable (see text).

and the amplitude $|B|$. For those two modes, the upper bound on $\ln\beta$ is set by the prior $s < 1$ in eq. (3.55b), which is saturated at $\ln\beta \simeq 7.5$. The best fit for \mathcal{B} lies at $s \simeq 1$, so we present in table 3.1 the second best⁹. We show in figure 3.6 the predicted C_l for mode \mathcal{B} .

The lower bands \mathcal{D} (and \mathcal{E}) are less significant and their likelihoods much less gaussian, so we only show their best fits. Despite their low significance, they are worthy of mention because they fall in the region overlapping with Planck’s search for features in the bispectrum (see below).

The best fits and 68% c.l. ranges [157] of the six Λ CDM parameters are quite accurately reproduced. We find two mild degeneracies ($|r| \lesssim 0.15$) of $\ln(-\tau_0)$ with ω_{CDM} and H_0 .

⁹The high- ℓ CMB polarization data of the new Planck release should put an upper bound on $\ln\beta$, as well as confirm that we are not fitting noise. This is an important reason for repeating this analysis with the new data.

FIGURE 3.6: CMB temperature power spectrum for mode \mathcal{B} .

Best fits and confidence intervals are also preserved for the nuisance parameters.

Due to the Fourier transform in eq. (3.58), our features oscillate as $\exp(i2k\tau_0)$. Thus it is natural to compare to other searches for linearly oscillating features in the Planck CMB power spectrum¹⁰. In [145], Meerburg et al. searched for constant amplitude oscillations with frequencies that compare to ours as $\omega_2 = 2|\tau_0|$. The search was done up to $\ln(-\tau_0) = 9$. In the overlapping region, $\omega_2 \in [160, 810]$, they find peaks at roughly $\ln(-\tau_0) \sim \{5.0, 5.1, 5.3, 5.6, 5.7\}$ ($|\Delta\chi_{\text{bf}}^2| \simeq 8$). We find three peaks in this region with similar significance; it could be that the discrepancies come from signals at scales at which our (localized) features are negligible.

Also, the Planck collaboration [146, sec. 8] searched for features motivated by step-inflation [135]. In 2013 they performed a search up to frequency $\ln(-\tau_0) = 12$ (in that parametrization $\eta_f = |\tau_0|$). The profile likelihood in [146, fig. 19, middle] reveals peaks at $\ln \eta_f \in [4.5, 4.8]$ ($|\Delta\chi_{\text{bf}}^2| \simeq 2$) and $\ln \eta_f \in [5.3, 5.7]$ ($|\Delta\chi_{\text{bf}}^2| \simeq 8$), which is consistent with our results. It is worth noting that in both searches above (also in [147]) the overall best fit occurs at $\ln(-\tau_0) \simeq 8.2$ ($|\Delta\chi_{\text{bf}}^2| \sim 10$), too high a frequency for the scope of our search.

Our analysis and the ones mentioned above were made with the 2013 Planck data. Since that date new data became available, in particular containing new polarization measurements. At the moment only the Planck collaboration has repeated the analysis [30], containing a new search for both step features and linear oscillations. For steps in the potential the best fit value reaches a maximum of $|\Delta\chi_{\text{bf}}^2| \sim 8$ for a slightly

¹⁰Logarithmic oscillations, in which the primordial power spectrum oscillates as $\cos(\omega \ln(k))$, is also a well studied and motivated template (see [30] and references therein).

smaller frequency ($\ln(-\tau_0) \simeq 7.1$) and different values for the amplitude and width of the envelope (the fit is similar to the one found by Benetti in [136]).

In all the cases mentioned above (and also including searches with templates with fewer parameters), the bayesian evidence does not prefer the feature model over the featureless power law spectra, which suggests that CMB power spectrum data alone cannot justify the introduction of these features. Nevertheless, one of the aims of this chapter is to show that low-significance fits can still predict correlated features in the bispectrum which are possibly observable with the current data. Model selection should be done taking into account both observables (or naturally, any other combination).

3.3.3 Comparison with the search for features in Planck's bispectrum

A first search for linearly oscillatory features was performed on Planck's bispectrum with the 2013 data (cf. [165, sec. 7.3.3]) using a constant feature model (i.e. with no envelope modulating the amplitude of the oscillation). The constant feature template is given by [166]

$$B(k_1, k_2, k_3) = \frac{6A^2 f_{\text{NL}}^{\text{feat}}}{(k_1 k_2 k_3)^2} \sin\left(2\pi \frac{\sum_{i=1}^3 k_i}{3k_c} + \phi\right), \quad (3.59)$$

where $A = A_s k_*^{1-n_s}$, A_s and n_s being the amplitude and spectral index of the primordial power spectrum, and $k_* = 0.05 \text{ Mpc}^{-1}$ a pivot scale. They sampled the amplitude $f_{\text{NL}}^{\text{feat}}$ over a coarse grid of wavelengths k_c and phases ϕ . Our features also present a linearly oscillatory pattern, which comes from the Fourier transform in (3.5). These oscillations enter the bispectrum approximately as $\exp(i \sum_i k_i \tau_0)$, cf. eq. (3.6). Thus, Planck's 2013 search falls inside $\ln(-\tau_0) \in [4.43, 5.34]$, while ours spans up to $\ln(-\tau_0) = 6$ ($k_c = 0.00519 \text{ Mpc}^{-1}$). The overlap includes our modes \mathcal{C} and \mathcal{D} (and also the discarded \mathcal{E}). In the range of $\ln(-\tau_0)$ probed here, we were not able to reproduce the improvement Planck appears to see for features at the first peak. On the other hand, we found good matching around the second and third peak scales between the best fit of \mathcal{D} with $k_c = 0.01327 \text{ Mpc}^{-1}$ and the 2.3σ signal of Planck bispectrum at $k_c = 0.01375 \text{ Mpc}^{-1}$ with $f_{\text{NL}}^{\text{feat}} = 345$ and $\phi = \pi/2$.

Having found an interesting hint for the presence of such a feature, it is important to know whether such good matching persists when considering additional data. In particular, the Planck search for features in the bispectrum was extended in 2015 [40]. New feature templates were tested, and the search was enlarged to higher frequencies (up to $\ln(-\tau_0) = 7.6$ for the constant feature model, and therefore covering all the modes \mathcal{A} to \mathcal{E}). Comparing our fits of the power spectrum with the new bispectrum search would require computing the best fit parameters for the power spectrum again, using

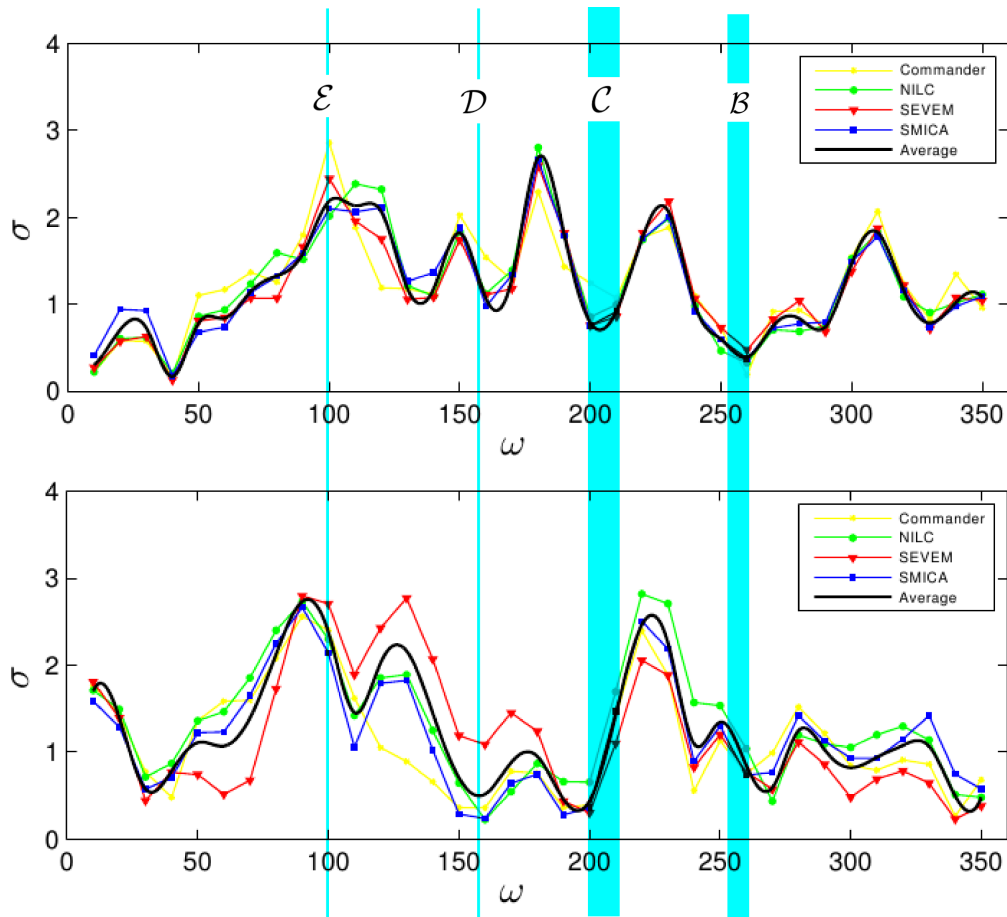


FIGURE 3.7: The likelihood for the constant feature models eq. (3.59), from Planck 2015 analysis [40]. Upper panel is for T only, and lower panel is T+E. We superimpose in turquoise the best-fits frequencies we found in the power spectrum with the 2013 data.

the new released data. This is going to be done in the future, and for the moment we will very qualitatively address what happens for the fits found with the 2013 data.

In order to facilitate the comparison we write in table 3.2 our power spectrum fits in terms of the frequency ω defined as $\omega \equiv 2\pi/3k_c (= -\tau_0)$. In figure (3.7) we show the

mode	\mathcal{A}	\mathcal{B}	\mathcal{C}	\mathcal{D}	\mathcal{E}
ω	(363) 369^{+10}_{-13}	(256) 257^{+4}_{-4}	(207) 206^{+5}_{-7}	158	100

TABLE 3.2: CMB power spectrum best fits (parentheses) and 68% c.l. intervals for modes \mathcal{A} to \mathcal{E} (shown in table 3.1) in terms of the frequency $\omega = 2\pi/3k_c = -\tau_0$.

likelihood for the template (3.59) up to $\omega = 350$ (where there is a better resolution of the data). We superimpose to this figure the frequencies we found in the 2013 power spectrum.

For templates with both oscillations and envelopes, the case of a step in the speed of sound and a step in the slow-roll parameters were analyzed. While the full shape is given

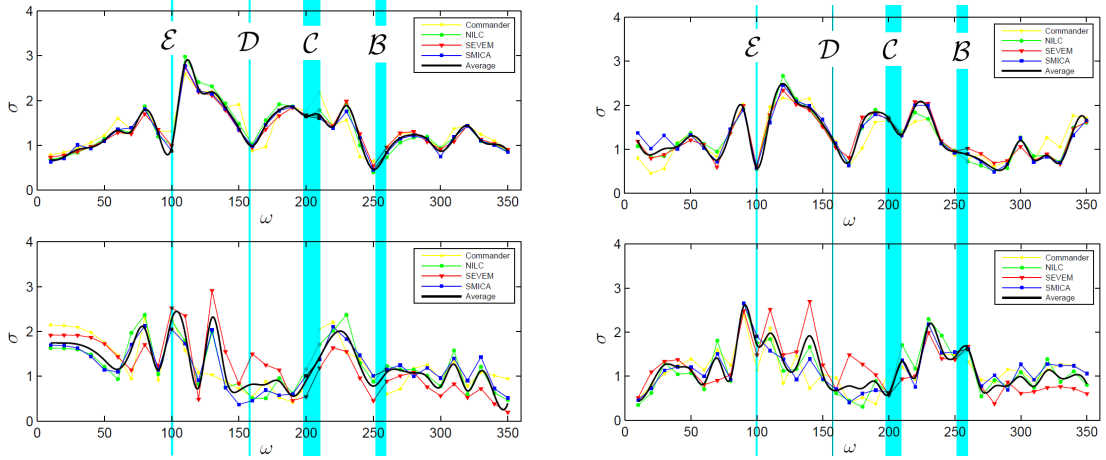


FIGURE 3.8: The likelihood for single feature models, whose dominant contribution is given in eqs. (3.60)-(3.61), from Planck 2015 analysis [40]. We superimpose in turquoise the best-fits frequencies we found in the power spectrum with the 2013 data. LEFT: Step in the potential (T-only top, and T+E bottom) RIGHT: Step in the speed of sound (T-only top, and T+E bottom).

by a very long formula, we can write the dominant contribution for each case. They are given by:

$$B_{K \sin}(k_1, k_2, k_3) = \frac{6A^2 f_{\text{NL}}^{\text{feat}}}{(k_1 k_2 k_3)^2} K \mathcal{D}(\alpha \omega K) \sin \left(2\pi \frac{\sum_{i=1}^3 k_i}{3k_c} + \phi \right), \quad (3.60)$$

$$B_{K^2 \cos}(k_1, k_2, k_3) = \frac{6A^2 f_{\text{NL}}^{\text{feat}}}{(k_1 k_2 k_3)^2} K^2 \mathcal{D}(\alpha \omega K) \cos \left(2\pi \frac{\sum_{i=1}^3 k_i}{3k_c} + \phi \right). \quad (3.61)$$

Here $f_{\text{NL}}^{\text{feat}}$ is a constant that sets the overall amplitude of the bispectrum, $\mathcal{D}(\alpha \omega)$ is the envelope function that modulates this amplitude in k -space, α is the sharpness of the step, and $K = k_1 + k_2 + k_3$. The envelope is taken to come from a tanh-step, i.e. $\mathcal{D}(\alpha \omega K) = \alpha \omega / (K \sinh(\alpha \omega K))$ (see eq. (3.32)). We show the likelihood for these models as a function of the frequency of oscillation ω in figure 3.8.

From figures (3.7) and (3.8) we can see that only mode \mathcal{E} correspond to a frequency that is a peak in the bispectrum ($\sigma \sim 2$ for all the envelopes). Some comments are in order. The likelihood values of figure (3.8) are obtained after marginalizing over the envelope factor α and the amplitude $f_{\text{NL}}^{\text{feat}}$. In our case they are not free parameters of the bispectrum since they are fixed by the fit to the power spectrum. Unfortunately we do not know how the likelihood changes as we vary these parameters. The likelihood values of figure (3.8) should then be understood as a maximum value for an arbitrary α and $f_{\text{NL}}^{\text{feat}}$. Furthermore, our template does not really correspond to any of the templates studied by Planck: while they considered a step in the speed of sound, i.e. an antisymmetric function, our test case is a symmetric reduction in the speed of sound. We know that the symmetry of the feature determines where does the envelope peaks, see e.g. figure

3.1, so this might be an important difference between our template and theirs. Whether the data can distinguish between these two templates is a question left for future work.

3.4 Conclusions

In this chapter we have studied moderately sharp features in the speed of sound from the point of view of theory and observations. In particular, we have shown that the effect of a transient reduction in the speed of sound can be calculated with the simple Slow Roll Fourier Transform (SRFT) approximation [108], in which the correlations between power spectrum and bispectrum are manifest. Additionally, we have presented an alternative way to calculate both the power spectrum and bispectrum, by consistently applying an approximation for moderately sharp features, both to the Generalized Slow Roll (GSR) power spectrum (eq. (3.29)) and to the in-in calculation of the bispectrum (eq. (3.45)). Within this regime, we have extended existing GSR calculations of the power spectrum to less sharp and arbitrary shapes of the speed of sound, and found excellent agreement with the SRFT approximation in the regime where both methods apply. Given that the regimes of validity of the two methods are not entirely coincident, we are now equipped with a robust machinery that will allow us to describe features in the speed of sound for a broader region of the parameter space. Broad features can be calculated with the SRFT approach, while sharp features can be calculated using GSR for the power spectrum (eq. (3.29)) and the in-in approach for the bispectrum (eq. (3.45)).

Furthermore, we have carried out a statistical search for localized oscillatory features in the CMB power spectrum produced by a transient reduction in the speed of sound. We have found a number of fits and calculated the associated primordial bispectra. The bispectrum prediction resembles templates that were tested by the Planck collaboration, so we can compare our predictions with the templates used in that search. Using the 2013 data and Planck bispectrum analysis, we found a surprisingly good agreement. This is remarkable, considering that these bispectrum features are *predicted from a search in the CMB power spectrum* with a very simple ansatz for c_s . The new release made by Planck calls for a new analysis, but from their bispectrum analysis it seems that a shift in the best fit frequencies of the power spectrum will be necessary in order to find an interesting correlation.

We emphasize that the CMB power spectrum data alone can hardly justify the introduction of features on top of the Λ CDM model; a gain of $|\Delta\chi^2| \lesssim 10$ is not uncommon. However, as we have shown, low-significance fits in the power spectrum can still predict correlated features that may be observable in the CMB bispectrum. Therefore, model selection should take into account both observables simultaneously.

Our results suggest that, by exploiting correlations between different observables, current data might already be sensitive enough to detect transient reductions in the speed of sound as mild as a few percent, opening a new window for the presence of extra degrees of freedom during inflation.

4

Slowly evolving speeds of sound

Having studied transient features in the speed of sound in the previous chapter, we study now the other phenomenological regime, i.e. the situations in which the speed of sound is slowly evolving. A slow evolution of the speed of sound greatly simplifies the calculation for the primordial correlation functions: the power spectra will still be described by a power law, with a slightly modified spectral index and tensor to scalar ratio, and its non gaussian signal is described by a simple analytical function. It is then possible to directly compare the predictions with the allowed (n_s, r) bounds coming from Planck, as shown in figure 1.3. We will show that a slowly evolving speed of sound can be easily generated in slow-roll inflation, provided the two-field completion resembles a spiral in field space.

This chapter is based on the following paper:

On the viability of $m^2\phi^2$ and natural inflation, A. Achúcarro, V. Atal and Y. Welling, JCAP **1507** (2015) 07, 008 [arXiv:1503.07486 [astro-ph.CO]].

4.1 Introduction

Precise observations of the cosmic microwave background and large scale structure allow today for a very accurate determination of the cosmological parameters [11]. This requires the theoretical predictions to be precise and robust, so that there are no uncertainties when interpreting the data, or, more realistically speaking, that any uncertainty is well understood. In the particular case of inflation [13, 14], the fact that this period might be driven by a single light scalar field, effectively uncoupled to any additional degree of freedom (at least during the time when observable perturbations are generated)

is a very appealing scenario in terms of predictability¹. Indeed, any given potential has unique and precise predictions, with the only ambiguity coming from uncertainties on which e-foldings correspond to the observable scales. The fact that many models of inflation have been ruled out by measurements of the spectral tilt and bounds on the amount of tensor perturbation, reaffirms this claim. In particular some of the simplest large field models like $m^2\phi^2$ [31] and natural inflation [32] are in tension with the data [30]. In this chapter we show that a particular class of two-field embeddings, where the additional field is super heavy, can bring these models back into consistency with the data, by changing the value of the slow-roll parameters as well as by generating a reduced speed of sound $c_s < 1$ for the fluctuations. We emphasize that this deformation is coming entirely from super massive degrees of freedom (masses much heavier than the Hubble parameter), and is an example of how important heavy fields may be in determining the low energy effective description.

In general, a heavy field may influence the low energy dynamics by either affecting the background, the perturbations or a combination of both. We would like to stress that this does not require any high energy excitations or particle production, and our discussion in this chapter focuses on the regime in which they do not occur. First of all, changes in the background may come when evaluating the action at the vacuum expectation value (v.e.v.) of the heavy field. Provided the kinetic energy is dominated by the light field, it is possible to write a Lagrangian in which we recover single-field inflation described by some effective potential (see e.g. [167, 168]). Changing the background will result in different values for the slow-roll parameters ϵ and η , and thus we call this the *background* model. Secondly, for certain (derivative) couplings between the light and heavy field, perturbations of the heavy field contribute to the low frequency mode and therefore to the low energy - single field - effective field theory (EFT) for the perturbations². The effect of this coupling has been widely studied, both in the cases when it is small [95, 106], and the cases in which it is large [41, 55, 73, 76, 78–80, 82, 83, 93, 101, 102, 169] (see [170] for a comparative study of some of these works). In the latter case, integrating out the heavy field results in a reduced speed of sound for the adiabatic fluctuations. This is a purely quantum effect that arises when considering the full two-field evolution for the perturbations.

As we will explicitly show through examples, a proper description of the system demands taking both effects into account. In order to do so, we embed inflation in a simple two-field realization such that inflation takes place on a turning trajectory whose radius of

¹At least if we ignore the issue of eternal inflation and the multiverse paradigm.

²The isocurvature modes are heavy and decay fast, they do not source the curvature perturbations after horizon crossing. This situation is different from so-called multifield inflation, where there are multiple light fields [66, 68], and quasi-single field inflation, where the mass of the heavy field is order of the Hubble parameter [74].

curvature is changing very slowly. In our embedding, the inflaton is the phase of a complex field where the $U(1)$ symmetry is mildly broken and the v.e.v. of the - massive - radial field is approximately the radius of curvature of the inflationary trajectory (see [171, 172] and [173] for realizations in field theory and supergravity respectively).

As already anticipated, we will show that within this framework quadratic inflation can be consistent with the data, and that subplanckian values of the effective (instantaneous) decay constant are no longer disfavored in natural inflation. This will require that the v.e.v. of the radial field takes subplanckian values. Different deformations of standard natural and chaotic inflation were discussed in e.g. [174–177], and [177–183] respectively. Unlike previous studies that included additional heavy fields to improve agreement with the data due to a flattening of the potential, in all cases described here the effective potential *steepens*. However the speed of sound effects dominate and move the predictions *downward* in the (n_s, r) plane, towards the best fit region. In addition, in some cases the speed of sound slowly decreases along the trajectory, causing a shift towards higher values of n_s .

The outline of the Chapter is as follows. In section 4.2 we introduce a simple two-field embedding of inflation with an additional heavy field. We explain how both the background and the curvature perturbations are affected by the presence of the heavy field. Furthermore we provide analytical expressions for the observables. In sections 4.3, 4.4 and 4.5 we study the predictions of the observables of quadratic, linear and natural inflation embedded in this two-field scenario. We show explicitly how the predictions in the (n_s, r) plane move towards the 1σ allowed region of Planck. Finally in section 4.6 we discuss our findings and conclude.

4.2 General setup

4.2.1 Two-field embedding

We embed inflation in a simple two field realization, given by the following Lagrangian:

$$\mathcal{L} = \frac{1}{2} \partial_\nu \rho \partial^\nu \rho + \frac{1}{2} \rho^2 \partial_\nu \theta \partial^\nu \theta - \frac{m_\rho^2}{2} (\rho - \rho_0)^2 - V(\theta). \quad (4.1)$$

Here we assume the inflaton to be the phase of a complex field, and the $U(1)$ symmetry has been mildly broken by a potential $V(\theta)$. This model was already studied in [78] (with a different kinetic term), and in [101], for the case of linear inflation (that we discuss below). This is not the most general Lagrangian consistent with the symmetries invoked. In fact we may also have different choices for the potential or the field space

metric, but we choose this form as the simplest starting case. We also notice that since the model becomes singular at $\rho = 0$, additional degrees of freedom should appear at some higher energy scale. Additionally, these models will have monodromy; the potential is not completely invariant after the phase θ has made a 2π cycle [184–187].

The standard logic (that we will show is inaccurate) is that, if the radial field is sufficiently heavy, the field ρ will rapidly reach its minimum at ρ_0 , so that one may truncate the model and consider the single field Lagrangian

$$\mathcal{L} = \frac{1}{2}\rho_0^2\partial_\nu\theta\partial^\nu\theta - V(\theta), \quad (4.2)$$

which by a field redefinition becomes:

$$\mathcal{L} = \frac{1}{2}\partial_\nu\phi\partial^\nu\phi - V(\phi/\rho_0). \quad (4.3)$$

We will show that truncating the model in this manner yields inaccurate predictions. The reason is twofold. First, because of the kinetic coupling the radial field will have a minimum at $\bar{\rho} \neq \rho_0$. Plugging this solution back in the Lagrangian will result in an EFT in which we recover single-field inflation described by an effective potential [167, 168]. In general, this will result in different predictions for both ϵ and η (the slow-roll parameters) at the observable scales. This single field description is possible provided the kinetic energy is dominated by the angular field, or more specifically that $\dot{\rho}^2 + \rho^2\dot{\theta}^2 = \left((d\rho/d\theta)^2 + \rho^2\right)\dot{\theta}^2 \sim \rho^2\dot{\theta}^2$. From this condition we will demand that $d\rho/d\theta \ll \rho$. Secondly, light and heavy field perturbations will be coupled through the angular velocity, $\dot{\theta}/H$, which, if large, will give rise to a low energy EFT with a reduced speed of sound c_s for the adiabatic fluctuations [73, 81, 82, 101].

The prediction for the system can then be computed with the usual relations³ $r = 16\epsilon c_s$ and $n_s = 1 - 2\epsilon - \eta - s$ with $\epsilon \equiv -\dot{H}/H^2$, $\eta \equiv \dot{\epsilon}/H\epsilon$ and $s \equiv \dot{c}_s/Hc_s$. From these expressions it is clear that a reduced speed of sound, $c_s < 1$, will contribute to moving the predictions of the model towards smaller values of r (taking into account that in general ϵ will also change while we go from $c_s = 1$ to $c_s \ll 1$). Additionally, n_s will also change making theories flow in the (n_s, r) plane⁴. In the following, we show how to exactly calculate these quantities.

³We actually use the more precise predictions for r as in [27], where the difference in freeze-out time between the scalar and tensor perturbation is considered [26]. This effect becomes relevant when $c_s \ll 1$. We also compute the power spectrum, from which we derive n_s , at second order in slow-roll, as in [27].

⁴In [188], the effect of c_s and s in the (n_s, r) plane for a phenomenological ansatz $c_s(N)$ was discussed.

4.2.2 Analytical predictions

The possibility to make analytical predictions for n_s and r depends on the ability to calculate the radius $\bar{\rho}(\theta)$ at which the radial field stabilizes, as a function of the parameters of the two-field embedding. While it is not generically possible to solve the full two-field model, there is a regime in which such analytical predictions are possible. This is the regime in which the time derivatives of ρ can be neglected in the equations of motion (e.o.m.). In order to show this explicitly, consider the e.o.m. for the system

$$\ddot{\rho} + 3H\dot{\rho} - \rho\dot{\theta}^2 + V_\rho = 0 \quad (4.4)$$

$$\rho^2\ddot{\theta} + 2\rho\dot{\rho}\dot{\theta} + 3H\rho^2\dot{\theta} + V_\theta = 0 \quad (4.5)$$

together with the Friedmann equation (from here on we set the reduced Planck mass $m_{pl} \equiv (8\pi)^{-1/2}M_{pl} = 1$)

$$3H^2 = \frac{1}{2}(\dot{\rho}^2 + \rho^2\dot{\theta}^2) + V. \quad (4.6)$$

where $V_\theta = \partial V/\partial\theta$ and $V_\rho = \partial V/\partial\rho$.

First, we assume that we can neglect the derivatives of ρ in the previous equations (which is a good approximation in all of the cases studied here). We assume then $\ddot{\rho}, 3H\dot{\rho} \ll \rho\dot{\theta}^2, V_\rho$ and $2\rho\dot{\rho}\dot{\theta} \ll 3H\rho^2\dot{\theta}, V_\theta, \rho^2\ddot{\theta}$. Let us note that the previous inequalities demand that, at the same time, $\frac{1}{\rho}\frac{d\bar{\rho}}{d\theta} \ll \frac{\dot{\theta}}{3H}$ and $\frac{1}{\rho}\frac{d\bar{\rho}}{d\theta} \ll \frac{3H}{2\dot{\theta}}$. This directly implies that

$$\frac{1}{\rho}\frac{d\bar{\rho}}{d\theta} \ll 1 \quad (4.7)$$

which is the condition for writing a single field model for the background (i.e. that the kinetic energy is dominated by the angular velocity). This condition does not mean that the field ρ has to be exactly constant, but rather that its time evolution is slow.

Furthermore, as θ plays - mainly - the role of the inflaton, we also drop $\ddot{\theta}$. This demands $\ddot{\theta} < 3H\dot{\theta}$. The simplified system then reads:

$$\rho\dot{\theta}^2 = V_\rho \quad (4.8)$$

$$3H\rho^2\dot{\theta} + V_\theta = 0 \quad (4.9)$$

and

$$3H^2 = V. \quad (4.10)$$

Importantly, let us note that there is no bound on $\dot{\theta}/H$ (as long as $\dot{\theta} < m_\rho < M_{pl}$). This quantity plays an important role in determining both the coupling of the perturbations

between the light and heavy field, and - as we will see below - the slow-roll parameters.

In principle with these equations we obtain $\bar{\rho}(\theta)$, plug the solution in the potential and find a canonical variable so that we have a single-field effective potential. However, in situations in which the solution $\bar{\rho}(\theta)$ is a complicated function of θ , it may be too difficult to follow this procedure, the main reason being that we need to find a canonical variable ϕ such that $\bar{\rho}\dot{\theta} = \dot{\phi}$. Nonetheless, the system can still be solved semi-analytically in a single field approach. If the kinetic energy is dominated by θ , then ϵ is given by

$$\epsilon = \frac{1}{2\bar{\rho}^2} \left(\frac{V_{\theta}}{V} \right)^2. \quad (4.11)$$

With this we can calculate $\eta = \dot{\epsilon}/\epsilon H$ giving

$$\eta = \frac{2}{\bar{\rho}^2} \left(\frac{V_{\theta\theta}}{V} \right) + 4\epsilon - 2\frac{\dot{\bar{\rho}}}{\bar{\rho}H}. \quad (4.12)$$

Importantly, the last term cannot be neglected. Indeed

$$\delta \equiv \frac{\dot{\bar{\rho}}}{\bar{\rho}H} \quad (4.13)$$

$$= \frac{1}{\bar{\rho}} \frac{d\bar{\rho}}{d\theta} \frac{\dot{\theta}}{H} = \frac{1}{\bar{\rho}} \frac{d\bar{\rho}}{d\theta} \frac{\sqrt{2\epsilon}}{\bar{\rho}}. \quad (4.14)$$

While the reduced e.o.m. demands $\delta \ll 1$, δ may be $\mathcal{O}(\epsilon, \eta)$. Then, we can calculate all of the relevant quantities for the background with the following relations⁵:

$$\epsilon = \frac{1}{2\bar{\rho}^2} \left(\frac{V_{\theta}}{V} \right)^2, \quad \eta = \frac{2}{\bar{\rho}^2} \left(\frac{V_{\theta\theta}}{V} \right) + 4\epsilon - 2\delta, \quad \delta = \frac{\dot{\bar{\rho}}}{\bar{\rho}H}, \quad N = \int \bar{\rho}^2 \frac{V}{V_{\theta}} d\theta, \quad (4.15)$$

where $\bar{\rho}$ is the solution to $\rho^3 V_{\rho} = V_{\theta}^2/3V$ and N is the number of e-folds before the end of inflation. From here it is clear that the time dependence of $\bar{\rho}$ has to be explicitly taken into account in order to make accurate predictions. This means that while we can neglect the derivatives of ρ in the e.o.m. its derivatives do play an important role in determining the observables of the model.

As for the perturbations, in a regime in which the angular acceleration $\ddot{\theta}$ is small in comparison with the effective mass of the heavy field [92] (given here by $m_{\text{eff}}^2 = m_{\rho}^2 - \dot{\theta}^2$ and demanding $m_{\text{eff}} \gg H$), the low energy EFT develops a speed of sound of the

⁵These expressions were derived assuming a separable potential. For non separable potentials they remain approximately valid provided $V_{\theta\rho}(d\bar{\rho}/d\theta) \ll V_{\theta\theta}$

fluctuations which is given by⁶

$$c_s^{-2} = 1 + 4 \frac{\dot{\theta}^2}{m_{\text{eff}}^2} \quad \text{where} \quad m_{\text{eff}}^2 = m_\rho^2 - \dot{\theta}^2. \quad (4.16)$$

We refer to [101] for a more detailed discussion. Moreover, it is easy to show that s can be written solely in terms of ϵ , η , δ and c_s :

$$s = \left(\epsilon - \frac{\eta}{2} + \delta \right) (1 - c_s^2) \left(\frac{3}{4} + \frac{1}{4c_s^2} \right). \quad (4.17)$$

With all these elements it is possible to compute all of the observables of the model, i.e. r and n_s , without having to solve any dynamical equation, as in the standard slow-roll computation. As can be seen from eq. (4.16), in order to have a substantial reduction in the speed of sound we will need large angular velocities, of the order of the effective heavy mass. This is consistent with slow-roll whenever the radius of curvature is small enough, and that is the reason why we will demand the condition $\rho_0 < 1$ to be satisfied.

Before closing this section, two comments are in order. First, it is important to ensure that the theory stays weakly coupled up to the scale where new physics cannot be further integrated out. In models with a reduced speed of sound, this places a theoretical lower bound on the speed of sound [79, 94]. Every case presented here is consistent with this bound, provided a scale dependent speed of sound - like the one we have - is taken into account.

Secondly, a reduction in the speed of sound unavoidably implies a cubic interaction for the adiabatic perturbation [34], producing potentially observable non-gaussianity. In particular, for the case of a nearly constant speed of sound we have [62][101]:

$$f_{NL}^{(eq)} = \frac{125}{108} \frac{\epsilon}{c_s^2} + \frac{5}{81} \frac{c_s^2}{2} \left(1 - \frac{1}{c_s^2} \right)^2 + \frac{35}{108} \left(1 - \frac{1}{c_s^2} \right). \quad (4.18)$$

This means that in order to have a measurable non gaussianity $|f_{NL}^{eq}| > 5$, we need $c_s < 0.2$ (which is still consistent with weak coupling [79, 94]). While it is interesting to search for such values of c_s , we will notice that much milder reductions in the speed of sound can already leave big imprints in the power spectrum, and we are thus going to focus mainly on mild reductions of c_s .

⁶The speed of sound presented here is the $k \rightarrow 0$ limit of the speed of sound obtained by integrating out the heavy mode. The k -dependence is not extremely important to compute the observables of the theory - at least for moderate reductions in c_s - but it becomes important in order to assess the overall consistency and predictivity of the theory [79, 94, 189]. Whenever needed, we use the full k -dependent c_s .

4.3 Quadratic inflation

Our first example to show how a heavy field may influence the low energy dynamics is a two-field embedding of the quadratic inflation model. The Lagrangian for the single field model [31] is given by:

$$\mathcal{L} = \frac{1}{2} \partial_\nu \phi \partial^\nu \phi - \frac{1}{2} m_\phi^2 \phi^2. \quad (4.19)$$

We embed this model in the two field scenario (4.1), and consider the following Lagrangian:

$$\mathcal{L} = \frac{1}{2} \partial_\nu \rho \partial^\nu \rho + \frac{1}{2} \rho^2 \partial_\nu \theta \partial^\nu \theta - \frac{m_\rho^2}{2} (\rho - \rho_0)^2 - \Lambda^4 \theta^2. \quad (4.20)$$

Assuming $\rho = \rho_0$, and defining $\phi = \rho_0 \theta$, we recover the single field Lagrangian with the mass m_ϕ given by $m_\phi^2 = 2\Lambda^4/\rho_0^2$. Thus, at the level of this truncation, both Lagrangians (4.19) and (4.20) are equivalent. Going beyond this simplification demands solving the full e.o.m. Fortunately we can rely on the reduced e.o.m. to find approximate solutions. Solving equations (4.8), (4.9) and (4.10), the minimum in the radial direction, $\bar{\rho}$, is given by the root of the following equation:

$$\bar{\rho}^3 (\bar{\rho} - \rho_0) - \frac{4}{3} \frac{\Lambda^4}{m_\rho^2} = 0, \quad (4.21)$$

while the angular velocity is given by

$$\dot{\theta} = -\frac{2}{\sqrt{3}} \frac{\Lambda^2}{\bar{\rho}^2}. \quad (4.22)$$

Here we have used $V = V(\theta)$, which, as we will remark below, is a very good approximation. With these solutions at hand we can then predict how the observables move in the (n_s, r) plane. In doing so we will split the effects on the background and perturbations.

Background model: All the relevant quantities for calculating the background can be found in equation (4.15). First of all, because $\bar{\rho} \neq \rho_0$, the potential V will have a contribution of the form $V_0 = \frac{m_\rho^2}{2} (\bar{\rho} - \rho_0)^2$. It is easy to show that this contribution is negligible in comparison with $V(\theta)$ in the computation of the slow-roll parameters at $N = 50 - 60$ ⁷. Thus, we can use $V \sim V(\theta)$. Under this simplification, and because $\bar{\rho} \sim cte$, the background model yields the same predictions as in the standard quadratic inflation, i.e. $\epsilon = 1/2N$ and $\eta = 1/N$.

⁷This approximation breaks down towards the end of inflation. The numerical results confirm that it does not affect the predictions at the observables scales.

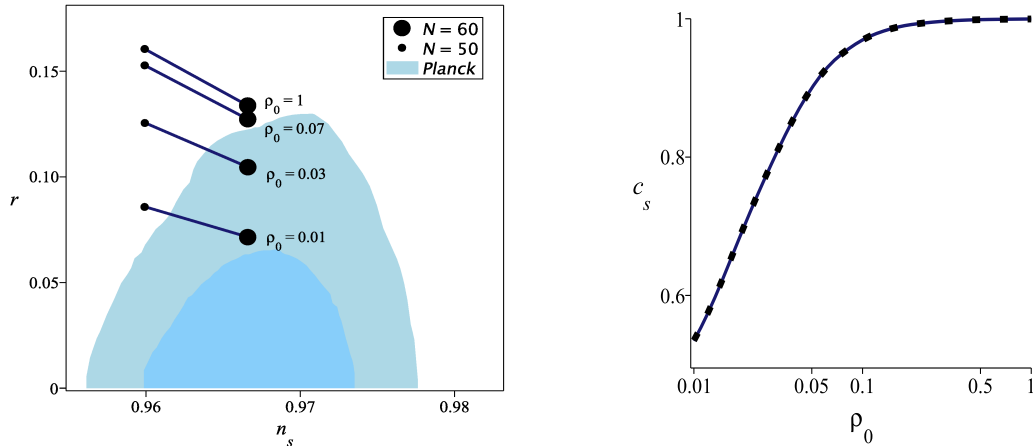


FIGURE 4.1: *Left*: The (n_s, r) plane for $m^2\phi^2$ inflation when embedded in the model given by (4.20), with the mass of the heavy field given by $m_{\text{eff}}^2 = 100H^2$. The predictions are calculated using the EFT, which is an excellent description for the full two-field system. The blue regions are the 1- σ and 2- σ allowed regions from Planck [30]. *Right*: Speed of sound of the adiabatic fluctuation, given by equation (4.16) for $N = 50 - 60$. The dotted line is computed using the numerical solution of the full two-field system (4.20), and the solid line is computed with the semi-analytical approximation of equation (4.15).

EFT for the perturbations: While the background does not change as we change ρ_0 , we find that perturbations develop a constant speed of sound which is noticeably different from 1 for values of $\rho_0 < 0.1$, as can be seen in the right panel of figure 4.1.

Putting all these elements together we compute the prediction for (n_s, r) . Since ϵ and η are unchanged, and $s \sim 0$, only the tensor to scalar ratio is going to be modified, and its modification will only be due to the change in c_s . We test these predictions with a numerical solution of the two-field system (partly done using the code from [190]), choosing ρ_0 ranging from 0.01 to 1 and m_ρ such that $(m_{\text{eff}}/H)^2 = 100$ in the observable scales. We fix Λ such that we have the right amplitude for the perturbations. Let us note that we have fixed the effective mass of the heavy field (which is always smaller than the bare mass m_ρ) such that it is much greater than the Hubble parameter. Our results are summarized in figure 4.1, displayed together with the experimental bounds from Planck⁸ [30]. First of all, there is very good agreement between the predictions of the analytical single field EFT and the full two-field system, and more importantly, there are sizeable effects in terms of where the predictions lie in the (n_s, r) plane.

In particular, we see that when decreasing ρ_0 the quadratic potential becomes more consistent with Planck confidence regions. This is not a surprising result, since we know that reduced speeds of sound lead to smaller values for the tensor to scalar ratio, but

⁸From the PLA-PR2-2015 official chains including TT,TE and low- l polarization data at <http://pla.esac.int/pla/>.

the fact that this can be achieved with the simple quadratic potential “UV completed” with an additional very massive field is worth noting. Let us note that larger reductions in the speed of sound can easily be attainable provided we consider smaller values for ρ_0 . This will further increase the consistency with the data as well as generating potentially observable non gaussianities (e.g for, $\rho_0 = 10^{-3}$ we find $|f_{NL}^{eq}| \sim 5$).

4.4 Linear inflation

We repeat the analysis, this time for the linear inflaton potential [184]. We consider the following Lagrangian:

$$\mathcal{L} = \frac{1}{2}\partial_\nu\rho\partial^\nu\rho + \frac{1}{2}\rho^2\partial_\nu\theta\partial^\nu\theta - \frac{m_\rho^2}{2}(\rho - \rho_0)^2 - \alpha\theta \quad (4.23)$$

This embedding was already studied in [101], where very small values of ρ_0 ($\rho_0 \sim 10^{-4}$) were considered in order to find large reductions in the speed of sound, as a working example of how decoupling works in this setup. We complement those results with the predictions for the values of ρ_0 considered here, in order to show how the theory flows from the vanilla linear potential to the new predictions. The v.e.v. of the radial field can be found by solving the reduced e.o.m.. Again, we can set $V = V(\theta)$, so that we have the following algebraic equation for the radial field $\bar{\rho}$:

$$\frac{\alpha}{3\bar{\rho}^4\theta} = m_\rho r^2 \left(1 - \frac{\rho_0}{\bar{\rho}}\right) \quad (4.24)$$

Here, the solution for $\bar{\rho}$ will explicitly depend on both θ and ρ_0 . However, the dynamics in ρ is such that its time derivatives are still negligible in the e.o.m. Because $\bar{\rho}(\theta)$ is a complicated function of θ , it is not easy to find an effective potential. Fortunately, we can solve the system by considering the slow-roll parameters as given in (4.15). The solution of this system is such that ϵ becomes *bigger* as we decrease ρ_0 . In principle this is bad news since we would not like to move away from the 1σ contour of Planck data (see figure 4.2).

Fortunately, as ρ_0 decreases, c_s decreases, which dominates over the increase in ϵ . This means that the tensor to scalar ratio r decreases as ρ_0 decreases. We show these effects in fig. 4.2 where we plot the full EFT i.e. considering the combined effect of background and perturbations, and the predictions considering only the effects on the background. We also add the prediction for the parameters considered in [101] ($\rho_0 = 6.8 \times 10^{-4}$, $m_{\text{eff}}^2 = 250H^2$).

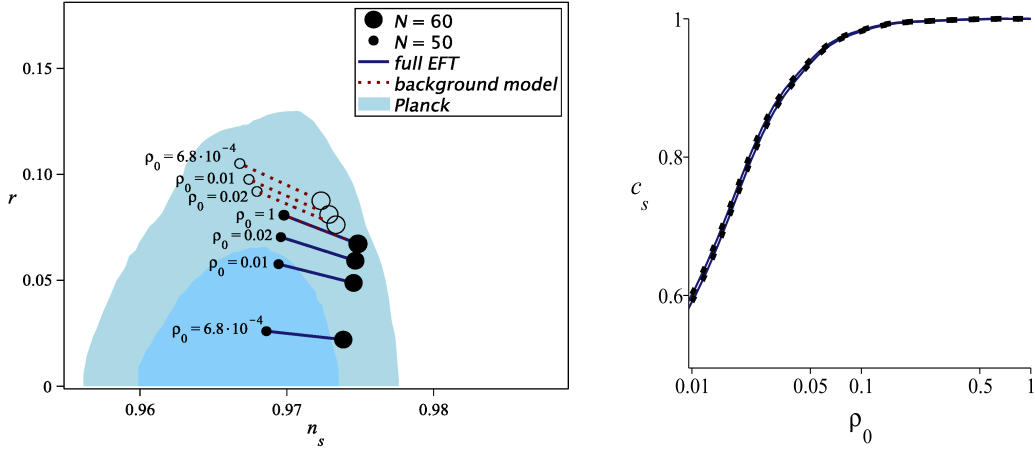


FIGURE 4.2: *Left*: The (n_s, r) plane for inflation with linear potential when embedded in the two-field model given by (4.23), with the mass of the heavy field given by $m_{\text{eff}}^2 = 100H^2$. The points are calculated using the EFT, which we have checked is an excellent approximation to the numerical two-field prediction. For comparison, we also plot the predictions if we had only considered the effects on the background (red dotted line). *Right*: Speed of sound of the adiabatic fluctuation equation (4.16) for $N = 50 - 60$. The dotted line is computed using the full two-field numerical solution of (4.23), and the solid line is the semi-analytical single-field approximation equation (4.15).

As for the quadratic potential, larger reductions in the speed of sound can easily be attainable provided we consider smaller values for ρ_0 . This will also increase the consistency with the data as well as generating potentially observable non gaussianities (e.g for, $\rho_0 = 10^{-3}$ we find $|f_{NL}^{eq}| \sim 5$).

4.5 Natural inflation

Finally, we consider the case for natural inflation [32]. The total Lagrangian is given by

$$\mathcal{L} = \frac{1}{2} \partial_\nu \rho \partial^\nu \rho + \frac{1}{2} \rho^2 \partial_\nu \theta \partial^\nu \theta - \frac{m_\rho^2}{2} (\rho - \rho_0)^2 - \Lambda^4 (1 + \cos(m\theta)). \quad (4.25)$$

This two-field completion is consistent with the original motivation of the inflaton being a Nambu-Goldstone boson, as the additional field ρ respects the $U(1)$ symmetry. If we assumed that the field ρ acquires its v.e.v. at the minimum of the potential, and defining the canonical field as $\phi = \rho_0 \theta$ we would get the standard potential, given by:

$$\mathcal{L} = \frac{1}{2} \partial_\nu \phi \partial^\nu \phi - \Lambda^4 \left(1 + \cos \left(\frac{\phi}{f_0} \right) \right). \quad (4.26)$$

where $f_0 = \rho_0/m$ would be the so-called decay constant. Again, we will show that in general the dynamics of the radial field cannot be neglected - even at energies below the spontaneous symmetry breaking scale - so that (4.26) is not a good description of (4.25).

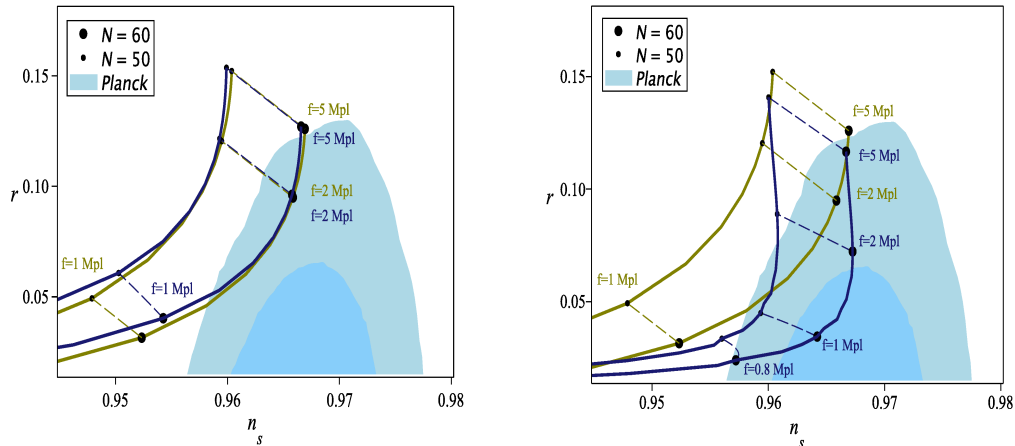


FIGURE 4.3: The (n_s, r) plane for inflation with the natural potential, with the mass of the heavy field given by $m_{\text{eff}}^2 \sim 100H^2$. The green line is the standard natural inflation scenario given by (4.26). The blue line is the two-field model in (4.25), for different values of the instantaneous decay constant $f = \bar{\rho}/m$. The agreement between the numerical and semi-analytical predictions is excellent. Although the potential steepens, the predictions moves towards the best fit region because of c_s . *Left*) $m = 0.01$ *Right*) $m = 0.002$

While the natural - or axionic - potential is well motivated from the point of view of generic extensions of the Standard Model, the fact that decay constants larger than M_{pl} are needed in order to achieve successful inflation is a problem from the point of view of the UV completion [191]. Attempts to construct effectively super planckian decay constants by considering several axions coupled together were first considered in [174, 175]. Here instead, we take a different route. We will show that the presence of a heavy degree of freedom can improve the situation, in the sense that the overlap in the (n_s, r) plane between the predictions and the experimentally allowed region is greater. Since we cannot write an effective potential of the form (4.26), it is not completely fair to talk about a decay constant in our model. However, if we consider an *instantaneous* decay constant i.e. $f = \bar{\rho}/m$ (which is changing adiabatically as $\dot{f}/Hf = \dot{\bar{\rho}}/H\bar{\rho} \ll 1$), we will show that indeed subplanckian values of f could be consistent with the data.

As in the case of the linear potential, it is a difficult task to find an effective potential, but we can compute the single field predictions by using the expressions for ϵ , η and ΔN as in eqs. (4.15) and c_s and s in eqs. (4.16) and (4.17). We compare these predictions with the two-field model, in this case by considering two values for m , $m = \{0.01, 0.002\}$, and find an excellent agreement. The results are shown in figures 4.3 and 4.4.

Interestingly, as in the case of the linear and quadratic potential, the predictions move towards the best fit region. While the potential steepens due to the presence of the heavy field (so one might think the two-field model is disfavored with respect to the single field model), the reduced speed of sound and its variations causes the predictions to move towards the allowed experimental region. We also notice that $0.8M_{pl} < f < 1M_{pl}$ is

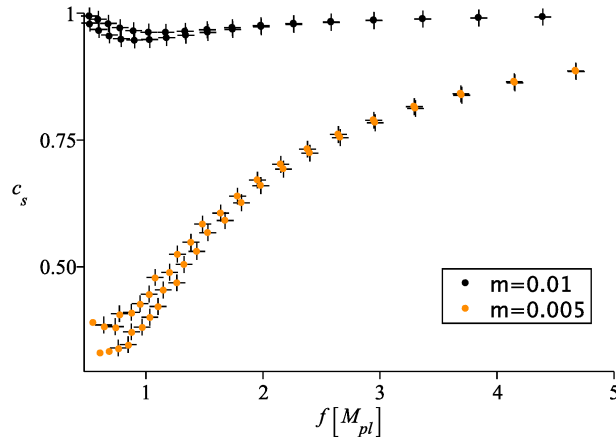


FIGURE 4.4: Speed of sound of the adiabatic fluctuations in the natural inflation model as a function of the instantaneous decay constant $f = \bar{\rho}/m$, for two values of m , $m = 0.01$ and $m = 0.002$. Each data point is double, representing the values for c_s at $N=50$ (lower) and $N=60$ (upper). The dots are computed using the full two-field model while the crosses are obtained using the semi-analytical single field approximation.

consistent with Planck data for the case $m = 0.002$. In the region where sub-planckian decay constants overlap with Planck contours, $|f_{NL}^{eq}| \sim 1$. Larger values of $|f_{NL}^{eq}|$ can be achieved by considering smaller values of m . Whether the Lagrangian (4.25) arises in some UV completion remains however an open question.

4.6 Conclusion

Natural inflation and quadratic inflation are theoretically appealing scenarios but their single field realizations are in tension with the data. In general, one expects the single field description to be an EFT in which the effects of massive fields have been integrated out. Crucially, while in some cases truncating the heavy field is a good approximation to construct the EFT, there is a regime in which the inflationary predictions can be very different from those of the single field truncated theory. This can happen even if the additional fields have masses much greater than the Hubble parameter. Considering that the heavy field tracks its instantaneous, adiabatic, ground state along the inflationary trajectory (which, on a turning trajectory, is displaced from the minimum of the potential) leads to modifications of the background evolution, as well as reducing the speed of sound of the light mode fluctuations. As we have shown, both effects are crucial in obtaining the correct predictions for where a model lies in the (n_s, r) plane, as well as the expected level of non gaussianities.

In this chapter we have illustrated this idea in a very simple two-field embedding of various large field inflation models, in which the inflaton is approximately the phase of a complex field where a $U(1)$ symmetry is mildly broken. We find that this embedding

can, in a weakly coupled regime, make models that are in tension with the data, viable. In particular, the quadratic potential and the natural potential with subplanckian values of the decay constant are no longer disfavored. Although the effective potential *steepens* in these examples, the effect of the speed of sound on the perturbations dominates: while ϵ increases, the tensor to scalar ratio goes *down* due to the reduced speed of sound, c_s . Furthermore, adiabatic changes in c_s along the trajectory can also modify of the spectral index. We have presented an analytic approximation which enables us to easily calculate all the relevant observables

Finally, we should add that this phenomenology is not restricted to the particular embedding studied here i.e. a flat field-space metric and a separable potential. The essential characteristic is that inflation happens on a curved trajectory (with respect to the field-space metric) with a large, sustained mass hierarchy. The same approximate symmetry that protects the inflaton mass and slow-roll parameters also keeps the radius of curvature and the mass of the heavy orthogonal direction approximately constant (for a recent discussion on adiabaticity and the slow-roll conditions see [101] and references therein). In this regime the radial field can be integrated out, and the isocurvature perturbations decay quickly outside the horizon. The resulting effective theory for the perturbations has a reduced speed of sound that changes slowly along the trajectory. As shown here, the effects of this reduction can be very important in obtaining the correct predictions for inflationary observables.

5

The two-field regime of natural inflation

In this last chapter we deviate from the “speed of sound” phenomenology in order to show a different mechanism by which multifield dynamics can affect the inflationary predictions. In particular, we show that the simplest two-field completion of natural inflation has a regime in which both fields are active and in which its predictions are within the Planck $1\text{-}\sigma$ confidence contour. We show this for the original model of natural inflation, in which inflation is achieved through the explicit breaking of a $U(1)$ symmetry. We consider the case in which the mass coming from explicit breaking of this symmetry is comparable to that from spontaneous breaking, which we show is consistent with a hierarchy between the corresponding energy scales. While both masses are comparable when the observable modes left the horizon, the mass hierarchy is restored in the last e-foldings of inflation, rendering the predictions consistent with the isocurvature bounds. For completeness, we also study the predictions for the case in which there is a large hierarchy of masses and an initial period of inflation driven by the (heavy) radial field.

This chapter is based on

- *The two-field regime of natural inflation*, A. Achúcarro, V. Atal and M. Kawasaki, F. Takahashi, JCAP **1512** (2015) 12, 044 [arXiv:1510.08775 [astro-ph.CO]].

5.1 Introduction

One of the most prominent models of inflation is natural inflation [32]. In its original version, the inflaton is the Nambu-Goldstone boson of a spontaneously broken $U(1)$ symmetry. In particular, the inflaton is the phase of a complex field whose modulus is strongly stabilized. A mass for the inflaton, stable under radiative corrections, can be generated via explicit symmetry breaking terms. For example, instanton effects can create such a potential, as in the case of the Peccei-Quinn mechanism for strong CP conservation [192–195]. The $U(1)$ symmetry is broken to a discrete subgroup $\phi \rightarrow \phi + 2\pi f$, and the potential for the inflaton (in this case an axion) is given by

$$V = \Lambda^4 (1 + \cos(\phi/f)) \ , \quad (5.1)$$

where f is the so-called axion decay constant, Λ is a dynamically generated scale that sets the overall magnitude of the potential and a cosmological constant has been tuned to make the potential vanish at the minimum of the potential. While this model is under good theoretical control for subplanckian values of f (where the Planck mass $M_{\text{pl}} = 1.22 \times 10^{19} \text{ GeV}$), recent data by the Planck satellite [30] seems not to be consistent with its predictions for the tilt of the power spectrum n_s , and tensor to scalar ratio r . Furthermore, the region in which the tension between the prediction and the observations is less severe is for super planckian values of f , in which one may expect the low energy effective theory to break down [191]¹. This has motivated the study of modifications of the single field potential (5.1), in order to test if the tension persists with theoretically and/or phenomenologically well motivated extensions. For example, the predictions in the (n_s, r) plane might be substantially affected when considering many axions [175, 199, 200], multiple sinusoidal functions [199, 201], extra non-renormalizable operators [202, 203], different periodic functions [204], and/or higher dimensional theories [205]. Some completions are based on the fact that the constants that determine the low energy potentials are, in general, vacuum expectation values (v.e.v) of additional fields, and that their dynamics can be non-trivial. For example, even if these additional fields are very heavy with respect to the energy scale of inflation, they can induce changes in the effective potential [176, 206, 207] and/or in the speed of sound of the inflaton fluctuations [208]. The Nambu-Goldstone boson may also take different functional forms, depending on the symmetry that is being broken [209–213], or, e.g. the field content in higher dimensional theories [184, 185].

¹However, several mechanisms to achieve the potential (5.1) with $f > M_{\text{pl}}$ consistent with a low energy description have been put forward in the literature [174, 187, 196, 197]. It has also been pointed out that non-perturbative dynamics in the single field potential can make the predictions for subplanckian values of f consistent with CMB data [198].

We aim to explore the multifield regime of natural inflation in a very simple completion in which, in addition to the angular field $\theta = \arg[\Phi]$ (which has a sinusoidal potential), there is a radial field $r = |\Phi|$ which is not strongly stabilized. We will work with *same* original model as proposed in [32], in which there is a quartic spontaneous symmetry breaking potential together with a term $V \propto \Phi + \bar{\Phi}$ that explicitly breaks the $U(1)$ symmetry. Irrespective of the hierarchy between the explicit and spontaneous symmetry breaking scales, the masses of both radial and angular field may or may not be comparable. On the one hand, if the radial field is very heavy with respect to the scale of inflation, its v.e.v will be strongly stabilized and determined only by the spontaneous symmetry breaking scale. The effective potential will then reduce to (5.1). This case is well understood, and its predictions were first computed in [32]. On the other hand, if both masses are similar none of the fields will be strongly stabilized, and the dynamics of both of them will become important. The objective of this paper is to study this latter case.

5.2 Natural models

We will study the following Lagrangian:

$$\mathcal{L} = \frac{1}{2} \partial_\mu \Phi \partial^\mu \bar{\Phi} - \lambda (r_0^2 - |\Phi|^2)^2 - \Lambda^3 (\Phi + \bar{\Phi}) , \quad (5.2)$$

which is a very simple completion of (5.1). Here r_0 is the scale of the spontaneous $U(1)$ breaking and Λ represents the scale of the explicit breaking. As we will see later, generating the right amplitude for the two-point function of the curvature perturbations fixes $r_0 \gg \Lambda$. Writing $\Phi = r e^{i\theta}$, the Lagrangian can be written as

$$\mathcal{L} = \frac{1}{2} \partial_\mu r \partial^\mu r + \frac{1}{2} r^2 \partial_\mu \theta \partial^\mu \theta - \lambda (r_0^2 - r^2)^2 - 2\Lambda^3 r \cos \theta . \quad (5.3)$$

It is useful to define the following dimensionless quantity

$$\beta = \frac{2\Lambda^3}{r_0^3 \lambda} , \quad (5.4)$$

so the potential can be written as

$$V = \mu^4 \left[\left(1 - \left(\frac{r}{r_0} \right)^2 \right)^2 + \beta \left(\frac{r}{r_0} \right) \cos \theta \right] \quad (5.5)$$

where $\mu^4 = \lambda r_0^4$. Written in this way, it is clear that the only parameters that determine the dynamics of the theory are r_0 and β , since μ is an overall factor which is fixed by

the amplitude of the two-point function². While both r_0 and β will determine the axion decay constant at low energies (equal to r_0 when $\beta \ll 1$), only β controls the hierarchy between the masses of the radial and angular field. Importantly, a value $\beta \sim \mathcal{O}(1)$ will still imply a hierarchy between Λ and r_0 , of the order $\Lambda/r_0 \sim 10^{-4}$, as a rather small value for μ (which implies a small value for λ when $r_0 \sim M_{\text{pl}}$) is needed in order to fix the amplitude for the two-point function. In other words, multifield dynamics ($\beta \sim \mathcal{O}(1)$) will still imply a hierarchy between both energy scales. As corrections to the potential are expected to go as $(\Lambda/r_0)^n$ -where n is some positive power- higher order contributions will still be under control.³

Defining $x = r/r_0$ and adding a cosmological constant V_0 , we write the potential as

$$\frac{V}{\mu^4} = (1 - x^2)^2 + \beta x \cos \theta + \frac{V_0}{\mu^4}. \quad (5.6)$$

Minimizing in the radial direction at $\theta = \pi$, we get

$$\left. \frac{dV}{dr} \right|_{\theta=\pi} = 0 \quad \rightarrow \quad 4(1 - x^2)x + \beta = 0. \quad (5.7)$$

Evaluating the potential at x satisfying (5.7) gives the contribution of the cosmological constant, which is then fixed once we choose values for r_0 and β . As the second term in (5.7) is non-zero, the absolute minimum is reached for values of $x \neq 1$ (or equivalently $r \neq r_0$). The deviation from $r = r_0$ is going to be negligible when $\beta \ll 1$ but becomes important for values of $\beta \sim 1$. Since in the minimum of the potential the field is stabilized at a radius $r \neq r_0$, the low energy effective theory will have a decay constant that is in general different from r_0 .

One necessary condition for having a single field description is that at the instantaneous minimum the mass of the orthogonal field is much bigger than the Hubble scale H .⁴ We can thus compute the mass eigenvalues at the minimum, and see how they change as we vary β . With canonical kinetic terms (as given in eq. (5.3)), the mass matrix is given by

$$V_{IJ}^I = \frac{\mu^4}{r_0^2} \begin{pmatrix} 12x^2 - 4 - \frac{\beta \sin \theta}{x} \\ -\frac{\beta \sin \theta}{x} & -\frac{\beta \cos \theta}{x} \end{pmatrix}, \quad (5.8)$$

²Furthermore, r_0 cannot be absorbed into the definition of r since the kinetic term only depends on r and not on the combination r/r_0 .

³Take for example the case in which Λ is generated by non-perturbative gravitational effects [214]. In this case $\Lambda^3 = e^{-S} M_{\text{pl}}^3$, where S is the action a wormhole configuration. Contributions of the order $e^{-nS} \cos(n\theta)$ are going to be $(\Lambda^3/M_{\text{pl}}^3)^n \cos(n\theta)$ which are small considering that $\Lambda/r_0 \ll 1$ and $r_0 \sim M_{\text{pl}}$.

⁴A single field description does not necessarily mean that the heavy field can be *truncated*. Even if there is no particle production, a heavy field may have a time-dependent v.e.v and/or be displaced from the minimum, modifying the low energy effective potential [168, 183, 215] and/or speed of sound of the fluctuations [55].

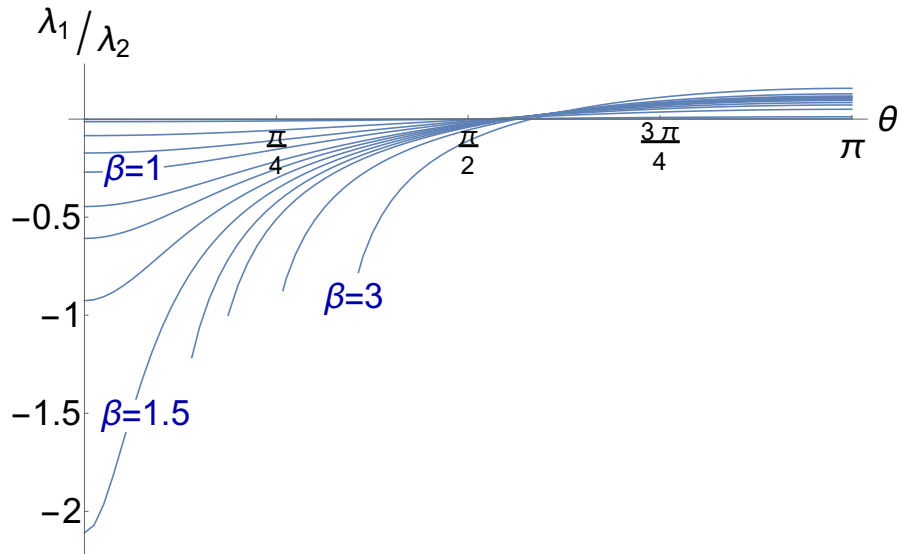


FIGURE 5.1: Ratio of the two eigenvalues of the mass matrix evaluated at the radial minimum, for different values of β .

and the eigenvalues are then:

$$\lambda_{1,2} = \frac{\mu^4}{r_0^2} \left[6x^2 - 2 - \frac{\beta \cos \theta}{2x} \pm \left[\left(6x^2 - 2 - \frac{\beta \cos \theta}{2x} \right)^2 - \Delta \right]^{1/2} \right] \quad (5.9)$$

with Δ the determinant of the mass matrix (ignoring the prefactor m^4/r_0^2). In the limit $\beta \ll 1$, λ_1 and λ_2 correspond to the mass (squared) eigenvalues of θ and r respectively. When $\beta \sim \mathcal{O}(1)$, the mass eigenstates are a linear combination of the radial and angular field. In figure 5.1 we evaluate the ratio λ_1/λ_2 at the radial instantaneous minimum of the potential, as a function of β .

We can see that for values of $\beta < 1$ there is a sufficient hierarchy in the mass eigenvalues at the minimum of the potential. Provided that there are no strong turns in the trajectory the field will track the instantaneous minimum of the potential. This is indeed the case, since the radius of curvature is large ($\sim M_{\text{pl}}$), and then the angular velocity $\dot{\theta}$ - which sets the strength of the centrifugal force that displaces the field from the instantaneous minimum - is small during inflation⁵. If the observable scales leave the horizon when the heavy radial field is stabilized in its minimum, the predictions for the inflationary observables will coincide with the single field predictions of (5.1). There is still the possibility that there is a first period of inflation driven by the heavy radial field, *à la* chaotic inflation, and if the observable scales leave the horizon during or before the transition this may cause departures from the single field predictions of (5.1). We

⁵If the radius of curvature is small (and then a monodromy in θ must be assumed to have large field inflation) then the effects of the displacement from the radial minimum may become very important [208].

compute the predictions for this particular case in the last section. The more interesting case is for $\beta \gtrsim 1$, for which the mass eigenvalues are of the same order in some part of the trajectory. Furthermore, for $\beta > 1.5$ there is no minimum in the radial direction for small values of θ . This will ensure that the dynamics are of a multi-field nature. As the hierarchy is restored when approaching the absolute minimum at $\theta = \pi$, the isocurvature perturbations will be eventually damped. We will study this case in section IV. Let us note that the presence or absence of a hierarchy between the masses does not ensure that inflation will happen, as inflation requires at least one of the eigenvalues to be smaller than the Hubble parameter. By numerically evaluating the background we will see that many trajectories have indeed enough e-foldings of inflation.

In any multifield model one should be concerned about the presence of isocurvature modes in the CMB, as they are heavily constrained by Planck data [30]. The constraints are usually stated in terms of the primordial isocurvature fraction, defined as

$$\beta_{iso}(k) = \frac{P_{II}(k)}{P_{\mathcal{R}\mathcal{R}}(k) + P_{II}(k)}, \quad (5.10)$$

where $P_{\mathcal{R}\mathcal{R}}(k)$ and $P_{II}(k)$ are the power spectra of the curvature and isocurvature perturbations. The Planck constraints are given specifically for a variety of models, in which the isocurvature component is attributed to one of the different elements of the plasma, and different correlations are assumed between the curvature and isocurvature components. None of these idealized situations corresponds exactly to our case as we do not specify, for example, a mechanism for reheating. We can however take a nominal value of $\beta_{iso} < 0.01$, which is the typical order of magnitude for these constraints.

As we argued in Chapter 2, while the isocurvature mode may be relevant when the observable scales left the horizon, the field with isocurvature perturbations can decay if it becomes heavy between horizon crossing and the end of inflation (see, e.g [85–88]). One can see from figure 5.1 that when the absolute minimum of the potential is reached (at $\theta = \pi$), the hierarchy between the eigenvalues is restored ($\lambda_2 \gg \lambda_1$). If the trajectories follow this minimum before the end of inflation, the isocurvature mode will be rapidly damped, and the model will be consistent with the Planck isocurvature bound. Furthermore, the amplitude of local non-gaussianity will also be damped during this period [85], and thus the level of non-gaussianity will be consistent with observations.

Another consequence of the presence of an additional dynamical direction in the axion potential has to do with the initial conditions. In the single field potential (5.1), a number N_* of e-folds are achieved by setting the initial angle at θ_* given by

$$\theta_* = 2 \arcsin \left[\left(1 + \frac{1}{2f^2} \right)^{1/2} e^{-N_*/2f^2} \right]. \quad (5.11)$$

It is then possible to assign a probability for having more than N_* e-folds by assuming, e.g. a linear probability distribution for θ_{ini} in the interval $[0, 2\pi]$. For example, for $f = 1M_{\text{pl}}$ there is a 20% probability of having more than 60 e-folds (ignoring the fact that the patches of the Universe that inflate are much bigger than those who don't, and that this enhances the probability of observing those patches). When considering the effects of the radial direction in field space, we will find that it is possible to inflate for values of $\theta_{\text{ini}} < \theta_*$. We now review the basics of multifield inflation, but refer the reader to Chapter 2 for further details.

5.3 Equations of motion

In order to compute the predictions for the model we first solve the background equations of motion. For a general multifield model with n -fields $\phi(t)^a$ (a ranging from 1 to n), and field space metric γ_{ab} , the background equations of motion are⁶

$$D_t \dot{\phi}_0^a + 3H \dot{\phi}_0^a + V^a = 0 \quad (5.12)$$

$$3H^2 = \dot{\phi}_0^2/2 + V, \quad (5.13)$$

where $\phi_0(t)^a$ is the time dependent background component of the field $\phi^a(t)$, $\dot{\phi}_0^2 \equiv \gamma_{ab} \dot{\phi}_0^a \dot{\phi}_0^b$, $H = \dot{a}/a$ and $D_t X^a = \dot{X}^a + \Gamma_{bc}^a \dot{\phi}_0^b X^c$ is a covariant time derivative, with

$$\Gamma_{bc}^a = \gamma^{ad} (\partial_b \gamma_{dc} + \partial_c \gamma_{bd} - \partial_d \gamma_{bc})/2. \quad (5.14)$$

In our case, working in polar coordinates such that $\phi^a(t) = (r, \theta)$ and with flat field space metric γ_{ab} ($\gamma_{11} = 1, \gamma_{22} = r^2$ and $\gamma_{12} = \gamma_{21} = 0$), the equations of motion reduce to:

$$\ddot{r} + 3H\dot{r} - r\dot{\theta}^2 + \frac{\mu^4}{r_0} \left[-2\frac{r}{r_0} \left(1 - \left(\frac{r}{r_0} \right)^2 \right) + \beta \cos \theta \right] = 0, \quad (5.15)$$

$$r^2 \ddot{\theta} + 2r\dot{r}\dot{\theta} + 3Hr^2\dot{\theta} - \mu^4 \beta \frac{r}{r_0} \sin \theta = 0, \quad (5.16)$$

and

$$3H^2 = \frac{1}{2}\dot{r}^2 + \frac{1}{2}r^2\dot{\theta}^2 + \mu^4 \left[\left(1 - \left(\frac{r}{r_0} \right)^2 \right)^2 + \beta \left(\frac{r}{r_0} \right) \cos \theta \right]. \quad (5.17)$$

Having solved the background trajectory, it is useful to define vectors parallel and perpendicular to the trajectory. This set of vectors forms a basis on which the equations for the perturbations can be projected. The curvature perturbations are nothing more than

⁶In this section, we set the reduced Planck mass $m_{\text{pl}} = M_{\text{pl}}/8\pi^2$ to 1.

the projection along the tangential direction, while the isocurvature perturbation is the projection on the perpendicular direction [55, 66, 67]. The tangential vector is given by $T^a = \dot{\phi}^a / \dot{\phi}_0$, and the normal vector is constructed such that $T_a N^a = 0$ and $N_a N^a = 1$ (indices are raised and lowered with the field space metric γ_{ab}). In the two-field case it is given by $N_a = (\det\gamma)^{1/2} \epsilon_{ab} T^b$ where ϵ_{ab} is the two dimensional Levi-Civita symbol with $\epsilon_{11} = \epsilon_{22} = 0$ and $\epsilon_{12} = -\epsilon_{21} = 1$, such that

$$T^a = \frac{1}{\sqrt{\dot{r}^2 + r^2 \dot{\theta}^2}} (\dot{r}, \dot{\theta}) \quad \text{and} \quad N^a = \frac{r}{\sqrt{\dot{r}^2 + r^2 \dot{\theta}^2}} (\dot{\theta}, -r^{-2} \dot{r}) . \quad (5.18)$$

The rate of change of the tangential vector defines the angular velocity of the trajectory $\dot{\theta}$, as $D_t T^a \equiv -\dot{\theta} N^a$. The slow-roll parameters can be written as

$$\epsilon \equiv -\dot{H}/H^2 \quad , \quad \eta^a \equiv -\frac{1}{H \dot{\phi}_0} D_t \dot{\phi}_0^a . \quad (5.19)$$

While the slow-roll parameter ϵ is a scalar, the change in the inflaton velocity is a two dimensional vector. We may decompose η^a along the normal and tangent directions by introducing two independent parameters η_{\parallel} and η_{\perp} as

$$\eta^a = \eta_{\parallel} T^a + \eta_{\perp} N^a . \quad (5.20)$$

Then, one finds that

$$\eta_{\parallel} = -\frac{\ddot{\phi}_0}{H \dot{\phi}_0} \quad \text{and} \quad \eta_{\perp} = -\frac{V_N}{H \dot{\phi}_0} \quad (5.21)$$

where $V_N = N^a \partial_a V$. It is easy to see that η_{\perp} is just the angular velocity in e-folds, $\eta_{\perp} = \dot{\theta}/H$, and that sufficient inflation only demands ϵ and η_{\parallel} to be small. In flat gauge, the curvature and isocurvature perturbations are given by [81]

$$\mathcal{R} \equiv -\frac{H}{\dot{\phi}^a} T_a \delta\phi^a \quad \text{and} \quad \mathcal{F} = N_a \delta\phi^a , \quad (5.22)$$

which satisfies the following equations of motions

$$\ddot{\mathcal{R}} + (3 + 2\epsilon - 2\eta_{\parallel}) H \dot{\mathcal{R}} + \frac{k^2}{a^2} \mathcal{R} = 2\dot{\theta} \frac{H}{\dot{\phi}_0} \left[\dot{\mathcal{F}} + \left(3 - \eta_{\parallel} - \epsilon + \frac{\ddot{\theta}}{H\dot{\theta}} \right) H \mathcal{F} \right] , \quad (5.23)$$

$$\ddot{\mathcal{F}} + 3H \dot{\mathcal{F}} + \frac{k^2}{a^2} \mathcal{F} + M_{\text{eff}}^2 \mathcal{F} = -2\dot{\theta} \frac{\dot{\phi}_0}{H} \dot{\mathcal{R}} . \quad (5.24)$$

where $M_{\text{eff}}^2 = m^2 - \dot{\theta}^2$, and $m^2 \equiv N^a N^b V_{ab}$ is the bare mass of the field \mathcal{F} . Imposing the Bunch Davies initial conditions when the modes are well inside the horizon, we compute the predictions for different initial positions in field space, and compare them with the Planck confidence contours in the (n_s, r) plane and bounds on isocurvature fluctuations. We repeat this analysis for different values of r_0 and β .

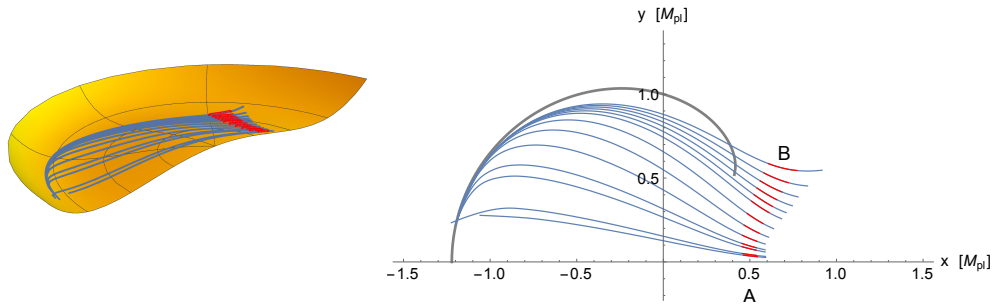


FIGURE 5.2: Different trajectories for different initial conditions in the case $\beta = 2.4$, where $x = r \cos \theta$ and $y = r \sin \theta$. We indicate in red where the pivot scale left the horizon (50 to 60 e-folds before the end of inflation). The gray line tracks the instantaneous minimum of the potential in the radial direction.

5.4 Trajectories with no mass hierarchy

In the case in which $\beta \sim 1$, which we will study in the following sections, both masses are comparable and we are completely in a two-field regime

5.4.1 Case 1: $r_0 = 1M_{\text{pl}}$

An important threshold value for the axion decay constant is the Planck mass. While $f \leq 1M_{\text{pl}}$ is in tension with the data, it seems difficult to achieve $f \geq 1M_{\text{pl}}$ in well controlled models. As we have seen, for values of $\beta \sim \mathcal{O}(1)$ the radial field is not massive enough to make the trajectories follow their instantaneous minimum. We have to numerically evolve the equations of motion in order to compute the trajectories. For a nominal value of $\beta = 2.4$, these trajectories can be seen in figure 5.2.

As one can see, the observable scales are placed at different values of r, θ for different initial conditions, therefore the predictions of the model will depend upon them. Additionally, nearly all of the trajectories converge at the end of inflation. This happens because the mass in the orthogonal direction is increasing, as can be seen in figure 5.3. While the orthogonal mass is sub-Hubble for most of the trajectory -which ensures the two-field effect to be important- it becomes super-Hubble for around 10 e-folds before the end of inflation. This will make the isocurvature perturbations suppressed and unobservable. There are however some trajectories, close to trajectory A in figure 5.2, in which the minimum is never reached before the end of inflation. We expect those trajectories to have a non-negligible amount of isocurvature fluctuations. In figure 5.4 we plot the amount of curvature and isocurvature perturbations (normalized by the single field prediction $P_0 \equiv H^2/8\pi^2\epsilon$, evaluated at horizon crossing) as a function of the number of e-folds N for k_{60} , the mode that left the horizon 60 e-folds before the end of inflation.

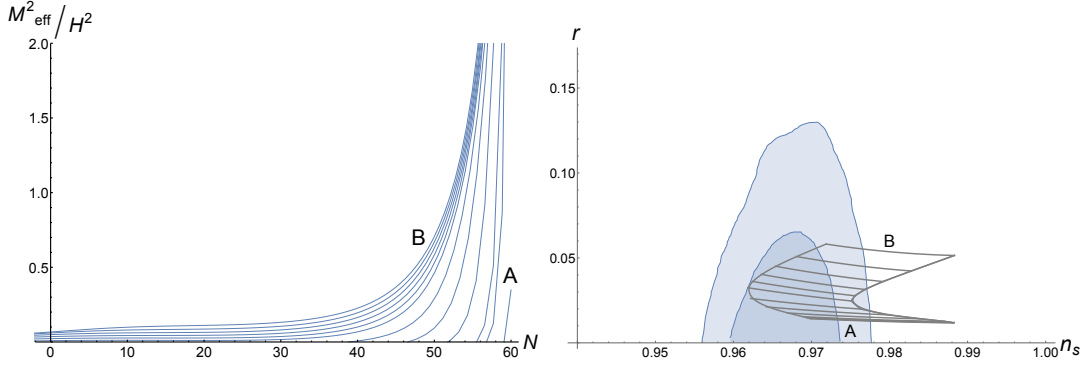


FIGURE 5.3: *Left*: The orthogonal mass to the trajectories for different initial conditions in the case $\beta = 2.4$, as a function of number of e-folds N ($N=60$ is the end of inflation). *Right*: The (n_s, r) plane for the different initial conditions. The width represents the predictions for 50 to 60 e-folds before the end of inflation, and the shaded regions are the 1 and 2- σ confidence contours as given by Planck.

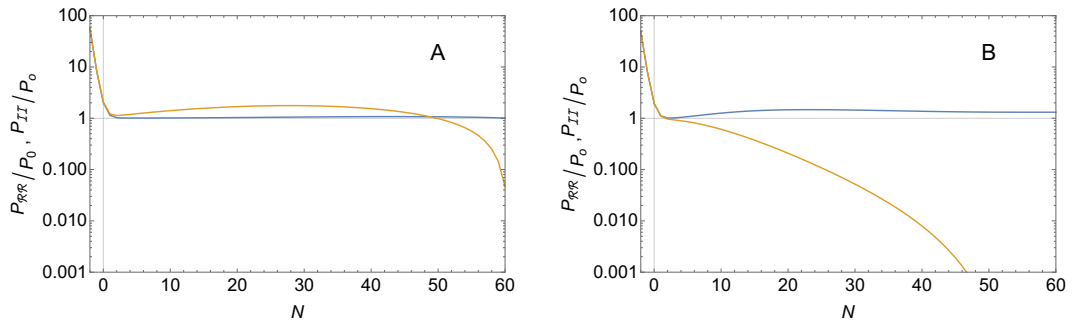


FIGURE 5.4: Curvature (blue) and isocurvature (yellow) perturbations for $\beta = 2.4$ and $r_0 = M_{\text{pl}}$, normalized to $P_0 \equiv H^2/8\pi^2\epsilon$ (with H and ϵ evaluated at horizon crossing). The left panel is for trajectory A, in which the isocurvature perturbations do not have time to decay. The right panel is for trajectory B, in which the isocurvature perturbations decay at the end of inflation.

We can see the isocurvature perturbations decay significantly in the last 10 e-folds of inflation for trajectories close to trajectory B -such that adiabaticity is reached- while they remain large for trajectories close to A. We can plot the amount of isocurvature perturbations as a function of the trajectory, which we choose to parametrize by θ_{60} , the angle of the trajectory 60 e-folds before the end of inflation.

From figure 5.5 we can see that only the trajectories with $\theta_{60} \ll 1$ will have unsuppressed isocurvature fluctuations. The only way to know whether this is a big or small subspace is with a theory of initial conditions, which we do not provide here.

For these values of the parameters ($r_0 = M_{\text{pl}}$ and $\beta = 2.4$) we find that $m^4 \sim 10^{-13} M_{\text{pl}}^4$ is needed in order to fix the amplitude of the primordial curvature perturbations ($H^2/8\pi^2\epsilon \sim 10^{-9}$). This translates into $\Lambda/r_0 \sim 10^{-4}$. This is the *same* order of magnitude needed in the single field natural potential: a smaller value of β (e.g. 0.01) needs

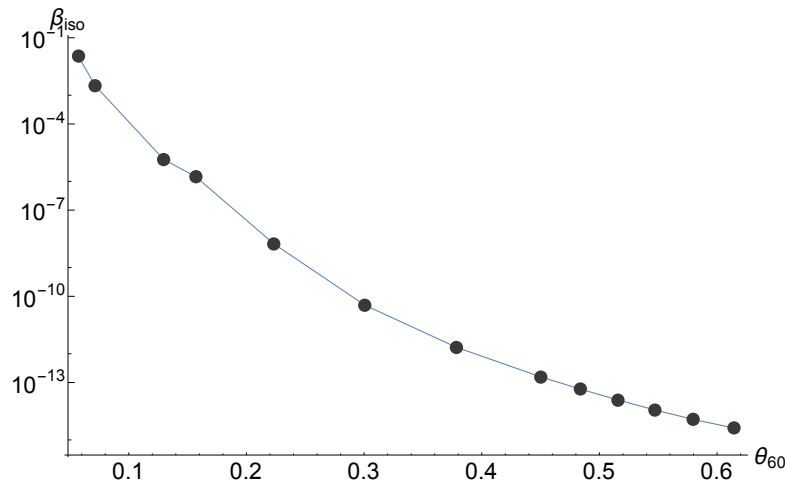


FIGURE 5.5: Isocurvature perturbations at the end of inflation for $\beta = 2.4$ and $r_0 = M_{\text{pl}}$ as a function of θ_{60} , the angle of the trajectory 60 e-folds before the end of inflation. Trajectories with smaller θ_{60} have larger amounts of isocurvature perturbation since they experience the mass hierarchy for a shorter time.

a larger value of $m^4 (\sim 10^{-11} M_{\text{pl}}^4)$ to generate the right amplitude for the fluctuations, resulting in Λ/r_0 of the same order.

5.4.2 Case II: $r_0 = 0.8M_{\text{pl}}$

As subplanckian values of the axion decay constant may be better understood in terms of an effective field theory, it is interesting to know whether the predictions for such values are also in better agreement with the data. We take $r_0 = 0.8M_{\text{pl}}$ as a test case. For comparison, in this case we choose a slightly smaller $\beta = 1.6$. We will expect then the trajectories to be more confined to the instantaneous minimum of the potential. We show the trajectories and their predictions in the (n_s, r) plane for different initial conditions in figure 5.6.

The amount of isocurvature perturbations for trajectories A and B are shown in figure 5.7. As all the trajectories reach the attractor several e-folds before the end of inflation, the isocurvature perturbations are strongly damped. A larger fraction of isocurvature perturbations can be found by increasing the value of β . We can also see that, for trajectories close to B, the sourcing of isocurvature to curvature fluctuations has a big impact on the latter. In this case the amplitude is enhanced by ~ 10 times compared to their value at horizon crossing. Additionally the running of the spectral index is enhanced.

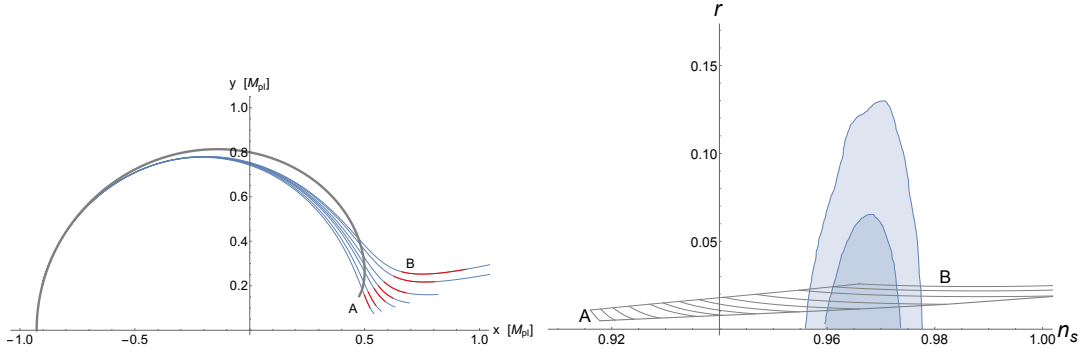


FIGURE 5.6: *Left*: Different trajectories for different initial conditions in the case $\beta = 1.6$. In red we show where the pivot scale left the horizon (50 to 60 e-folds before the end of inflation). The gray line is the minimum of the potential in the radial direction. *Right*: Predictions in the (n_s, r) plane for the depicted trajectories. The width represents the predictions for 50 to 60 e-folds before the end of inflation.

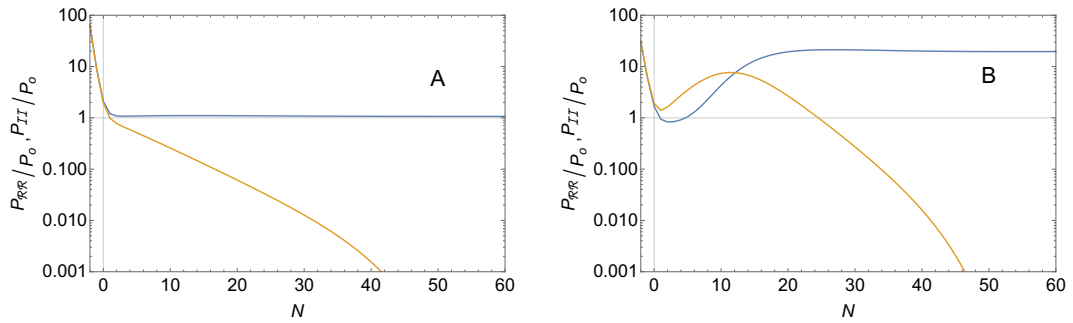


FIGURE 5.7: Curvature (blue) and isocurvature (yellow) perturbations for $\beta = 1.6$ and $r_0 = 0.8M_{\text{pl}}$, normalized to $P_0 \equiv H^2/8\pi^2\epsilon$ (with H and ϵ evaluated at horizon crossing). For both trajectories A and B, left and right panel respectively, the isocurvature mode has decayed at the end of inflation. For trajectory B the amplitude of the curvature mode is severely affected by isocurvature perturbations.

5.5 Trajectories with mass hierarchy

For completeness, we also compute the predictions in the case in which the $U(1)$ symmetry is mildly broken. In this case $\beta \ll 1$ and the hierarchy of masses between the radial and angular field is large throughout the trajectory. Let us note that if the field is at a large radius, the system will also inflate, *à la* chaotic inflation. The dynamics admits then three distinct situations.

- Inflation starts either in r or θ , ends in θ , and the observable e-folds left when the inflaton was θ (e.g. trajectory C in fig. 5.8)
- There is a first period of inflation in the radial direction, a second period in θ , and the observable e-folds left during the transition. (e.g. trajectory D in fig. 5.8)

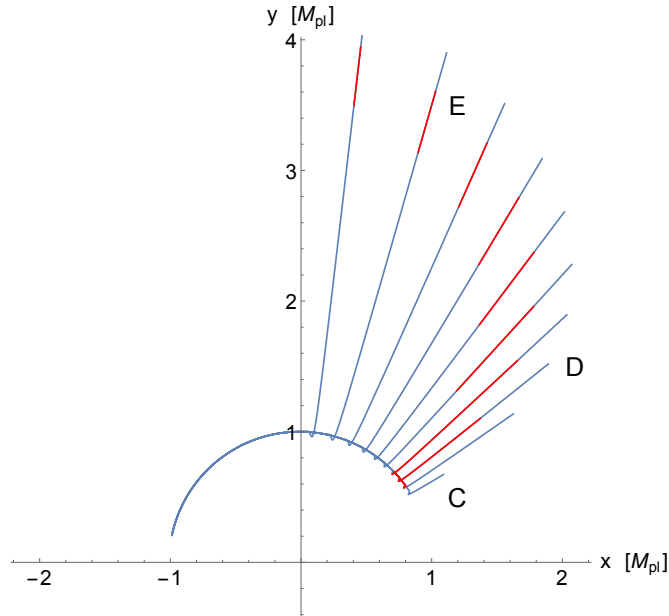


FIGURE 5.8: Different trajectories for different initial conditions in the case $\beta = 0.08$. In red is where the observable scales left the horizon (50 to 60 e-folds before the end of inflation).

- There is a first period of inflation in the radial direction, a second period in θ , and the observable e-folds left when the inflaton was r . Both periods of inflation could be matched or not. (e.g. trajectory E in fig. 5.8)

The transition from inflating in r to inflating in θ will produce a local peak in the slow-roll parameters, as can be seen in figure 5.9. The predictions for these cases are different. The first case will yield the same predictions as the single natural inflation potential. The second and third are more interesting. For trajectories like D and E and we expect large values for the slow-roll parameters at horizon crossing. If it were not for the additional e-folding provided by θ , those scales would correspond to very few e-folds before the end of inflation, in which the slow-roll parameters are big. This will also imply that the predictions for the primordial power spectrum may largely differ from a power law. In single field inflation, a period of fast roll at the time when the largest observable scales left the horizon might be an interesting mechanism to generate a smaller amplitude for the curvature perturbations at those scales [216–219], as suggested by observations (most recently, Planck 2015 results[30]). As explained in [220], this does not generalize to multifield models, as curvature perturbations may grow after horizon crossing. We find that this is the case in our model, such that perturbations on large scales are in general bigger than at smaller scales. Now, because of the small oscillatory feature in the slow-roll parameters, there is a zone in which the perturbations become smaller than the flat power spectrum. In figure 5.9 we show the power spectrum in the cases in which the predictions do not resemble a power law in all the range of observable

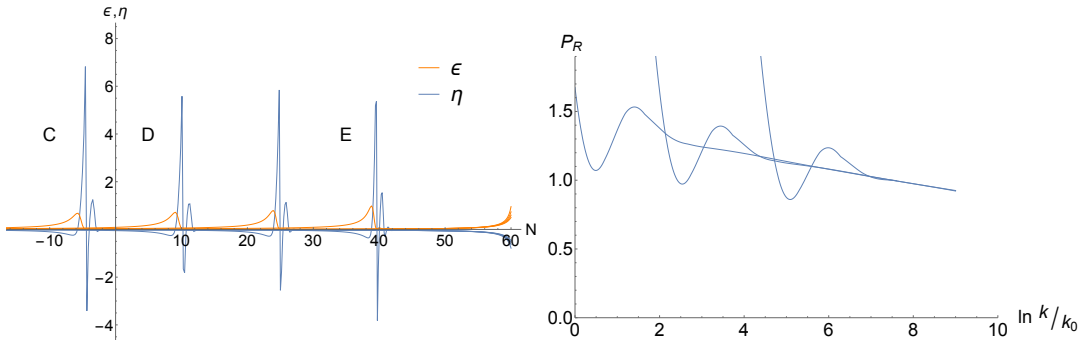


FIGURE 5.9: *Left:* The slow parameters ϵ and η ($\equiv \dot{\epsilon}/H\epsilon$) as a function of e-folds ($N=60$ is the end of inflation). *Right:* Power spectrum for different trajectories in the case $\beta = 0.08$, as a function of $\ln(k/k_0)$, with k_0 the scale that left the horizon 60 e-folds before the end of inflation.

e-folds, which is the case for trajectories that are subject to a turn in these scales. The rest of the trajectories are ruled out by direct computation of (n_s, r) .

5.6 Conclusions

Pseudo Nambu-Goldstone bosons are interesting candidates for driving inflation. However, the single field description with a sinusoidal potential leads to predictions that are in tension with the most recent CMB data. In this paper, we have shown that the simplest two-field completion of natural inflation (the original model proposed by Freese et al. in [32]), has a regime in which its predictions are consistent with observations. To do so, we have considered the possibility that the mass of the angular field (an axion) is of the same order as its radial partner. The normalization of the two-point function then fixes a hierarchy between the scales of spontaneous and explicit symmetry breaking, thus keeping higher order corrections under control. Isocurvature perturbations, while important for sourcing the curvature perturbations around the time of horizon crossing, decay before the end of inflation, since a mass hierarchy is created at the end of the inflationary trajectory. This makes the model also compatible with Planck isocurvature bounds.

For completeness, we have also computed the predictions for the more standard regime in which the radial field is very massive, but in the case in which the initial conditions are such that there are two stages of inflation, first in the radial direction and then in the angular direction. We find that in general this will imply an initial period of fast roll, which in this particular multifield setting (and contrary to single field models) provides an enhancement of power on large scales.

Bibliography

- [1] E. Hubble, “A relation between distance and radial velocity among extra-galactic nebulae,” *PNAS*, vol. 15, p. 169, 1929.
- [2] G. Lemaître, “Un univers homogène de masse constante et de rayon croissant, rendant compte de la vitesse radiale des nébuleuses extra-galactiques,” *Ann.Soc.Sci.Bruxelles*, vol. A 47, p. 49, 1927.
- [3] J.-P. Luminet, “Lemaître’s Big Bang,” *1503.08304*, 2014.
- [4] E. W. Kolb and M. S. Turner, *The Early Universe*. Addison-Wesley, 1990. Frontiers in Physics, 69.
- [5] A. R. B. H. and G. G., “The Origin of Chemical Elements,” *Phys.Rev*, vol. 73, p. 803, 1948.
- [6] R. Alpher and H. R., “On the Relative Abundance of the Elements,” *Nature*, vol. 162, pp. 774–775, 1949.
- [7] A. A. Penzias and R. W. Wilson, “A Measurement of excess antenna temperature at 4080-Mc/s,” *Astrophys. J.*, vol. 142, pp. 419–421, 1965.
- [8] R. H. Dicke, P. J. E. Peebles, P. G. Roll, and D. T. Wilkinson, “Cosmic Black-Body Radiation,” *Astrophys. J.*, vol. 142, pp. 414–419, 1965.
- [9] J. C. Mather *et al.*, “Measurement of the Cosmic Microwave Background spectrum by the COBE FIRAS instrument,” *Astrophys. J.*, vol. 420, pp. 439–444, 1994.
- [10] G. F. Smoot *et al.*, “Structure in the COBE differential microwave radiometer first year maps,” *Astrophys. J.*, vol. 396, pp. L1–L5, 1992.
- [11] R. Adam *et al.*, “Planck 2015 results. I. Overview of products and scientific results,” 2015.
- [12] P. A. R. Ade *et al.*, “Planck 2015 results. XIII. Cosmological parameters,” 2015.
- [13] A. H. Guth, “The Inflationary Universe: A Possible Solution to the Horizon and Flatness Problems,” *Phys.Rev.*, vol. D23, pp. 347–356, 1981.

- [14] A. A. Starobinsky, “Relict Gravitation Radiation Spectrum and Initial State of the Universe. (In Russian),” *JETP Lett.*, vol. 30, pp. 682–685, 1979.
- [15] K. Sato, “First Order Phase Transition of a Vacuum and Expansion of the Universe,” *Mon.Not.Roy.Astron.Soc.*, vol. 195, pp. 467–479, 1981.
- [16] A. D. Linde, “A New Inflationary Universe Scenario: A Possible Solution of the Horizon, Flatness, Homogeneity, Isotropy and Primordial Monopole Problems,” *Phys.Lett.*, vol. B108, pp. 389–393, 1982.
- [17] A. Albrecht and P. J. Steinhardt, “Cosmology for Grand Unified Theories with Radiatively Induced Symmetry Breaking,” *Phys.Rev.Lett.*, vol. 48, pp. 1220–1223, 1982.
- [18] A. H. Guth and E. J. Weinberg, “Could the universe have recovered from a slow first-order phase transition?,” *Nuclear Physics B*, vol. 212, no. 2, pp. 321 – 364, 1983.
- [19] V. F. Mukhanov and G. V. Chibisov, “Quantum Fluctuation and Nonsingular Universe. (In Russian),” *JETP Lett.*, vol. 33, pp. 532–535, 1981.
- [20] A. Riotto, “Inflation and the theory of cosmological perturbations,” in *Astroparticle physics and cosmology. Proceedings: Summer School, Trieste, Italy, Jun 17-Jul 5 2002*, pp. 317–413, 2002.
- [21] M. Sasaki, “Large Scale Quantum Fluctuations in the Inflationary Universe,” *Prog. Theor. Phys.*, vol. 76, p. 1036, 1986.
- [22] V. F. Mukhanov, “Quantum Theory of Gauge Invariant Cosmological Perturbations,” *Sov. Phys. JETP*, vol. 67, pp. 1297–1302, 1988. [Zh. Eksp. Teor. Fiz.94N7,1(1988)].
- [23] T. S. Bunch and P. C. W. Davies, “Quantum Field Theory in de Sitter Space: Renormalization by Point Splitting,” *Proc. Roy. Soc. Lond.*, vol. A360, pp. 117–134, 1978.
- [24] S. Weinberg, “Adiabatic modes in cosmology,” *Phys. Rev.*, vol. D67, p. 123504, 2003.
- [25] J. Garriga and V. F. Mukhanov, “Perturbations in k-inflation,” *Phys.Lett.*, vol. B458, pp. 219–225, 1999.
- [26] D. Baumann, D. Green, and R. A. Porto, “B-modes and the Nature of Inflation,” *JCAP*, vol. 1501, no. 01, p. 016, 2015.

- [27] G. A. Palma and A. Soto, “B-modes and the sound speed of primordial fluctuations,” 2014.
- [28] A. Lewis, A. Challinor, and A. Lasenby, “Efficient computation of CMB anisotropies in closed FRW models,” *Astrophys.J.*, vol. 538, pp. 473–476, 2000.
- [29] J. Lesgourgues, “The Cosmic Linear Anisotropy Solving System (CLASS) I: Overview,” 2011.
- [30] P. A. R. Ade *et al.*, “Planck 2015 results. XX. Constraints on inflation,” 2015.
- [31] A. D. Linde, “Chaotic Inflation,” *Phys.Lett.*, vol. B129, pp. 177–181, 1983.
- [32] K. Freese, J. A. Frieman, and A. V. Olinto, “Natural inflation with pseudo - Nambu-Goldstone bosons,” *Phys.Rev.Lett.*, vol. 65, pp. 3233–3236, 1990.
- [33] P. A. R. Ade *et al.*, “BICEP2 / Keck Array VI: Improved Constraints On Cosmology and Foregrounds When Adding 95 GHz Data From Keck Array,” 2015.
- [34] C. Cheung, P. Creminelli, A. L. Fitzpatrick, J. Kaplan, and L. Senatore, “The Effective Field Theory of Inflation,” *JHEP*, vol. 0803, p. 014, 2008.
- [35] A. P. S. Yadav and B. D. Wandelt, “Primordial Non-Gaussianity in the Cosmic Microwave Background,” *Advances in Astronomy*, vol. 2010, p. 71, 2010.
- [36] V. Acquaviva, N. Bartolo, S. Matarrese, and A. Riotto, “Second order cosmological perturbations from inflation,” *Nucl.Phys.*, vol. B667, pp. 119–148, 2003.
- [37] J. M. Maldacena, “Non-Gaussian features of primordial fluctuations in single field inflationary models,” *JHEP*, vol. 0305, p. 013, 2003.
- [38] L. Senatore, K. M. Smith, and M. Zaldarriaga, “Non-Gaussianities in Single Field Inflation and their Optimal Limits from the WMAP 5-year Data,” *JCAP*, vol. 1001, p. 028, 2010.
- [39] E. Komatsu and D. N. Spergel, “Acoustic signatures in the primary microwave background bispectrum,” *Phys. Rev.*, vol. D63, p. 063002, 2001.
- [40] P. A. R. Ade *et al.*, “Planck 2015 results. XVII. Constraints on primordial non-Gaussianity,” 2015.
- [41] D. Baumann, D. Green, H. Lee, and R. A. Porto, “Signs of Analyticity in Single-Field Inflation,” 2015.
- [42] E. Silverstein and D. Tong, “Scalar speed limits and cosmology: Acceleration from D-cceleration,” *Phys. Rev.*, vol. D70, p. 103505, 2004.

-
- [43] M. Alishahiha, E. Silverstein, and D. Tong, “DBI in the sky,” *Phys. Rev.*, vol. D70, p. 123505, 2004.
- [44] A. A. Starobinsky, “Spectrum of adiabatic perturbations in the universe when there are singularities in the inflation potential,” *JETP Lett.*, vol. 55, pp. 489–494, 1992.
- [45] D. Polarski and A. A. Starobinsky, “Spectra of perturbations produced by double inflation with an intermediate matter dominated stage,” *Nucl. Phys.*, vol. B385, pp. 623–650, 1992.
- [46] D. J. H. Chung, E. W. Kolb, A. Riotto, and I. I. Tkachev, “Probing Planckian physics: Resonant production of particles during inflation and features in the primordial power spectrum,” *Phys. Rev.*, vol. D62, p. 043508, 2000.
- [47] J. A. Adams, B. Cresswell, and R. Easther, “Inflationary perturbations from a potential with a step,” *Phys.Rev.*, vol. D64, p. 123514, 2001.
- [48] J.-O. Gong, “Breaking scale invariance from a singular inflaton potential,” *JCAP*, vol. 0507, p. 015, 2005.
- [49] A. Ashoorioon and A. Krause, “Power Spectrum and Signatures for Cascade Inflation,” 2006.
- [50] A. E. Romano and M. Sasaki, “Effects of particle production during inflation,” *Phys. Rev.*, vol. D78, p. 103522, 2008.
- [51] A. Ashoorioon, A. Krause, and K. Turzynski, “Energy Transfer in Multi Field Inflation and Cosmological Perturbations,” *JCAP*, vol. 0902, p. 014, 2009.
- [52] S. H. H. Tye, J. Xu, and Y. Zhang, “Multi-field Inflation with a Random Potential,” *JCAP*, vol. 0904, p. 018, 2009.
- [53] S. H. H. Tye and J. Xu, “A Meandering Inflaton,” *Phys. Lett.*, vol. B683, pp. 326–330, 2010.
- [54] N. Barnaby, “On Features and Nongaussianity from Inflationary Particle Production,” *Phys. Rev.*, vol. D82, p. 106009, 2010.
- [55] A. Achúcarro, J.-O. Gong, S. Hardeman, G. A. Palma, and S. P. Patil, “Features of heavy physics in the CMB power spectrum,” *JCAP*, vol. 1101, p. 030, 2011.
- [56] X. Chen, “Primordial Features as Evidence for Inflation,” *JCAP*, vol. 1201, p. 038, 2012.

- [57] A. D. Linde and V. F. Mukhanov, “Nongaussian isocurvature perturbations from inflation,” *Phys. Rev.*, vol. D56, pp. 535–539, 1997.
- [58] N. Bartolo, S. Matarrese, and A. Riotto, “Nongaussianity from inflation,” *Phys. Rev.*, vol. D65, p. 103505, 2002.
- [59] F. Bernardeau and J.-P. Uzan, “NonGaussianity in multifield inflation,” *Phys. Rev.*, vol. D66, p. 103506, 2002.
- [60] D. H. Lyth, C. Ungarelli, and D. Wands, “The Primordial density perturbation in the curvaton scenario,” *Phys. Rev.*, vol. D67, p. 023503, 2003.
- [61] N. Bartolo, E. Komatsu, S. Matarrese, and A. Riotto, “Non-Gaussianity from inflation: Theory and observations,” *Phys. Rept.*, vol. 402, pp. 103–266, 2004.
- [62] X. Chen, M.-x. Huang, S. Kachru, and G. Shiu, “Observational signatures and non-Gaussianities of general single field inflation,” *JCAP*, vol. 0701, p. 002, 2007.
- [63] A. D. Linde, “Generation of Isothermal Density Perturbations in the Inflationary Universe,” *Phys. Lett.*, vol. B158, pp. 375–380, 1985.
- [64] A. A. Starobinsky, “Multicomponent de Sitter (Inflationary) Stages and the Generation of Perturbations,” *JETP Lett.*, vol. 42, pp. 152–155, 1985. [Pisma Zh. Eksp. Teor. Fiz.42,124(1985)].
- [65] D. Polarski and A. A. Starobinsky, “Isocurvature perturbations in multiple inflationary models,” *Phys. Rev.*, vol. D50, pp. 6123–6129, 1994.
- [66] C. Gordon, D. Wands, B. A. Bassett, and R. Maartens, “Adiabatic and entropy perturbations from inflation,” *Phys.Rev.*, vol. D63, p. 023506, 2001.
- [67] S. Groot Nibbelink and B. J. W. van Tent, “Density perturbations arising from multiple field slow roll inflation,” 2000.
- [68] S. Groot Nibbelink and B. van Tent, “Scalar perturbations during multiple field slow-roll inflation,” *Class.Quant.Grav.*, vol. 19, pp. 613–640, 2002.
- [69] F. Di Marco, F. Finelli, and R. Brandenberger, “Adiabatic and isocurvature perturbations for multifield generalized Einstein models,” *Phys. Rev.*, vol. D67, p. 063512, 2003.
- [70] Z. Lalak, D. Langlois, S. Pokorski, and K. Turzynski, “Curvature and isocurvature perturbations in two-field inflation,” *JCAP*, vol. 0707, p. 014, 2007.
- [71] K.-Y. Choi, J.-O. Gong, and D. Jeong, “Evolution of the curvature perturbation during and after multi-field inflation,” *JCAP*, vol. 0902, p. 032, 2009.

- [72] C. P. Burgess, “Introduction to Effective Field Theory,” *Ann. Rev. Nucl. Part. Sci.*, vol. 57, pp. 329–362, 2007.
- [73] A. J. Tolley and M. Wyman, “The Gelaton Scenario: Equilateral non-Gaussianity from multi-field dynamics,” *Phys.Rev.*, vol. D81, p. 043502, 2010.
- [74] X. Chen and Y. Wang, “Large non-Gaussianities with Intermediate Shapes from Quasi-Single Field Inflation,” *Phys.Rev.*, vol. D81, p. 063511, 2010.
- [75] X. Chen and Y. Wang, “Quasi-Single Field Inflation and Non-Gaussianities,” *JCAP*, vol. 1004, p. 027, 2010.
- [76] A. Achúcarro, J.-O. Gong, S. Hardeman, G. A. Palma, and S. P. Patil, “Mass hierarchies and non-decoupling in multi-scalar field dynamics,” *Phys.Rev.*, vol. D84, p. 043502, 2011.
- [77] S. Cremonini, Z. Lalak, and K. Turzyski, “On Non-Canonical Kinetic Terms and the Tilt of the Power Spectrum,” *Phys. Rev.*, vol. D82, p. 047301, 2010.
- [78] S. Cremonini, Z. Lalak, and K. Turzyski, “Strongly Coupled Perturbations in Two-Field Inflationary Models,” *JCAP*, vol. 1103, p. 016, 2011.
- [79] D. Baumann and D. Green, “Equilateral Non-Gaussianity and New Physics on the Horizon,” *JCAP*, vol. 1109, p. 014, 2011.
- [80] G. Shiu and J. Xu, “Effective Field Theory and Decoupling in Multi-field Inflation: An Illustrative Case Study,” *Phys.Rev.*, vol. D84, p. 103509, 2011.
- [81] A. Achúcarro, J.-O. Gong, S. Hardeman, G. A. Palma, and S. P. Patil, “Effective theories of single field inflation when heavy fields matter,” *JHEP*, vol. 1205, p. 066, 2012.
- [82] X. Gao, D. Langlois, and S. Mizuno, “Influence of heavy modes on perturbations in multiple field inflation,” *JCAP*, vol. 1210, p. 040, 2012.
- [83] S. Cespedes and G. A. Palma, “Cosmic inflation in a landscape of heavy-fields,” *JCAP*, vol. 1310, p. 051, 2013.
- [84] W. Hu and M. J. White, “Acoustic signatures in the cosmic microwave background,” *Astrophys. J.*, vol. 471, pp. 30–51, 1996.
- [85] J. Meyers and N. Sivanandam, “Non-Gaussianities in Multifield Inflation: Superhorizon Evolution, Adiabaticity, and the Fate of f_{nl} ,” *Phys. Rev.*, vol. D83, p. 103517, 2011.

- [86] S. Renaux-Petel and K. Turzynski, “On reaching the adiabatic limit in multi-field inflation,” *JCAP*, vol. 1506, no. 06, p. 010, 2015.
- [87] J. Ellis, M. A. G. Garcia, D. V. Nanopoulos, and K. A. Olive, “Two-Field Analysis of No-Scale Supergravity Inflation,” *JCAP*, vol. 1501, no. 01, p. 010, 2015.
- [88] S. Bielleman, L. E. Ibanez, F. G. Pedro, and I. Valenzuela, “Multifield Dynamics in Higgs-Otic Inflation,” 2015.
- [89] S. Weinberg, “Must cosmological perturbations remain non-adiabatic after multi-field inflation?,” *Phys. Rev.*, vol. D70, p. 083522, 2004.
- [90] G. A. Palma, “Untangling features in the primordial spectra,” *JCAP*, vol. 1504, no. 04, p. 035, 2015.
- [91] S. Mooij, G. A. Palma, G. Panotopoulos, and A. Soto, “Consistency relations for sharp features in the primordial spectra,” *JCAP*, vol. 1510, no. 10, p. 062, 2015.
- [92] S. Cespedes, V. Atal, and G. A. Palma, “On the importance of heavy fields during inflation,” *JCAP*, vol. 1205, p. 008, 2012.
- [93] A. Avgoustidis, S. Cremonini, A.-C. Davis, R. H. Ribeiro, K. Turzynski, *et al.*, “Decoupling Survives Inflation: A Critical Look at Effective Field Theory Violations During Inflation,” *JCAP*, vol. 1206, p. 025, 2012.
- [94] R. Gwyn, G. A. Palma, M. Sakellariadou, and S. Sypsas, “Effective field theory of weakly coupled inflationary models,” *JCAP*, vol. 1304, p. 004, 2013.
- [95] X. Chen and Y. Wang, “Quasi-Single Field Inflation with Large Mass,” *JCAP*, vol. 1209, p. 021, 2012.
- [96] E. Komatsu *et al.*, “Seven-Year Wilkinson Microwave Anisotropy Probe (WMAP) Observations: Cosmological Interpretation,” *Astrophys. J. Suppl.*, vol. 192, p. 18, 2011.
- [97] D. Cannone, N. Bartolo, and S. Matarrese, “Perturbative Unitarity of Inflationary Models with Features,” 2014.
- [98] P. Adshead and W. Hu, “Bounds on non-adiabatic evolution in single-field inflation,” 2014.
- [99] G. German, G. G. Ross, and S. Sarkar, “Low scale inflation,” *Nucl. Phys.*, vol. B608, pp. 423–450, 2001.
- [100] R. Allahverdi, K. Enqvist, J. Garcia-Bellido, and A. Mazumdar, “Gauge invariant MSSM inflaton,” *Phys. Rev. Lett.*, vol. 97, p. 191304, 2006.

-
- [101] A. Achúcarro, V. Atal, S. Céspedes, J.-O. Gong, G. A. Palma, *et al.*, “Heavy fields, reduced speeds of sound and decoupling during inflation,” *Phys.Rev.*, vol. D86, p. 121301, 2012.
- [102] C. Burgess, M. Horbatsch, and S. Patil, “Inflating in a Trough: Single-Field Effective Theory from Multiple-Field Curved Valleys,” *JHEP*, vol. 1301, p. 133, 2013.
- [103] E. Castillo, B. Koch, and G. Palma, “On the integration of fields and quanta in time dependent backgrounds,” 2013.
- [104] C. Burgess, J. M. Cline, and R. Holman, “Effective field theories and inflation,” *JCAP*, vol. 0310, p. 004, 2003.
- [105] S. Weinberg, “Effective Field Theory for Inflation,” *Phys.Rev.*, vol. D77, p. 123541, 2008.
- [106] S. Pi and M. Sasaki, “Curvature Perturbation Spectrum in Two-field Inflation with a Turning Trajectory,” *JCAP*, vol. 1210, p. 051, 2012.
- [107] W. Hu, “Generalized Slow Roll for Non-Canonical Kinetic Terms,” *Phys.Rev.*, vol. D84, p. 027303, 2011.
- [108] A. Achúcarro, J.-O. Gong, G. A. Palma, and S. P. Patil, “Correlating features in the primordial spectra,” *Phys.Rev.*, vol. D87, p. 121301, 2013.
- [109] M. Park and L. Sorbo, “Sudden variations in the speed of sound during inflation: features in the power spectrum and bispectrum,” *Phys.Rev.*, vol. D85, p. 083520, 2012.
- [110] V. Miranda, W. Hu, and P. Adshead, “Warp Features in DBI Inflation,” *Phys.Rev.*, vol. D86, p. 063529, 2012.
- [111] M. Nakashima, R. Saito, Y.-i. Takamizu, and J. Yokoyama, “The effect of varying sound velocity on primordial curvature perturbations,” *Prog.Theor.Phys.*, vol. 125, pp. 1035–1052, 2011.
- [112] R. Bean, X. Chen, G. Hailu, S.-H. H. Tye, and J. Xu, “Duality Cascade in Brane Inflation,” *JCAP*, vol. 0803, p. 026, 2008.
- [113] N. Bartolo, D. Cannone, and S. Matarrese, “The Effective Field Theory of Inflation Models with Sharp Features,” *JCAP*, vol. 1310, p. 038, 2013.
- [114] P. Adshead, W. Hu, and V. Miranda, “Bispectrum in Single-Field Inflation Beyond Slow-Roll,” *Phys.Rev.*, vol. D88, p. 023507, 2013.

- [115] R. H. Ribeiro, “Inflationary signatures of single-field models beyond slow-roll,” *JCAP*, vol. 1205, p. 037, 2012.
- [116] Y.-F. Cai and H.-Y. Xia, “Inflation with multiple sound speeds: a model of multiple DBI type actions and non-Gaussianities,” *Phys.Lett.*, vol. B677, pp. 226–234, 2009.
- [117] R. Saito and Y.-i. Takamizu, “Localized Features in Non-Gaussianity from Heavy Physics,” *JCAP*, vol. 1306, p. 031, 2013.
- [118] Y.-F. Cai, W. Zhao, and Y. Zhang, “CMB Power Asymmetry from Primordial Sound Speed Parameter,” *Phys.Rev.*, vol. D89, p. 023005, 2014.
- [119] J.-O. Gong, K. Schalm, and G. Shiu, “Correlating correlation functions of primordial perturbations,” 2014.
- [120] L.-M. Wang and M. Kamionkowski, “The Cosmic microwave background bispectrum and inflation,” *Phys.Rev.*, vol. D61, p. 063504, 2000.
- [121] X. Chen, R. Easther, and E. A. Lim, “Generation and Characterization of Large Non-Gaussianities in Single Field Inflation,” *JCAP*, vol. 0804, p. 010, 2008.
- [122] F. Arroja, A. E. Romano, and M. Sasaki, “Large and strong scale dependent bispectrum in single field inflation from a sharp feature in the mass,” *Phys.Rev.*, vol. D84, p. 123503, 2011.
- [123] J. Martin and L. Sriramkumar, “The scalar bi-spectrum in the Starobinsky model: The equilateral case,” *JCAP*, vol. 1201, p. 008, 2012.
- [124] P. Adshead, C. Dvorkin, W. Hu, and E. A. Lim, “Non-Gaussianity from Step Features in the Inflationary Potential,” *Phys.Rev.*, vol. D85, p. 023531, 2012.
- [125] F. Arroja and M. Sasaki, “Strong scale dependent bispectrum in the Starobinsky model of inflation,” *JCAP*, vol. 1208, p. 012, 2012.
- [126] Y.-i. Takamizu, S. Mukohyama, M. Sasaki, and Y. Tanaka, “Non-Gaussianity of superhorizon curvature perturbations beyond δN formalism,” *JCAP*, vol. 1006, p. 019, 2010.
- [127] U. H. Danielsson, “A Note on inflation and transPlanckian physics,” *Phys.Rev.*, vol. D66, p. 023511, 2002.
- [128] B. R. Greene, K. Schalm, G. Shiu, and J. P. van der Schaar, “Decoupling in an expanding universe: Backreaction barely constrains short distance effects in the CMB,” *JCAP*, vol. 0502, p. 001, 2005.

- [129] P. D. Meerburg, J. P. van der Schaar, and P. S. Corasaniti, “Signatures of Initial State Modifications on Bispectrum Statistics,” *JCAP*, vol. 0905, p. 018, 2009.
- [130] M. G. Jackson and K. Schalm, “Model Independent Signatures of New Physics in the Inflationary Power Spectrum,” *Phys.Rev.Lett.*, vol. 108, p. 111301, 2012.
- [131] X. Gao, D. Langlois, and S. Mizuno, “Oscillatory features in the curvature power spectrum after a sudden turn of the inflationary trajectory,” *JCAP*, vol. 10, p. 23, 2013.
- [132] T. Noumi and M. Yamaguchi, “Primordial spectra from sudden turning trajectory,” 2013.
- [133] L. Covi, J. Hamann, A. Melchiorri, A. Slosar, and I. Sorbera, “Inflation and WMAP three year data: Features have a Future!,” *Phys.Rev.*, vol. D74, p. 083509, 2006.
- [134] M. Benetti, M. Lattanzi, E. Calabrese, and A. Melchiorri, “Features in the primordial spectrum: new constraints from WMAP7+ACT data and prospects for Planck,” *Phys.Rev.*, vol. D84, p. 063509, 2011.
- [135] P. Adshead and W. Hu, “Fast Computation of First-Order Feature-Bispectrum Corrections,” *Phys.Rev.*, vol. D85, p. 103531, 2012.
- [136] M. Benetti, “Updating constraints on inflationary features in the primordial power spectrum with the Planck data,” *Phys.Rev.*, vol. D88, p. 087302, Oct. 2013.
- [137] J. Hamann, L. Covi, A. Melchiorri, and A. Slosar, “New Constraints on Oscillations in the Primordial Spectrum of Inflationary Perturbations,” *Phys.Rev.*, vol. D76, p. 023503, 2007.
- [138] M. Benetti, S. Pandolfi, M. Lattanzi, M. Martinelli, and A. Melchiorri, “Featuring the primordial power spectrum: new constraints on interrupted slow-roll from CMB and LRG data,” *Phys.Rev.*, vol. D87, p. 023519, 2013.
- [139] J. Martin and C. Ringeval, “Superimposed oscillations in the WMAP data?,” *Phys.Rev.*, vol. D69, p. 083515, 2004.
- [140] R. Flauger, L. McAllister, E. Pajer, A. Westphal, and G. Xu, “Oscillations in the CMB from Axion Monodromy Inflation,” *JCAP*, vol. 1006, p. 009, 2010.
- [141] M. Aich, D. K. Hazra, L. Sriramkumar, and T. Souradeep, “Oscillations in the inflaton potential: Complete numerical treatment and comparison with the recent and forthcoming CMB datasets,” *Phys.Rev.*, vol. D87, p. 083526, 2013.

- [142] P. D. Meerburg, R. A. M. J. Wijers, and J. P. van der Schaar, “WMAP7 constraints on oscillations in the primordial power spectrum,” *MNRAS*, vol. 421, pp. 369–380, Mar. 2012.
- [143] H. Peiris, R. Easther, and R. Flauger, “Constraining Monodromy Inflation,” *JCAP*, vol. 1309, p. 018, 2013.
- [144] P. D. Meerburg, D. N. Spergel, and B. D. Wandelt, “Searching for Oscillations in the Primordial Power Spectrum: Perturbative Approach (Paper I),” 2013.
- [145] P. D. Meerburg and D. N. Spergel, “Searching for Oscillations in the Primordial Power Spectrum: Constraints from Planck (Paper II),” 2013.
- [146] P. Ade *et al.*, “Planck 2013 results. XXII. Constraints on inflation,” 2013.
- [147] V. Miranda and W. Hu, “Inflationary Steps in the Planck Data,” 2013.
- [148] E. D. Stewart, “The Spectrum of density perturbations produced during inflation to leading order in a general slow roll approximation,” *Phys.Rev.*, vol. D65, p. 103508, 2002.
- [149] J.-O. Gong and E. D. Stewart, “The Density perturbation power spectrum to second order corrections in the slow roll expansion,” *Phys.Lett.*, vol. B510, pp. 1–9, 2001.
- [150] J. Choe, J.-O. Gong, and E. D. Stewart, “Second order general slow-roll power spectrum,” *JCAP*, vol. 0407, p. 012, 2004.
- [151] C. Dvorkin and W. Hu, “Generalized Slow Roll for Large Power Spectrum Features,” *Phys.Rev.*, vol. D81, p. 023518, 2010.
- [152] P. Adshead, W. Hu, C. Dvorkin, and H. V. Peiris, “Fast Computation of Bispectrum Features with Generalized Slow Roll,” *Phys.Rev.*, vol. D84, p. 043519, 2011.
- [153] L. Keldysh, “Diagram technique for nonequilibrium processes,” *Zh.Eksp.Teor.Fiz.*, vol. 47, pp. 1515–1527, 1964.
- [154] S. Weinberg, “Quantum contributions to cosmological correlations,” *Phys.Rev.*, vol. D72, p. 043514, 2005.
- [155] P. Creminelli and M. Zaldarriaga, “Single field consistency relation for the 3-point function,” *JCAP*, vol. 0410, p. 006, 2004.
- [156] A. Achúcarro, V. Atal, P. Ortiz, and J. Torrado, “Localized correlated features in the CMB power spectrum and primordial bispectrum from a transient reduction in the speed of sound,” *Phys.Rev.*, vol. D89, p. 103006, 2014.

- [157] P. Ade *et al.*, “Planck 2013 results. XVI. Cosmological parameters,” 2013.
- [158] D. Blas, J. Lesgourgues, and T. Tram, “The Cosmic Linear Anisotropy Solving System (CLASS) II: Approximation schemes,” *JCAP*, vol. 1107, p. 034, 2011.
- [159] P. Ade *et al.*, “Planck 2013 results. XV. CMB power spectra and likelihood,” 2013.
- [160] C. Bennett *et al.*, “Nine-Year Wilkinson Microwave Anisotropy Probe (WMAP) Observations: Final Maps and Results,” *Astrophys.J.Suppl.*, vol. 208, p. 20, 2013.
- [161] B. Audren, J. Lesgourgues, K. Benabed, and S. Prunet, “Conservative Constraints on Early Cosmology: an illustration of the Monte Python cosmological parameter inference code,” *JCAP*, vol. 1302, p. 001, 2013.
- [162] F. Feroz and M. Hobson, “Multimodal nested sampling: an efficient and robust alternative to MCMC methods for astronomical data analysis,” *Mon.Not.Roy.Astron.Soc.*, vol. 384, p. 449, 2008.
- [163] F. Feroz, M. Hobson, and M. Bridges, “MultiNest: an efficient and robust Bayesian inference tool for cosmology and particle physics,” *Mon.Not.Roy.Astron.Soc.*, vol. 398, pp. 1601–1614, 2009.
- [164] L. Verde, “Statistical methods in cosmology,” *Lect.Notes Phys.*, vol. 800, pp. 147–177, 2010.
- [165] P. Ade *et al.*, “Planck 2013 Results. XXIV. Constraints on primordial non-Gaussianity,” 2013.
- [166] X. Chen, R. Easther, and E. A. Lim, “Large Non-Gaussianities in Single Field Inflation,” *JCAP*, vol. 0706, p. 023, 2007.
- [167] S. Rubin, “Effect of massive fields on inflation,” *Journal of Experimental and Theoretical Physics Letters*, vol. 74, no. 5, pp. 247–250, 2001.
- [168] X. Dong, B. Horn, E. Silverstein, and A. Westphal, “Simple exercises to flatten your potential,” *Phys.Rev.*, vol. D84, p. 026011, 2011.
- [169] C. M. Peterson and M. Tegmark, “Testing Two-Field Inflation,” *Phys.Rev.*, vol. D83, p. 023522, 2011.
- [170] A. Achúcarro and Y. Welling, “Multiple Field Inflation and Signatures of Heavy Physics in the CMB,” 2015.
- [171] J. McDonald, “Sub-Planckian Two-Field Inflation Consistent with the Lyth Bound,” *JCAP*, vol. 1409, no. 09, p. 027, 2014.

- [172] G. Barenboim and W.-I. Park, “Spiral Inflation,” *Phys.Lett.*, vol. B741, pp. 252–255, 2015.
- [173] T. Li, Z. Li, and D. V. Nanopoulos, “Helical Phase Inflation,” *Phys.Rev.*, vol. D91, no. 6, p. 061303, 2015.
- [174] J. E. Kim, H. P. Nilles, and M. Peloso, “Completing natural inflation,” *JCAP*, vol. 0501, p. 005, 2005.
- [175] S. Dimopoulos, S. Kachru, J. McGreevy, and J. G. Wacker, “N-flation,” *JCAP*, vol. 0808, p. 003, 2008.
- [176] R. Kappl, H. P. Nilles, and M. W. Winkler, “Natural Inflation and Low Energy Supersymmetry,” 2015.
- [177] T. Li, Z. Li, and D. V. Nanopoulos, “Symmetry Breaking Indication for Supergravity Inflation in Light of the Planck 2015,” 2015.
- [178] C. Pallis, “Non-minimally gravity-coupled inflationary models,” *Physics Letters B*, vol. 692, no. 5, pp. 287 – 296, 2010.
- [179] R. Kallosh, A. Linde, and D. Roest, “Universal Attractor for Inflation at Strong Coupling,” *Phys.Rev.Lett.*, vol. 112, no. 1, p. 011303, 2014.
- [180] A. Ashoorioon, K. Dimopoulos, M. Sheikh-Jabbari, and G. Shiu, “Reconciliation of High Energy Scale Models of Inflation with Planck,” *JCAP*, vol. 1402, p. 025, 2014.
- [181] K. Kannike, G. H?tsi, L. Pizza, A. Racioppi, M. Raidal, *et al.*, “Dynamically Induced Planck Scale and Inflation,” *JHEP*, vol. 1505, p. 065, 2015.
- [182] L. Boubekeur, E. Giusarma, O. Mena, and H. Ram?rez, “Does Current Data Prefer a Non-minimally Coupled Inflaton?,” *Phys.Rev.*, vol. D91, p. 103004, 2015.
- [183] W. Buchmuller, E. Dudas, L. Heurtier, A. Westphal, C. Wieck, *et al.*, “Challenges for Large-Field Inflation and Moduli Stabilization,” *JHEP*, vol. 1504, p. 058, 2015.
- [184] L. McAllister, E. Silverstein, and A. Westphal, “Gravity Waves and Linear Inflation from Axion Monodromy,” *Phys.Rev.*, vol. D82, p. 046003, 2010.
- [185] N. Kaloper and L. Sorbo, “A Natural Framework for Chaotic Inflation,” *Phys.Rev.Lett.*, vol. 102, p. 121301, 2009.
- [186] N. Kaloper, A. Lawrence, and L. Sorbo, “An Ignoble Approach to Large Field Inflation,” *JCAP*, vol. 1103, p. 023, 2011.

- [187] K. Harigaya and M. Ibe, “Simple realization of inflaton potential on a Riemann surface,” *Phys.Lett.*, vol. B738, pp. 301–304, 2014.
- [188] I. Zavala, “Effects of the speed of sound at large-N,” *Phys.Rev.*, vol. D91, no. 6, p. 063005, 2015.
- [189] R. Gwyn, G. A. Palma, M. Sakellariadou, and S. Sypsas, “On degenerate models of cosmic inflation,” *JCAP*, vol. 1410, no. 10, p. 005, 2014.
- [190] M. Dias, J. Frazer, and D. Seery, “Computing observables in curved multifield models of inflation - A guide (with code) to the transport method,” 2015.
- [191] T. Banks, M. Dine, P. J. Fox, and E. Gorbatov, “On the possibility of large axion decay constants,” *JCAP*, vol. 0306, p. 001, 2003.
- [192] R. D. Peccei and H. R. Quinn, “CP Conservation in the Presence of Instantons,” *Phys. Rev. Lett.*, vol. 38, pp. 1440–1443, 1977.
- [193] R. D. Peccei and H. R. Quinn, “Constraints Imposed by CP Conservation in the Presence of Instantons,” *Phys. Rev.*, vol. D16, pp. 1791–1797, 1977.
- [194] S. Weinberg, “A New Light Boson?,” *Phys. Rev. Lett.*, vol. 40, pp. 223–226, 1978.
- [195] F. Wilczek, “Problem of Strong p and t Invariance in the Presence of Instantons,” *Phys. Rev. Lett.*, vol. 40, pp. 279–282, 1978.
- [196] M. Dine, P. Draper, and A. Monteux, “Monodromy Inflation in SUSY QCD,” *JHEP*, vol. 07, p. 146, 2014.
- [197] K. Yonekura, “Notes on natural inflation,” *JCAP*, vol. 1410, no. 10, p. 054, 2014.
- [198] A. Albrecht, R. Holman, and B. J. Richard, “Spinodal Instabilities and Super-Planckian Excursions in Natural Inflation,” *Phys. Rev. Lett.*, vol. 114, p. 171301, 2015.
- [199] M. Czerny and F. Takahashi, “Multi-Natural Inflation,” *Phys. Lett.*, vol. B733, pp. 241–246, 2014.
- [200] M. Peloso and C. Unal, “Trajectories with suppressed tensor-to-scalar ratio in Aligned Natural Inflation,” *JCAP*, vol. 1506, no. 06, p. 040, 2015.
- [201] M. Czerny, T. Higaki, and F. Takahashi, “Multi-Natural Inflation in Supergravity,” *JHEP*, vol. 05, p. 144, 2014.
- [202] D. Croon and V. Sanz, “Saving Natural Inflation,” *JCAP*, vol. 1502, no. 02, p. 008, 2015.

- [203] J. McDonald, “A Minimal Sub-Planckian Axion Inflation Model with Large Tensor-to-Scalar Ratio,” *JCAP*, vol. 1501, no. 01, p. 018, 2015.
- [204] T. Higaki and F. Takahashi, “Elliptic inflation: interpolating from natural inflation to R^2 -inflation,” *JHEP*, vol. 03, p. 129, 2015.
- [205] I. P. Neupane, “Natural Braneworld Inflation in Light of Recent Results from Planck and BICEP2,” *Phys. Rev.*, vol. D90, no. 12, p. 123502, 2014.
- [206] E. Dudas and C. Wieck, “Moduli backreaction and supersymmetry breaking in string-inspired inflation models,” 2015.
- [207] T. Li, Z. Li, and D. V. Nanopoulos, “Helical Phase Inflation via Non-Geometric Flux Compactifications: from Natural to Starobinsky-like Inflation,” 2015.
- [208] A. Achúcarro, V. Atal, and Y. Welling, “On the viability of $m^2\phi^2$ and natural inflation,” *JCAP*, vol. 1507, p. 008, 2015.
- [209] J. D. Cohn and E. D. Stewart, “NonAbelian discrete gauge symmetries and inflation,” *Phys. Lett.*, vol. B475, pp. 231–235, 2000.
- [210] G. G. Ross and G. German, “Hybrid natural inflation from non Abelian discrete symmetry,” *Phys. Lett.*, vol. B684, pp. 199–204, 2010.
- [211] C. P. Burgess, M. Cicoli, F. Quevedo, and M. Williams, “Inflating with Large Effective Fields,” *JCAP*, vol. 1411, p. 045, 2014.
- [212] C. Burgess and D. Roest, “Inflation by Alignment,” *JCAP*, vol. 1506, no. 06, p. 012, 2015.
- [213] D. Croon, V. Sanz, and J. Setford, “Goldstone Inflation,” 2015.
- [214] R. Kallosh, A. D. Linde, D. A. Linde, and L. Susskind, “Gravity and global symmetries,” *Phys. Rev.*, vol. D52, pp. 912–935, 1995.
- [215] S. G. Rubin, “Effect of massive fields on inflation,” *JETP Lett.*, vol. 74, pp. 247–250, 2001. [Pisma Zh. Eksp. Teor. Fiz.74,275(2001)].
- [216] C. R. Contaldi, M. Peloso, L. Kofman, and A. D. Linde, “Suppressing the lower multipoles in the CMB anisotropies,” *JCAP*, vol. 0307, p. 002, 2003.
- [217] M. Cicoli, S. Downes, and B. Dutta, “Power Suppression at Large Scales in String Inflation,” *JCAP*, vol. 1312, p. 007, 2013.
- [218] F. G. Pedro and A. Westphal, “Low- ℓ CMB power loss in string inflation,” *JHEP*, vol. 1404, p. 034, 2014.

-
- [219] R. Bousso, D. Harlow, and L. Senatore, “Inflation after False Vacuum Decay: Observational Prospects after Planck,” *Phys. Rev.*, vol. D91, no. 8, p. 083527, 2015.
- [220] J. J. Blanco-Pillado, M. Dias, J. Frazer, and K. Sousa, “Large Scale Power Suppression in a Multifield Landscape,” 2015.

Publications

- *The two-field regime of natural inflation*, A. Achúcarro, V. Atal and M. Kawasaki, F. Takahashi, JCAP **1512** (2015) 12, 044 [arXiv:1510.08775 [astro-ph.CO]].
- *On the viability of $m^2\phi^2$ and natural inflation*, A. Achúcarro, V. Atal and Y. Welling, JCAP **1507** (2015) 07, 008 [arXiv:1503.07486 [astro-ph.CO]].
- *Inflation with moderately sharp features in the speed of sound: Generalized slow roll and in-in formalism for power spectrum and bispectrum*, A. Achúcarro, V. Atal, B. Hu, P. Ortiz and J. Torrado, Phys. Rev. D **90** (2014) 2, 023511 [arXiv:1404.7522 [astro-ph.CO]].
- *“Localized correlated features in the CMB power spectrum and primordial bispectrum from a transient reduction in the speed of sound,”*, A. Achúcarro, V. Atal, P. Ortiz and J. Torrado, Phys. Rev. D **89** (2014) 10, 103006 [arXiv:1311.2552 [astro-ph.CO]].
- *“Heavy fields, reduced speeds of sound and decoupling during inflation”*, A. Achúcarro, V. Atal, S. Céspedes, J. O. Gong, G. A. Palma and S. P. Patil, Phys. Rev. D **86** (2012) 121301 [arXiv:1205.0710 [hep-th]].
- *“On the importance of heavy fields during inflation“*, S. Céspedes, V. Atal and G. A. Palma, JCAP **1205** (2012) 008 [arXiv:1201.4848 [hep-th]].
- *“Bigravitational inflation”*, V. Atal, L. E. Campusano and G. A. Palma, Phys. Rev. D **86** (2012) 123521 [arXiv:1109.3224 [hep-th]].

Summary

Early Time Cosmology

Not even the most optimistic scientists and philosophers of the past could have guessed the impressive descriptive power of our current cosmological model. While it is certain that outstanding achievements have been made in every branch of the natural sciences, it is particularly remarkable that a substantial development has also been reached in our understanding of the Cosmos. Indeed, it is not at all clear from first principles that any kind of knowledge can be reached in the understanding of a system of which we are just a tiny, tiny part. In fact, the Universe is at least, 10^{26} times larger and 10^8 times older than ourselves⁷.

According to the theory of General Relativity, the geometry of space and time is affected by the energy density of the different components that make up part of the Universe, and *vice versa*. This interconnection is what determines the history of the Universe and the evolution of its internal constituents. The interplay between this theoretical framework and observations suggests that the Universe started expanding from a spacetime singularity 13.8×10^9 years ago. The history of the establishment of this model is of course long and complex, but it is fair to say that it can be traced back to the works of Lemaître and Hubble, where the recession of distant galaxies was first established. The natural reticence to the logical consequences of such model - implying a dynamical cosmos and the apparent presence of a spacetime singularity in the past- could only be overcome after the accumulation of overwhelming observational evidence sustained by elegant mathematics. factor to many of the new developments in physics: to astonish the human⁸.

Our current cosmological model further suggests that most of the present day energy in the cosmos comes from two unknowns constituents: the so-called dark matter and dark energy. The reader, amazed by the fact that we were able to describe such an old and vast Universe, might feel betrayed, as we have really little idea of what is the microscopic nature of the most important components of the present Universe. The reason for this “knowledge within ignorance” to be possible is that only a few numbers are enough to describe the influence of such

⁷If, as Protagoras said, man is the measure of all things, then we might metaphorically declare: man is of the size of the Universe!

⁸Of course, physics is just one example in which this feeling can be proven. Any deep interrogation, experience or contemplation of any phenomena, however simple, will certainly create such state of mind.

constituents on large cosmological scales, such as their equation of state parameter (relating pressure to density) and their present energy density. This simplification is common in everyday life: we only need to know a few functional characteristics of the objects that surround us in order to make use of them. While a superficial knowledge of dark energy and dark matter might be good enough for explaining some cosmological observations, a deeper understanding of the microscopic nature of these elements (or whatever they might be) is by all means necessary in order to provide a complete and fully satisfactory model of nature.

The presence of dark energy and dark matter are not the only mysterious phenomena for which we have no satisfactory full explanation. An additional conundrum of our standard cosmological model is the overall homogeneity of the Universe. This refers to the observation that *at sufficiently large scales* galaxies are evenly distributed through space⁹. Moreover, even the present highly inhomogeneous small scale regions (dense clusters of galaxies versus voids depleted of any trace of matter) are the result of very tiny initial perturbations of a highly homogeneous initial state.

Furthermore, the initial state of homogeneity is not only deduced from our present state but it is actually measured by looking at the so-called Cosmic Microwave Background. This is a relic radiation of our Universe emitted about 380.000 years after the spacetime ‘singularity’. This corresponds to a 0.001% of its present age, so it can be considered as a photograph of its primeval state. The Cosmic Microwave Background, commonly known as the CMB, is indeed a highly homogeneous sea of radiation (described by one single temperature), whose small temperature inhomogeneities are only of the order of one part in 10^5 .

The homogeneity of the observable Universe, combined with its finite age, is a problem for cosmologists because it challenges one of the most basic principles in physics, causality. Light rays, which define the maximum speed at which information can travel, have only traveled a finite distance since the beginning of time. Therefore, any observer in the Universe is only causally connected to a finite portion of their surroundings. Now, if the CMB temperature of the different portions of our observable Universe is the same, we would expect all of these different portions to be causally connected. Then comes the problem: in our present cosmological model, only very small regions of space were causally connected at the

⁹These *sufficiently large scales* are the scales we need to consider in cosmology, since they are not affected by the ‘environmental’ local forces (as the gravitational attraction of galaxies and cluster of galaxies) and follow instead the macroscopic flow of spacetime.

time when the CMB was created¹⁰. Therefore, how did all these causally disconnected regions manage to reach the very same temperature, if they never shared any information?

This thesis studies some aspects of the favourite solution to this conundrum, the idea of cosmic inflation. In very simple words, this theory states that the Universe, in a very primitive stage of evolution, expanded almost exponentially. This first burst of exponential expansion causes our Universe to emerge from a very tiny primeval volume which was indeed in causal contact before the inflationary expansion. This solves the homogeneity problem. Quite impressively, an inflationary era not only homogenizes the primordial Universe but also creates small density and tensor fluctuations¹¹. As the density fluctuations are needed in order to seed the present inhomogeneities, the theory of inflation is then basically providing a mechanism for the emergence of all the structures that we can see around us.

An idealized history of the expansion of the Universe is just a first step towards the establishment of a viable cosmological model. We also have to provide an explanation for why the Universe evolved in this particular way. As we said previously, the dynamics of the Universe, i.e., whether it expands, contracts or stays static, depends on its energy content. It follows that in order to have an initial era of inflation, some unknown “matter” field must be the cause. This hypothetical field is called the inflaton.

In physics, it is useful to classify fields according to their symmetries. One possibility is to classify them according to the way they change as we perform a rotation of the spacetime coordinates. This classification is very important, since the symmetry properties of a given field determine the structure of their equations of motion. The simplest fields which could cause inflation are *scalar* fields, which are fields that are invariant under spacetime rotations¹². Still, the supposition that the inflaton might be a scalar field is not yet enough for making this a satisfactory model, since this field might not exist in nature! Whether the inflaton field is present in nature or not, we do not know, since we have no idea of what is the correct description of the fundamental particles at the energy scale at which inflation might have happened. Let us note that the Standard Model of Particles has been tested up to the TeV scale (at the LHC experiment), but that inflation might have happened at energies which are of the order of 10^{13} times higher. Any

¹⁰The causally connected regions correspond to regions in the sky of the angular size of the moon.

¹¹Tensor fluctuations correspond to gravitational waves.

¹²For example, a fundamental scalar field is the recently discovered Higgs field.

theory about how particle physics is like at those energies is then highly speculative. In physics we like, however, to speculate. Ideally we do it following ideas which have proven to be good guiding principles for the explanation of physical phenomena. As we already mentioned, one of this principles is symmetry. In particular, we like to think about particles and forces as the representations of certain symmetries. Following this abstract principle physicists have been able to predict the existence of new particles, that were later discovered in the laboratory. Moreover, apparently disjoint phenomena have proven to be part of the same symmetry group.

This opens the possibility that all particle interactions might be fundamentally described by only one single symmetry group. This might be relevant for the theory of inflation, since one of the features of all the known ‘unification’ routes is that they predict the existence of many particles at high energies. This is exactly what inflation needs, since the inflaton should presumably be an unknown new particle living at higher energies¹³. However, a closer look shows that this may not be an ‘easy marriage’.

On the one hand, the statistical properties of the CMB tell us that if inflation happened it should have been dominated by one *single* field. On the other hand, high energy theories (predicting particles from symmetries) generically predict the existence of many fields. Both pictures are consistent with each other if the spectrum of the multifield theory obeys some very specific properties. If one and only one of these particles is light and all the rest are heavy¹⁴, then the many-particle theory is *effectively* reduced to the theory of a single light particle.

The reason for the possibility of constructing an effective theory, is that nature can be described at different levels. At different length scales (or, equivalently, energy scales) the degrees of freedom needed to describe a system might be different. For example, a stream of water might be understood macroscopically as a liquid with certain properties as density and viscosity. However when we look at the stream of water at a microscopic scale, we need molecules interacting through electrical

¹³A possible unification of the fundamental forces is only *one* of the possible motivations for considering the presence of additional fields at higher energies. Indeed, one might be much more agnostic as inflation doesn’t need all the ingredients of the theories of unification to be feasible. For example, even the Higgs field could play the role of the inflaton (needing an additional coupling between the Higgs field and gravity to be feasible). Whether physicists are more attracted by the minimality of adding just one new interaction to the Standard Model of Particles (as in Higgs inflation), or are inspired by (much) more complicated theories of unification (that have the additional advantage of explaining some other ‘conundrums’ present in our models), we consider it to be a matter of taste.

¹⁴By light/heavy we mean particles with masses much smaller/larger than the energy scale of inflation (that is related to the rate of expansion at that time). We can do this comparison between mass and energy since they are related through the famous Einstein formula $E = mc^2$.

forces to describe the system. Both are descriptions of the same system, but at different scales.

Importantly, we do not need to know the microscopic description in order to study the system at the macroscopic scale. Indeed, the macroscopic properties of the system can simply be measured at the macroscopic scale. In physics this phenomenon is known as *decoupling*, and the systematic understanding on how it operates provides a framework for addressing many problems in modern physics. This principle is, to some extent, a big relief: we don't need to understand the physics of the fundamental particles in order to study the mechanical properties of water!

From another point of view, this is exactly what has been preventing us from succeeding in finding an ultimate model for all the fundamental interactions. Indeed, we are constrained to build accelerators to directly probe very high energy (small scale) particles. Today these accelerators reach only 0.00000000001 % of all the energy scales we would like to probe. We might then say to have rediscovered what Heraclitus said more than 2000 years ago: "Nature loves to hide".

While nature loves to hide, it leaves some traces. Indeed, all the properties of the macroscopic system, e.g. viscosity for water, emerge from the details of the microscopic theory. Making the connection between the small and large scales might be very difficult, but if we are able to do it, we can gain knowledge about the microphysics by looking at the system macroscopically. This has tremendous consequences, since it tells us that we can gain knowledge about very high energy physics without the need of large accelerators to directly probe those energies.

This Thesis

In this thesis we have studied the situation in which the extra and very heavy fields can leave an imprint in the 'speed of propagation' of the inflaton density waves (known as the speed of sound). This is an example in which we can relate a macroscopic variable (e.g. the speed of sound of the inflaton's perturbations) with the microscopic details of the theory (e.g. the presence of very massive fields).

As the inflaton's perturbations seed the perturbations seen in the CMB, the speed of sound of the inflaton can have important consequences in the statistics of the CMB. Depending on the time dependence of the speed of sound, these effects are different in nature. In this thesis we have studied the case in which the speed of sound is allowed to vary very smoothly and very rapidly.

The former situation, in which the speed of sound varies smoothly, is quite simple to analyse. Indeed, no new mathematical or statistical tools are needed in order to compute predictions and compare them with observations. Let us note that the question whether the high energy degrees of freedom leave a trace in the low energy theory or not is totally circumstantial, as it depends on how these different fields are coupled, for which there is no a priori preference. In this thesis, we have shown how a particular class of interactions leading to “spiral” trajectories in field space, can lead to measurable effects. These models are the inspiration for the cover of this thesis.

The second part of this thesis concerns the study of a rapidly varying speed of sound. This situation demands the use of more sophisticated techniques for calculating the predictions of such models since we are no longer allowed to use approximations based on smooth and slow evolution of the variables. Moreover, in order to know whether such models are good for fitting the data we need to perform a direct and sophisticated comparison with the CMB maps. We perform an analysis based on the fact that, in models with a reduced speed of sound, there is a very specific correlation between the two- and the three-point function¹⁵. While we find some hints that such correlation could be present in the 2013 Planck satellite data of the CMB, the most recent data from 2015 seems not to favour its presence. An extended analysis with the new data is needed, which we plan to carry out in the future.

The last chapter of this thesis deals with the predictions of the so-called natural model of inflation. As we said previously, for inflation to be successful we need the presence of one very light field. However, we cannot simply say that a field is light and then forget about it. One of the most important lessons in modern physics is that the masses and charges of particles are not simple constants, but receive corrections from quantum effects involving all the remaining particles present in the theory (including also self-corrections). In the case of inflation, these effects might dominate the inflaton mass to the point where it is not light enough to support inflation. This is indeed the case for one interesting class of inflationary models, the so-called large-field models¹⁶. Large-field models are very appealing since they produce a relatively high amount of gravitational waves, whose detection could be very important for understanding the details of inflation, or even, to put

¹⁵These are measures of the correlation of the inflaton perturbations between two or three points in space. These quantities are very useful for statistically describing any map.

¹⁶Large-field models are those in which the inflaton field traverses a large ‘distance’ in field space. It more precisely means that the difference between the field values at the beginning and at the end of inflation is of the order of the Planck mass.

the inflationary paradigm under stress. It is then very unsatisfactory that we do not know how to consistently describe, in generality, this class of models.

One of the few models of large-field inflation in which this is not a problem is the case of natural inflation, in which there is symmetry ‘protecting’ the mass of the inflaton. It refers to the generic situation in which a model for inflation respects more symmetries when we consider a massless version of the same model. Then, one can show that quantum corrections will not increase the mass to dangerous levels. This scenario might sound very appealing from a fundamental level, but the prediction of its simplest version are in tension with the observed properties of the CMB. Indeed, this theory predicts a ratio of temperature to tensor perturbations which is too high, and/or a spectrum of the temperature perturbations which is too ‘red’ (meaning that the amplitude of the two-point correlation function at large scales is too big when compared with the small scales). In the last chapter we reconsider the predictions for natural inflation. While in the original model only one field is driving the dynamics, we show that in the case in which there is an additional field the predictions for such a model are indeed consistent with the observations.

Conclusions

In this thesis we present various aspects of early time cosmology. Our motivation is not only to acquire an understanding of the overall dynamics of the Universe but also to understand what might be the spectrum of particles and forces at energy scales which are today impossible to probe directly. In particular, we show how observations of the cosmos might reveal the presence of some heavy unknown particles. Discovering such particles would open the gate to a present day hidden sector of Particle Physics, and its implications might be enormous for solving many of the long-standing open questions in modern physics.

Samenvatting

Kosmologie van het vroege heelal

Zelfs de meest optimistisch ingestelde wetenschappers en filosofen uit het verleden zouden ons indrukwekkende model voor kosmologie niet voor mogelijk hebben gehouden. Het mag duidelijk zijn dat in alle takken van de natuurwetenschappen baanbrekende ontdekkingen zijn gedaan, maar het is in het bijzonder fascinerend dat we vandaag de dag zo ontzettend veel begrijpen over de kosmos. Het is immers verbluffend dat we iets kunnen leren over een systeem waar we zelf maar een minuscule deel van uit maken. Om precies te zijn, het heelal is minstens 10^{26} keer groter en 10^8 keer ouder dan dat we zelf zijn¹⁷.

Volgens de algemene relativiteitstheorie wordt de geometrie van het heelal beïnvloed door de energiedichtheid van haar verschillende bestanddelen en vice versa. Deze wederzijdse connectie bepaalt de geschiedenis van het heelal en de tijdsevolutie van haar elementen. Als men de waarnemingen hiermee vergelijkt dan lijkt het erop dat het heelal zo'n 13.8×10^9 jaar geleden is ontstaan vanuit een singulariteit in de ruimtetijd. De geschiedenis van de ontwikkeling van dit theoretische model is natuurlijk langdurig en complex, maar de belangrijkste fundamenten zijn gelegd in de werken van Lemaître en Hubble, waarin voor het eerst is waargenomen dat sterrenstelsels van ons vandaan bewegen. De natuurlijke terughoudende reactie op de implicaties van zo'n model – namelijk een dynamisch heelal en een ruimtetijd singulariteit in het verleden – kon alleen overwonnen worden door de opeenstapeling van massa's overtuigende waarnemingen ondersteund door elegante wiskunde.

Uit het huidige kosmologische model blijkt verder dat het grootste gedeelte van de energiehuishouding uit twee onbekende elementen bestaat: de zogenaamde donkere materie en donkere energie. De lezer, gefascineerd door het feit dat we in staat zijn zo'n oud en enorm heelal te beschrijven, zal zich misschien bedonderd voelen, aangezien we eigenlijk vrij weinig weten over de microscopische eigenschappen van de belangrijkste componenten van het huidige heelal. De reden dat we “kennis binnen onzekerheid” kunnen hebben, komt doordat we slechts een paar getallen nodig hebben om de invloed van deze bestanddelen op de grootste schalen te kunnen beschrijven. Voorbeelden hiervan zijn de toestandsvergelijking (de relatie tussen druk en energiedichtheid) en de energiedichtheid van de betreffende componenten

¹⁷Als een man de maat is van alle dingen, zoals Protagoras zei, dan kunnen we figuurlijk zeggen: een man is zo groot als het heelal!

op de dag van vandaag. Deze vereenvoudiging is iets wat we dagelijks tegenkomen: we hoeven slechts een paar functionele eigenschappen van objecten om ons heen te weten om ze te kunnen gebruiken. Hoewel een oppervlakkige beschrijving van donkere energie en donkere materie goed genoeg blijkt om bepaalde kosmologische waarnemingen te kunnen verklaren, zal een meer diepgaand begrip van de onderliggende microscopische wetten zeker nodig zijn om een compleet en meer bevredigend model van de natuur te hebben.

De aanwezigheid van donkere energie en donkere materie zijn niet de enige onopgeloste mysteriën. Een ander raadsel van het standaard kosmologische model is de homogeniteit van de heelal, meer precies de waarneming dat *voldoende grote schalen* sterrenstelsels gelijkmatig verdeeld zijn over de ruimte¹⁸. Bovendien zijn zelfs de huidige inhomogene kleine regio's (dichtbevolkte clusters met sterrenstelsels versus lege ruimte zonder ook maar een spoor van materie) het resultaat van zeer kleine fluctuaties in een verder homogene begin toestand.

De mate van homogeniteit kan niet alleen worden afgeleid uit de huidige staat van het heelal, maar ook door naar de zogenaamde kosmische achtergrondstraling te kijken. Deze straling is een relikwie van het heelal en zo'n 380.000 jaar na de ruimtetijd 'singulariteit' uitgezonden. Dit komt overeen met 0.001% van de huidige leeftijd van het heelal, en kan daarom gezien worden als een baby foto. De kosmische achtergrondstraling, ook wel de CMB genaamd, is inderdaad één zeer homogene zee van straling (beschreven door één enkele temperatuur), met kleine variaties in de temperatuur van de orde 0.001%.

De homogeniteit van het waarneembare heelal, samen met zijn eindige leeftijd, is een probleem voor kosmologen omdat het een van de belangrijkste principes in natuurkunde schendt, causaliteit. Licht, wat met de hoogste snelheid dat fysisch toegestaan is reist, kan slecht een eindige afstand reizen sinds het ontstaan van het heelal. Dit betekent dat elke waarnemer in het heelal slechts in causaal contact staat met een deel van zijn gehele omgeving. Nu we zien dat de temperatuur van de CMB van alle verschillende plekken van het waarneembare heelal gelijk is, verwachten we dat al deze delen in causaal contact met elkaar geweest moeten zijn. Het probleem is nu dat het huidige kosmologische model voorspelt dat de causale regio's ten tijde van de CMB zeer klein waren¹⁹. Hoe kan het dat al deze

¹⁸Deze *groot genoeg schalen* zijn de schalen die we moeten bestuderen in kosmologie, aangezien ze niet worden beïnvloed door de omgevende lokale krachten (zoals de gravitationele aantrekking tussen sterrenstelsels en clusters van sterrenstelsels) en daarom volgen ze de grootschalige stroming in de ruimtetijd

¹⁹De voorspelde causale regio's hebben een hoekgrootte gelijk aan die van de maan nu

losstaande delen toch precies dezelfde temperatuur hebben, ondanks het feit dat ze nooit informatie hebben kunnen uitwisselen?

In dit proefschrift worden enkele aspecten behandeld van de favoriete oplossing van dit raadsel, het idee van kosmische inflatie. Deze theorie zegt dat het heelal, toen het nog heel jong was, bijna exponentieel snel is uitgezet. Deze eerste explosie van exponentiële expansie maakt dat het heelal voortkomt uit een zeer klein oerstukje waarin alles in causaal contact was voordat de inflatie inzette. Dit lost het homogeniteitsprobleem op. Wat zeer indrukwekkend is, is dat een periode van inflatie niet alleen het heelal homogeen maakt, maar ook kleine dichtheidsvariaties en tensorfluctuaties²⁰ genereert. Aangezien de dichtheidsfluctuaties de zaadjes zijn van de huidige inhomogeniteiten, voorziet de theorie van inflatie ons met een mechanisme dat alles heeft gecreëerd wat we om ons heen zien.

Een geïdealiseerde geschiedenis van de expansie van het heelal is slechts de eerste stap naar de verwezelijking van een levensvatbaar kosmologisch model. We moeten daarnaast ook een verklaring hebben waarom het heelal op deze manier is geëvolueerd. Zoals we al eerder hebben aangegeven, hangt de dynamische ontwikkeling van het universum – d.w.z. of deze uitdijt, krimpt of statisch is – van zijn energie bestanddelen af. Hieruit blijkt dat voor een beginperiode van inflatie, een onbekend ‘materie’ veld nodig is. Dit hypothetische veld wordt het inflaton genoemd.

In de natuurkunde blijkt het handig te zijn om velden te classificeren overeenkomstig hun symmetrieën. Eén mogelijkheid om ze te classificeren is gerelateerd aan de manier waarop ze veranderen als we een rotatie van de ruimtetijd coördinaten uitvoeren. Deze classificatie is erg belangrijk, aangezien de symmetrieën van een veld de structuur van zijn bewegingsvergelijkingen bepaalt. De meest simpele velden die inflatie kunnen teweeg brengen zijn *scalair* velden, welke invariant zijn onder ruimtetijd rotaties²¹. Ondanks het vermoeden dat het inflaton een scalair veld is, maakt dit het nog geen bevredigend model, aangezien dit veld misschien in de natuur niet bestaat! Of het inflaton wel of niet bestaat weten we niet aangezien de juiste beschrijving van de elementaire deeltjes op de energieschaal van het inflaton onbekend is. Het standaard model voor elementaire deeltjes is tot aan de TeV energieschaal gemeten (bij het LHC experiment), maar inflatie zou plaats gevonden hebben op een energieschaal die 10^{13} maal hoger is. Elke theorie hoe de natuurkunde van de elementaire deeltjes werkt op die energieschaal

²⁰Tensorfluctuaties komen overeen met gravitatiegolven.

²¹Een voorbeeld van een scalair veld is het recentelijk ontdekte Higgs veld

is speculatief. Gelukkig houden we ervan te speculeren in de natuurkunde. Idealiter doen we dit volgens de ideeën welke de juiste basisprincipes zijn gebleken om natuurkundige verschijnselen te verklaren. Zoals al eerder genoemd is één van die principes symmetrie. In het bijzonder zien we deeltjes en krachten als representaties van bepaalde symmetrieën. Volgens dit abstracte principe zijn natuurkundigen erin geslaagd om nieuwe deeltjes te voorspellen, welke vervolgens in het lab gemeten zijn. Bovendien is gebleken dat schijnbaar verschillende fenomenen gevolg zijn van dezelfde symmetrie groep.

Dit zou het mogelijk kunnen maken dat alle interacties tussen deeltjes op een meer fundamenteel niveau beschreven kunnen worden door één enkele symmetrie groep. Dit kan belangrijk zijn voor de theorie van inflatie, aangezien één van de eigenschappen van alle ‘unificatie’ modellen is dat ze deeltjes voorspellen op een hoge energieschaal. Dit is precies wat nodig is voor inflatie, aangezien het inflaton waarschijnlijk een deeltje is wat op een hogere energieschaal leeft²². Als we dit idee wat beter bekijken, zien we wel dat dit geen gemakkelijke opgave is.

Aan de ene kant vertelt de statistiek van het CMB ons dat inflatie, als het plaatsgevonden heeft, gedomineerd zou moeten zijn door één enkel veld. Aan de andere kant voorspellen fundamentele theorieën (die, die deeltjes uit symmetrieën voorspellen) héél veel velden. Deze twee voorstellingen zijn met elkaar te verenigen als het spectrum van een theorie met meerdere velden aan specifieke eigenschappen voldoet. Als één veld licht is en de rest heel zwaar²³, dan is de theorie met meerdere velden effectief te reduceren tot een theorie met één enkel, licht deeltje.

De reden dat het mogelijk is om een effectieve theorie te construeren is dat de natuur beschreven kan worden op verschillende niveaus. Op verschillende lengteschalen (ofwel energieschalen) kunnen de vrijheidsgraden, die nodig zijn om het systeem te beschrijven, anders zijn. Een voorbeeld is dat een waterstroompje op grote schalen gezien kan worden als een vloeistof met bepaalde eigenschappen

²²Een mogelijke unificatie van de fundamentele krachten is slechts één van de mogelijke motivaties om het bestaan van nieuwe deeltjes op hogere energieën te beschouwen. Men kan ook meer agnostisch zijn aangezien inflatie niet alle ingredienten van unificatie nodig heeft om mogelijk te zijn. Het Higgs veld kan bijvoorbeeld ook de rol van het inflaton spelen (waarbij wel een extra koppeling tussen het Higgs veld en de zwaartekracht nodig is). Of natuurkundigen zich meer aangetrokken voelen tot een minimaal model waarbij slechts een nieuwe interactie nodig is in het standaard model van de elementaire deeltjes (zoals in Higgs inflatie), of geïnspireerd zijn door een meer ingewikkelde unificatie theorie (die het voordeel hebben om andere open vragen op te lossen), zullen we vanaf nu beschouwen als een eigen voorkeur.

²³Met licht/zwaar bedoelen we deeltjes met massa's veel lichter/zwaarder dan de energieschaal van inflatie (welke gerelateerd is aan de expansie snelheid op dat moment). We kunnen massa en energie met elkaar vergelijken aangezien ze aan elkaar gerelateerd zijn door de beroemde formule van Einstein $E = mc^2$.

zoals dichtheid en viscositeit. Maar als we naar het stroompje kijken op microscopische schaal, dan hebben we moleculen nodig die met elkaar wisselwerken met elektrische krachten. Beide beschrijven hetzelfde systeem, maar op verschillende schalen.

Het belangrijke punt is dat we de microscopische details niet nodig hebben om het systeem te kunnen bestuderen op macroscopische lengteschalen. De macroscopische eigenschappen kunnen immers gemeten worden op dezelfde schaal. In de natuurkunde wordt dit fenomeen *loskoppeling* genoemd, en de systematische manier om dit aan te pakken geeft een raamwerk waarin veel problemen binnen de moderne natuurkunde worden benaderd. Gelukkig maar, nu hoeven we immers niet de natuurkunde van elementaire deeltjes te begrijpen om water te kunnen bestuderen!

Vanuit een ander oogpunt gezien, dit is precies wat ons ervan weerhouden heeft om een succesvol model te vinden voor alle fundamentele krachten. We kunnen niet zomaar versnellers bouwen die de hoogste energieschalen meten. Vandaag de dag kunnen de deeltjesversnellers slechts 0.0000000001% van alle energieschalen meten die we zouden willen meten. Oftewel we hebben herontdekt wat Heraclitus meer dan 2000 jaar geleden heeft gezegd: “De natuur houdt ervan om zich te verstoppen”.

Ondanks dat de natuur zich graag verstoppt, laat het daarbij toch wat sporen na. Namelijk alle macroscopische eigenschappen van een systeem, bijvoorbeeld de viscositeit van water, zijn in principe af te leiden uit de microscopische details. Om de connectie tussen de kleine en de grote schalen te maken, zal lastig zijn, maar als het ons lukt dan kunnen we toch wat leren over de microscopische details door naar de macroscopische eigenschappen te kijken. Dit heeft fantastische gevolgen, namelijk dat we nog steeds iets zouden kunnen leren over fundamentele natuurkunde zonder deeltjesversnellers die deze energieën direct meten.

Terug naar inflatie. We hebben gezegd dat we een effectieve beschrijving kunnen afleiden in het geval dat er naast het inflaton veld nog meerdere zware deeltjes zijn. Wat zijn de gevolgen van deze zware deeltjes in de ‘macroscopische’ beschrijving van inflatie? Dit is precies het onderwerp van mijn proefschrift.

Dit proefschrift

In dit proefschrift hebben we een mogelijkheid bekeken waarin de extra en zeer zware velden een verandering aan kunnen brengen op de ‘propagatie snelheid’ van

de inflaton dichtheidsgolven (vanaf nu de geluidssnelheid genoemd). Dit is een voorbeeld waarbij we de macroscopische variabele (oftewel de geluidssnelheid van de inflaton perturbaties) kunnen relateren aan de microscopische details van de theorie (oftewel de aanwezigheid van de massieve velden).

Aangezien de fluctuaties in het inflaton veld een bron zijn voor de temperatuur variaties in de CMB, kan de geluidssnelheid van de inflaton fluctuaties belangrijke gevolgen hebben voor de statistische eigenschappen van de CMB. Deze effecten hangen af van de tijdsafhankelijkheid van de geluidssnelheid. In dit proefschrift hebben we de gevallen bekeken dat de geluidssnelheid langzaam varieert en snel varieert. Het eerste geval, waarin de geluidssnelheid langzaam varieert, is makkelijk te analyseren. Er zijn geen nieuwe wiskundige of statistische instrumenten nodig om de voorspellingen te maken en te vergelijken met waarnemingen. We moeten er wel bijzeggen dat of de hoog energetische vrijheidsgraden wel of niet een spoor achterlaten in de beschrijving van laag-energetische fenomenen sterk afhangt van hoe de velden met elkaar gekoppeld zijn, waarvoor a priori geen voorkeur bestaat. In dit proefschrift laten we zien dat een klasse van interacties die tot ‘spiraalvormige’ banen in de veldenruimte leidt, meetbare effecten kan veroorzaken. Deze modellen zijn de inspiratie voor de omslag van dit proefschrift.

Het tweede gedeelte van het proefschrift gaat over de studie van een snel variërende geluidssnelheid. In dit geval hebben we meer geavanceerde technieken nodig om de voorspellingen te doen aangezien we geen benaderingen kunnen doen gebaseerd op langzaam variërende variabelen. Om te zien of zulke modellen in overeenstemming zijn met de data moeten we een directe en geavanceerde vergelijking doen met de ruimtelijke verdeling van de CMB. We doen een analyse gebaseerd op het feit dat, in modellen met een lagere geluidssnelheid, er een specifieke correlatie is tussen de twee- en driepuntsfunctie²⁴. Ondanks het feit dat we een hint van zo’n correlatie vinden in de Planck 2013 data van de CMB, lijkt deze correlatie te verdwijnen in de meest recente data (van 2015), een meer geavanceerder analyse van de nieuwe data is nodig, welke we in de toekomst plannen te doen.

Het laatste hoofdstuk van dit proefschrift gaat over de voorspellingen van het zogenaamde ‘natural model’ voor inflatie. Zoals eerder vermeld, om inflatie te laten plaatsvinden, hebben we een licht veld nodig. Alleen kunnen we niet gewoon zeggen dat het zo is en het hierbij laten. Een van de belangrijkste lessen die we geleerd hebben in de moderne natuurkunde is dat de massa’s en ladingen van

²⁴Dit zijn grootheden die de correlaties tussen inflaton perturbaties meten tussen twee of drie punten in de ruimte. Deze grootheden zijn in het bijzonder handig om de statistische eigenschappen van een kaart te beschrijven.

velden niet constant zijn, maar gecorrigeerd worden door quantum effecten van alle deeltjes in de theorie inclusief henzelf. In het geval van inflatie zou het kunnen zijn dat dit de massa van het inflaton veld naar boven drijft waardoor inflatie niet meer kan plaatsvinden. Dit is inderdaad het geval voor een klasse van inflatie modellen, de zogenaamde ‘large-field’ modellen²⁵. De large-field modellen zijn aantrekkelijk aangezien ze veel zwaartekrachtsgolven produceren. De detectie hiervan zou erg belangrijk kunnen zijn om de details van inflatie te begrijpen of om de theorie van inflatie juist onder druk te zetten. Helaas weten we dus niet hoe we deze klasse van modellen op een consistente manier kunnen beschrijven.

Eén van de weinige modellen voor large-field inflatie die deze problemen niet heeft, is ‘natural inflation’. In dit geval is er een symmetrie die de massa van het inflaton veld beschermt. Dit refereert naar de algemene situatie waarin een model voor inflatie meer symmetrieën respecteert als we een versie bekijken waarin het inflaton massaloos is. In dit geval kan men aantonen dat de massa niet gevaarlijk hoge waarden aanneemt. Dit scenario klinkt erg aantrekkelijk als fundamentele theorie, maar helaas is het in strijd met de waarnemingen van de CMB. Deze theorie voorspelt namelijk een verhouding van dichtheidsfluctuaties tot tensorfluctuaties welke te hoog is, en ook een spectrum wat te ‘rood’ is (dit betekent dat de amplitude van de tweepuntsrelatie te hoog is op grote schalen vergeleken met de kleine schalen). In het laatste hoofdstuk herzien we de voorspellingen van natural inflation. In tegenstelling tot het originele model waarin slechts één veld de drijvende kracht is, bekijken we nu een geval waarin er nog een extra veld is waardoor de voorspellingen inderdaad consistent zijn met de waarnemingen.

Conclusies

In dit proefschrift laten we enkele aspecten zien van de kosmologie van het vroege heelal. Onze motivatie is niet alleen de algehele evolutie van het universum te begrijpen maar ook het spectrum van deeltjes en krachten op energieschalen die vandaag onmogelijk zijn om te meten. In het bijzonder laten we zien hoe waarnemingen van de kosmos nieuwe deeltjes aan het licht kan brengen. Wanneer we zulke deeltjes ontdekken zal er een nieuwe deur open gaan om een verborgen sector van de deeltjesfysica te bestuderen. De bijbehorende gevolgen zullen enorm zijn voor het oplossen van vele open vragen binnen de moderne natuurkunde.

²⁵Dit zijn modellen waarin het inflaton een grote afstand aflegt in de veldenruimte. Dit betekent dat het verschil van de begin en eindwaarde van het veld van dezelfde orde van grootte van de Plank massa is.

Curriculum Vitae

I was born on the 11 July of 1986, in the city of Santiago, Chile. Upon completing my primary and secondary school I entered the Faculty of Physical and Mathematical Sciences of Universidad de Chile. After my Bachelor, I joined the Astronomy Department at Cerro Calán, where I obtained a Master degree in Astronomy. Part of my Master thesis involved an experimental research project at Cardiff University in Wales. In 2011 I joined the Instituut Lorentz of Leiden University. I enrolled in the PhD program as a Huygens fellow to work under the supervision of Prof. dr. Ana Achúcarro. During my PhD I made a long term visit to the Institute for the Physics and Mathematics of the Universe (IPMU) in Japan, where I joined the group of Prof. dr. Masahiro Kawasaki. During these years I had the privilege to attend many schools and conferences in Japan, US, and many countries in Europe. Beginning in September, I will be a postdoctoral researcher at the University of Barcelona.

Acknowledgements

I first would like to thank my advisor Ana Achúcarro for her guidance and support during this PhD. I always found her door wide open, for which I am most grateful. I would also like to thank my co-promotor Gonzalo Palma for initiating me in the world of research, and for the many discussions we had during this period. I am indebted to both of you for not only guiding my route as a physicist, but also for being examples on how to teach and perform scientific research with passion, honesty and good faith.

During my research I had the privilege to closely work with very talented colleagues. My deepest gratitude are to Pablo, Jesus, Bin and Yvette for sharing their passion with me. I will further like to extend my gratitude to all the members of the Cosmology and the Particle Physics groups of the Lorentz Institute. I was very pleased to have shared my time with you. My sincere gratitude also to Fran and Marianne for their precious help and positive vibes. Part of my research was done in the the Institute for the Physics and Mathematics of the Universe in Japan, which very warmly opened to me the doors of their Institute. I am in particular thankful to Masahiro Kawasaki for making me part of his group, and for being very open for discussion and collaboration.

From my time in Leiden I am mostly proud of having met extraordinary friends. It is pretty impossible naming all of them. My thoughts are with all the people with whom I have shared nights around the dining table of Oude Rijn-4. To all of you, thanks for sharing your desires, creativity and joy with me. For constantly reminding me about the magical nature of the world, I thank Manuela.

Finally, it would have been much more difficult to pursuit my dreams if it wasn't for the support and care of my family. For each one of you, my deepest gratitude.

